

5-14-2010

## Luminescent Quantum Dot and Protein Composite Nanoparticles for Bioanalytical Applications

Arriel Wicks  
*University of New Orleans*

Follow this and additional works at: <https://scholarworks.uno.edu/td>

---

### Recommended Citation

Wicks, Arriel, "Luminescent Quantum Dot and Protein Composite Nanoparticles for Bioanalytical Applications" (2010). *University of New Orleans Theses and Dissertations*. 1149.  
<https://scholarworks.uno.edu/td/1149>

This Dissertation is protected by copyright and/or related rights. It has been brought to you by ScholarWorks@UNO with permission from the rights-holder(s). You are free to use this Dissertation in any way that is permitted by the copyright and related rights legislation that applies to your use. For other uses you need to obtain permission from the rights-holder(s) directly, unless additional rights are indicated by a Creative Commons license in the record and/or on the work itself.

This Dissertation has been accepted for inclusion in University of New Orleans Theses and Dissertations by an authorized administrator of ScholarWorks@UNO. For more information, please contact [scholarworks@uno.edu](mailto:scholarworks@uno.edu).

Luminescent Quantum Dot and Protein Composite Nanoparticles for Bioanalytical Applications

A Dissertation

Submitted to the Graduate Faculty of the  
University of New Orleans  
in partial fulfillment of the  
requirements for the degree of

Doctor of Philosophy  
in  
Chemistry

By

Arriel Wicks

B.S. Louisiana State University, 2005

May, 2010

## **Dedication**

I would like to dedicate this dissertation to my loving and supporting parents Ralph and Esther Wicks.

## **Acknowledgements**

I would like to thank my research advisor Professor Zeev Rosenzweig and my research co-advisor Professor Matthew A. Tarr for their support, guidance, and encouragement during graduate school. I would like to thank my LaSPACE fellowship for allowing me to continue my studies by providing monetary support for the past five years.

I would also like to express my gratitude to my advisory committee members Professor Richard B. Cole, Professor Gabriel Caruntu, and Professor Ferdinand Poudeu for their comments and suggestions throughout my graduate research.

I thank Dr. Laurie Locascio and Dr. Michael Gaitan for hosting our research group at NIST after Hurricane Katrina.

I thank Dr. Jibao He from Tulane University for all the TEM and SEM analysis.

I give special thanks to Professor Isiah Warner from Louisiana State University for urging me to pursue my Ph.D. in chemistry, encouraging me, and providing support.

I thank my past and present research group members for their advice, help, and friendship.

I also thank my close friends Lavette Bell, Netosha Macdonald, Toi Armstead, Dana Brown, Kawanda Richardson, and Silas Casher for your encouragement and friendship throughout my time in graduate school.

I would like to greatly thank my family for their undying support and encouragement. I could not have made it this far without them. I thank my father, Ralph Wicks; my mother, Esther Wicks; my brother, Dedrick Robinson; my grandmother, Mary Jeffries; and all my aunts, uncles and cousins.

## Table of Contents

List of Figures .....	v
List of Schemes.....	ix
Abstract.....	x
Chapter 1 Introduction .....	1
1.1 Objectives and aims .....	1
1.2 Significance.....	2
1.3 Fluorescence Principle .....	2
1.4 Quantum Dots .....	5
1.5 Human Serum Albumin .....	12
1.6 References.....	10
Chapter 2 Experimental .....	18
2.1 Chemicals and Supplies .....	18
2.2 Characterization .....	19
2.3 References.....	24
Chapter 3 Preparation and Characterization of Highly Stable Silica-Quantum Dot Composites .....	25
3.1 Abstract.....	25
3.2 Introduction.....	26
3.3 Experimental.....	28
3.4 Results and Discussion .....	31
3.5 Summary and Conclusions .....	44
3.6 References.....	46
Chapter 4 Quantum Dot-Mesoporous Silica Microcomposites for Biomarker Analysis ..	49
4.1 Abstract.....	49
4.2 Introduction.....	50
4.3 Experimental.....	54
4.4 Results and Discussion .....	59
4.5 Summary and Conclusions .....	79
4.6 References.....	82
Chapter 5 Enzymenatic Release of Fluorescent Drug Analogue from Human Serum Albumin Naoparticles .....	85
5.1 Abstract.....	85
5.2 Introduction.....	85
5.3 Experimental.....	88
5.4 Results and Discussion .....	90

5.5 Summary and Conclusions .....	97
5.6 References.....	98
Chapter 6 Summary and Discussion.....	103
Vita.....	107

## List of Figures

<b>Figure 1.1-</b> Jablonski Diagram.....	3
---	---

**Figure 3.1** - Digital fluorescence microscope images and fluorescence spectra ( $\lambda_{ex} = 400 \text{ nm}$ ) of  $3 \mu\text{m}$  mesoporous silica particles that contain 545 nm green emitting CdSe/ZnS QD (a), 655 nm red emitting CdSe/ZnS QD (b), and green and red emitting QD mixtures with 1:2 (c), 1:1 (d), and 3:1 (e) ratios. A typical exposure time was 150 msec.....33

**Figure 3.2** – Characterization of mesoporous silica (a) SEM image of mesoporous silica particles without quantum dots, (b) microtomeTEM image of mesoporous silica particles without quantum dots, (c) EDS spectrum of mesoporous silica particles without quantum dots, (d) SEM image of mesoporous silica particles with quantum dots, (e) microtomeTEM image of mesoporous silica particles with quantum dots, and (f) EDS spectrum of mesoporous silica particles with quantum dots.....34

**Figure 3.3** - Photostability measurements of (a) mesoporous silica particles with 655 nm quantum dots, (b) mesoporous silica particles with 545 nm quantum dots, (c) free 545 nm quantum dots, (d) free 655 nm quantum dots, (e) mesoporous silica with rhodamine DHPE, and (f) mesoporous silica with fluorescein DHPE.....35

**Figure 3.4** - Fluorescence intensity measurements of supernatant samples collected daily from solutions of mesoporous silica microparticles loaded with fluorescein-DHPE (a), rhodamine-DHPE (b), green emitting ( $\lambda_{ex}=400 \text{ nm}$ ,  $\lambda_{em} = 545 \text{ nm}$ ) QD (c) and red-emitting ( $\lambda_{ex} = 400 \text{ nm}$ ,  $\lambda_{em} = 655 \text{ nm}$ ) QD (d).....37

**Figure 3.5** - Effect of temperature on the stability of the silica-quantum dot composites..39

**Figure 3.6** - Stability of quantum dots in mesoporous silica with and without MPTMS. a) particles deoxygenated by argon that were stored in the dark, b) particles deoxygenated by argon that were stored in room light, c) particles with no argon stored in the dark, and d) particles with no argon stored in room light.....40

**Figure 3.7** - Dependence of the binding of the fluorescent anti-HER2/neu labeled particles on the concentration of HER2/neu: Plot of fluorescence intensity versus HER2/neu concentration of (a) 545 nm and (b) 655 nm SiQDs, and digital fluorescence microscopy images of (c) Unlabeled anti-HER2 silica with  $10 \mu\text{g/ml}$  HER2/neu, (d)  $0 \mu\text{g/ml}$  HER2/neu, (e)  $65 \text{ ng/ml}$  HER2/neu, (f)

50  $\mu\text{g/ml}$  ER, (g) 10  $\mu\text{g/ml}$  PR, (h) 85  $\text{ng/ml}$  HER2/neu, (i) 0.1  $\mu\text{g/ml}$  HER2/neu, (j) 2  $\mu\text{g/ml}$  HER2/neu, (k) 5  $\mu\text{g/ml}$  HER2/neu, and (l) 10  $\mu\text{g/ml}$  HER2/neu.....42

**Figure 4.1-** Anti-HER2/neu modified fluorescent silica particles for detection of HER2/neu. (a) the reactive methoxy groups are hydrolyzed upon addition of water, (b) condensation covalently links the silane to the oxide surface of quantum dot encoded mesoporous silica particles, (c) streptavidin is covalently bound to the silica particles via thiol-maleimide chemistry, (d) biotinylated HER2/neu is added and bound to streptavidin modified particles, and (e) direct detection assay performed.....57

**Figure 4.2-**Dependence of the binding of the fluorescent anti-HER2/neu labeled particles on the concentration of HER2/neu exposed to the glass well plate before addition of the antibody labeled beads: plot of mean number of particles attached to glass versus HER2/neu concentration.....61

**Figure 4.3.** Dependence of the binding of the fluorescent anti-HER2/neu labeled particles on the concentration of HER2/neu exposed to the glass well plate before addition of the antibody labeled beads: (a) digital fluorescence microscopy images of unlabeled anti-HER2 silica with 10  $\mu\text{g/mL}$  HER2/neu, (b) 0  $\mu\text{g/mL}$  HER2/neu, (c) 10  $\mu\text{g/mL}$  PR, (d) 50  $\mu\text{g/mL}$  ERa, (e) 65  $\text{ng/mL}$  HER2/neu, (f) 85  $\text{ng/mL}$  HER2/neu, (g) 0.1  $\mu\text{g/mL}$  HER2/neu, (h) 2  $\mu\text{g/mL}$  HER2/neu, (i) 5  $\mu\text{g/mL}$  HER2/neu, and (j) 10  $\mu\text{g/mL}$  HER2/neu.....62

**Figure 4.4.** Stability of HER2/neu plate prepared in advance (a) 545 nm quantum dots in silica and (b) 655 nm quantum dots in silica.....63

**Figure 4.5.** Dependence of the binding of the fluorescent anti-ERa labeled particles on the concentration of ERa exposed to the glass well plate before addition of the antibody labeled beads: plot of mean number of particles attached to glass versus ERa concentration.....64

**Figure 4.6.** Dependence of the binding of the fluorescent anti-ERa labeled particles on the concentration of ERa (a) digital fluorescence microscopy images of unlabeled anti- ERa silica with 50  $\mu\text{g/ml}$  ERa, (b) 0  $\mu\text{g/ml}$  ERa, (c) 85  $\text{ng/ml}$  ERa, (d) 10  $\mu\text{g/ml}$  HER2/neu, (e) 10  $\mu\text{g/ml}$  PR, (f) 100  $\text{ng/ml}$  ERa, (g) 2  $\mu\text{g/ml}$  ERa, (h) 5  $\mu\text{g/ml}$  ERa, and (i) 10  $\mu\text{g/ml}$  ERa, and (j) 50  $\mu\text{g/ml}$  ERa.....65

**Figure 4.7.** Dependence of the binding of the fluorescent anti-PR labeled particles on the concentration of PR exposed to the glass well plate before addition of the antibody labeled beads: plot of mean number of particles attached to glass versus PR concentration.....66

**Figure 4.8.** Dependence of the binding of the fluorescent anti-PR labeled particles on the concentration of PR: (a) digital fluorescence microscopy images of unlabeled anti- PR silica with 10  $\mu\text{g/ml}$  PR, (b) 0  $\mu\text{g/ml}$  PR, (c) 100  $\text{ng/ml}$  ERa, (d) 10  $\mu\text{g/ml}$  HER2/neu, (e) 50  $\mu\text{g/ml}$  ERa, (f) 200  $\text{ng/ml}$  PR, (g) 500  $\text{ng/mL}$ , (h) 1  $\mu\text{g/ml}$  PR, (ij) 2  $\mu\text{g/ml}$  PR, (j) 5  $\mu\text{g/ml}$  PR, and (k) 10  $\mu\text{g/ml}$  PR.....67

**Figure 4.9.** Fluorescence microscope images of a) EDC/sulfo-NHS activated capture HER2/neu antibody bound to amino-modified glass plate and b) EDC/sulfo-NHS activated carboxylic acid modified glass plate bound to amino groups of capture HER2/neu antibody.....69

**Figure 4.10.** Fluorescence microscope images of a) sandwich assay with 10 $\mu$ g/mL HER2/neu and b) direct detection assay with 10 $\mu$ g/mL HER2/neu.....69

**Figure 4.11.** Dependence of the binding of the fluorescent anti-HER2/neu labeled particles on the concentration of HER2/neu: plot of mean number of particles attached to glass versus HER2/neu concentration.....70

**Figure 4.12.** Dependence of the binding of the fluorescent anti-HER2/neu labeled particles on the concentration of HER2/neu: (a) digital fluorescence microscopy images of anti-HER2 silica with 85 ng/mL HER2/neu, (b) 25ng/mL HER2/neu, (c) 15 ng/mL HER2/neu, (d) 10 ng/mL HER2/neu, (e) 4 ng/mL HER2/neu, and (f) 3 ng/mL HER2/neu.....71

**Figure 4.13.** Dependence of the binding of the fluorescent anti-ERa labeled particles on the concentration of ERa: plot of mean number of particles attached to glass versus ERa concentration.....72

**Figure 4.14.** Dependence of the binding of the fluorescent anti-ERa labeled particles on the concentration of ERa: (a) digital fluorescence microscopy images of anti- ERa silica with 100 ng/mL ERa, (b) 25 ng/mL ERa, (c) 15 ng/mL ERa, (d) 10 ng/mL ERa, and (e) 6 ng/mL ERa. ....73

**Figure 4.15.** Dependence of the binding of the fluorescent anti-PR labeled particles on the concentration of PR: plot of mean number of particles attached to glass versus PR concentration. ....74

**Figure 4.16.** Dependence of the binding of the fluorescent anti-PR labeled particles on the concentration of PR: (a) digital fluorescence microscopy images of anti- PR silica with 200 ng/mL PR, (b) 25 ng/mL PR, (c) 15 ng/mL PR, (d) 12 ng/mL PR, and (e) 11 ng/mL PR.75

**Figure 4.17.** Multiplexed detection of (a) 3 ng/mL HER2/neu, 6 ng/mL ERa, and 11 ng/mL PR and (b) the fluorescence spectrum of 495 nm, 560 nm, and 655 nm SiQDs.....76

**Figure 4.18.** Sandwich detection of HER2/neu with InP/ZnS QDs of (a) 17 ng/mL HER2/neu, (b) 25 ng/mL HER2/neu, and (c) 50 ng/mL HER2/neu.....78

**Figure 4.19.** Sandwich detection of ERa with InP/ZnS QDs of (a) 25 ng/mL ERa, (b) 40 ng/mL ERa, and (c) 50 ng/mL ERa.....78

**Figure 4.20.** Sandwich detection of PR with InP/ZnS QDs of (a) 32 ng/mL PR, (b) 40 ng/mL PR, and (c) 50 ng/mL PR.....79

**Figure 4.21.** Multiplexed detection of (a) 17 ng/mL HER2/neu, 25 ng/mL ERa, and 32 ng/mL PR.....79

**Figure 5.1.** Cryo-TEM images of a) 1 micron HSA and b) 100 nm HSA.....90

**Figure 5.2.** Images of a) HSA nanoparticles at  $t = 0$  min in room light, b) HSA nanoparticles at  $t = 15$  min in room light, c) HSA nanoparticles at  $t = 0$  min under UVlight, and d) HSA nanoparticles at  $t = 15$  min under UV light.....92

**Figure 5.3.** Effect of collagenase concentration on BODIPY-vinblastine release from HSA nanoparticles. a) 10  $\mu\text{g/mL}$  collagenase, b) 8  $\mu\text{g/mL}$  collagenase, c) 6  $\mu\text{g/mL}$  collagenase, d) 2  $\mu\text{g/mL}$  collagenase, e) 0  $\mu\text{g/mL}$  collagenase, and f) unlabeled HSA particles with 10  $\mu\text{g/mL}$  collagenase.....93

**Figure 5.4.** Effect of MMP-11 concentration on BODIPY-vinblastine release from HSA nanoparticles. a) 10  $\mu\text{g/mL}$  MMP-11, b) 8  $\mu\text{g/mL}$  MMP-11, c) 6  $\mu\text{g/mL}$  MMP-11, d) 2  $\mu\text{g/mL}$  MMP-11, e) 0  $\mu\text{g/mL}$  MMP-11, and f) unlabeled HSA particles with 10  $\mu\text{g/mL}$  MMP-11 .....94

**Figure 5.5.** Effect of MMP-11 concentration of BODIPY-vinblastine release from HSA nanoparticles suspended in solution. a) fluorescence spectra and b) corresponding plot of the fluorescence intensity of supernatant as a function of enzyme degradation time.....95

**Figure 5.6.** Stern-Volmer plot of fluorophore populations. a) Free BODIPY and b) BODIPY inside HSA nanoparticles.....96

## List of Schemes

Scheme 3.1. Schematic representation of the sythesis of CdSe/ZnS core/shell quantum dots .....	29
Scheme 3.2. Schematic representation of the interaction between the C-18 hydrocarbon chain of the pore wall and the TOPO molecules on the quantum dot surface.....	38
Scheme 4.1. General scheme of FISH. <a href="http://www.genome.gov">www.genome.gov</a> .....	52
Scheme 4.2. Scheme of IHC.....	53

## ABSTRACT

The first project focused on the preparation, characterization, and application of dual emission quantum dot encoded mesoporous silica microparticles. The quantum dots were added in precisely controlled ratios and were stably encapsulated within the pores of the silica. Several experiments were performed to test the superior stability of the quantum dot-silica composites over dye-loaded silica particles. The composite particles exhibited very high fluorescence, were functionalized with antibodies, and were used as signal transducers for the detection of a protein expressed by breast cancer cells.

The second project focused in more detail on the detection capabilities of the quantum dot-silica composites. Three different types of quantum dot-silica composites were prepared. Each type was loaded with a separate type of quantum dot with distinct emission wavelengths and was functionalized with separate antibodies for detection of three different breast cancer biomarkers. These three composite sensors were used together for the simultaneous detection of each of the breast cancer markers. The initial strategy utilized the direct detection method in which the antigen is nonspecifically adsorbed to a glass plate. An improved second strategy was more sensitive and used a capture antibody which was covalently bound to a glass plate to immobilize the antigen.

The third project focused on the preparation and application of magnetic, fluorescent human serum albumin nanoparticle composites. A fluorescent drug analogue and iron oxide nanoparticles were encapsulated into 100 nm human serum albumin nanoparticles. The advantage of these composite particles is that they could be used as a theranostic tool which

could target, detect, and treat diseased tissue in a single application. Release of the drug analogue from the nanocomposites was achieved by addition of proteolytic enzymes that are expressed or overexpressed in cancer cells. The temporal release of the fluorescent drug analogue was measured as a function of enzyme concentration. The amount of drug released was directly proportional to enzyme concentration.

Keywords: Nanoparticles; quantum dots; fluorescence; multiplexing; enzymatic degradation; breast cancer detection

# **Chapter 1**

## **Introduction**

### **1.1 Objectives and Aims**

The main objective of the research projects was to develop luminescent quantum dot composite particles for the detection of breast cancer markers and to measure the release of a fluorescent drug analogue from biodegradable human serum albumin (HSA) nanoparticles. Quantum dots offer several advantages over conventional fluorophores. One of the major advantages is the broad absorption spectra of quantum dots. This enables quantum dots with different emission wavelengths to be excited by a single wavelength. This is important because it allows for multiplexing. The specific aims of study were i) to prepare and characterize highly stable silica-quantum dot composites, ii) to develop quantum dot-mesoporous silica microcomposites for biomarker analysis, and iii) to prepare and apply BODIPY-Vinblastine encoded magnetic HSA particles for the detection of a breast cancer marker and to measure the release as a function of enzyme concentration.

### **1.2 Significance**

The ability for a sensitive assay to rapidly and reliably detect levels of breast cancer markers is in high demand in cancer research. It is important for early diagnosis and improved prognosis. The current methods to detect levels of breast cancer markers use fluorophores to measure gene

expression and protein localization. Fluorophores have several chemical and photophysical limitations, such as broad emission spectra, poor photostability, low fluorescence quantum yields, and the inability to perform multicolor detection. However, luminescent quantum dots have unique electronic and optical properties that make them very desirable in biological research. A major field of study in cancer research is the simultaneous detection of cancer markers. The ability to detect cancer markers early can reduce cost and improve prognosis. One research project focused on the development of a fluoroimmunoassay that can simultaneously detect three very common breast cancer markers. Another research project focused on measuring the release of drug analogue from magnetic, fluorescent HSA composites. The composite particles can be used in cancer research for both magnetic targeting and treatment such as magnetic hyperthermia.

## **1.3 Fluorescence Principle**

### **1.3.1 Jablonski Diagram**

Fluorescence is the emission of one or more photons by an atom or molecule activated by the absorption of a photon of electromagnetic radiation. This phenomenon can be illustrated by the Jablonski Diagram (Figure 1.1).

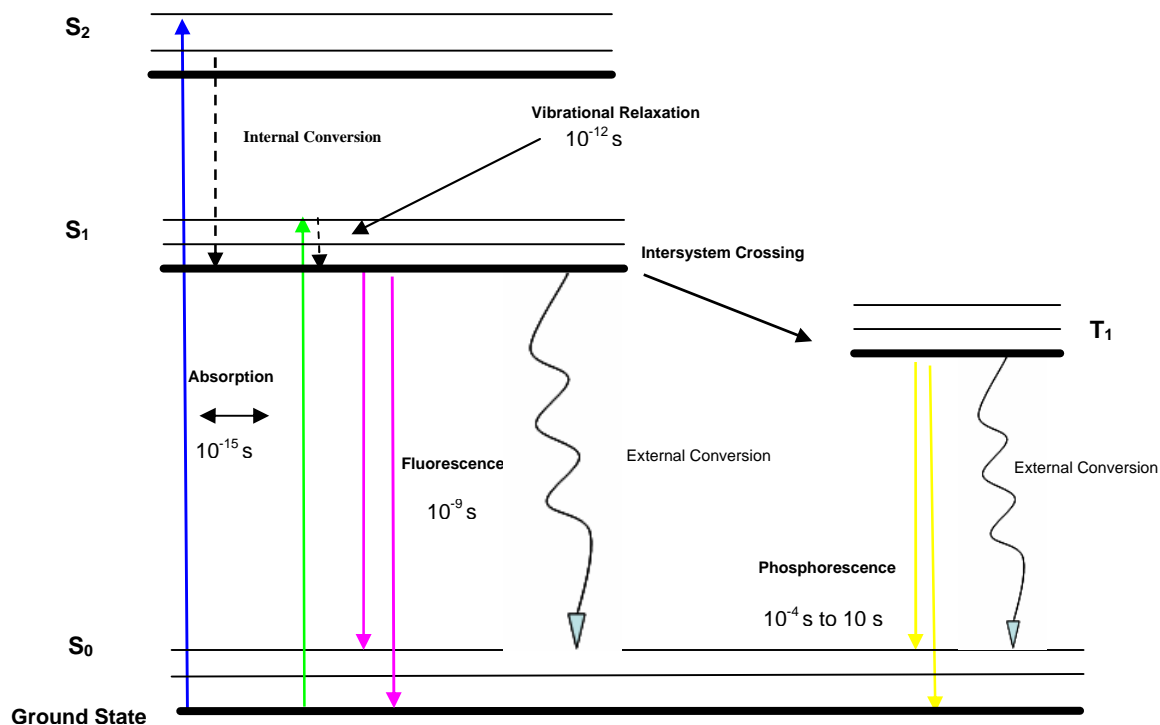


**Figure 1.1** The Jablonski (energy-level) diagram for a photoluminescent molecule. S<sub>0</sub>, S<sub>1</sub>, and S<sub>2</sub> are the singlet ground state and the first and second excited electronic states, respectively. T<sub>1</sub> is the first electronic triplet state.

Fluorescence occurs when the electron of a fluorophore is excited by the absorption of electromagnetic radiation to produce a higher energy singlet state (S<sub>1</sub> or S<sub>2</sub>) and returns to the ground (S<sub>0</sub>) state by emission of a photon. Emission involves the transition from the lowest vibrational level of the first excited electronic singlet state. The lifetime of fluorescence is about  $10^{-7}$  to  $10^{-9}$  s. The absorption of a photon of radiation occurs in about  $10^{-14}$  to  $10^{-15}$  s. After absorption, the electron is excited to any of the higher energy vibrational levels (depicted by the blue and green arrows in Figure 1.1). The four significant nonradiative deactivation processes are internal conversion, vibrational relaxation, external conversion, and intersystem crossing. Internal conversion takes place whenever the electron relaxes to the lowest vibrational level of S<sub>1</sub> or when a molecule moves to a lower energy electronic state without emission of radiation. The excited electron returns to its ground state via vibrational relaxation (shown by the dotted arrows in

Figure 1.1) and light is emitted. Vibrational relaxation occurs in about  $10^{-12}$  s. The vibrational energy is immediately lost because of collisions between the molecules of the excited fluorophore and the molecules of the solvent.<sup>1, 2</sup> External conversion is the deactivation of an electronic excited state caused by interaction and energy transfer between the excited fluorophore and the solvents or other solutes. In fluorescence, the emission spectrum is the mirror image of  $S_0 \rightarrow S_1$  of the absorbance spectrum because the same transitions are involved in both absorption and emission, and the vibrational levels of  $S_0$  and  $S_1$  are similar. For a given molecule, fluorescence occurs at longer wavelengths than absorbance because the energy of emission is less than that of absorption. This energy difference occurs because upon excitation into higher electronic and vibrational energy levels, the energy is rapidly dissipated as a result of vibrational relaxation and internal conversion. Therefore, emission usually occurs from the lowest vibrational level of  $S_1$ .

In fluorescence, the spin of the excited electron in the singlet state is paired with the ground state electron. When the spin of an electron in  $S_1$  are reversed, there is a transition from  $S_1$  to  $T_1$ . This is called intersystem crossing. Emission from  $T_1$  is called phosphorescence. Because transition from  $T_1$  to  $S_0$  is forbidden, the phosphorescence lifetime is much longer than fluorescence ( $10^{-4}$  s to 10 s vs  $10^{-7}$  to  $10^{-9}$  s). Both fluorescence and phosphorescence are the same in that excitation is caused by absorption of photons. Fluorescence is different from phosphorescence because the electronic energy transitions in fluorescence do not involve a change in electron spin.

### 1.3.2 Factors that Affect Fluorescence

The chemical environment and structure of a substance determine whether it will fluoresce and have a high or low quantum yield. The quantum yield is the ratio of the number of photons emitted to the total number of photons absorbed.<sup>2</sup> Highly fluorescent molecules have quantum yields that approach unity; whereas, non-fluorescent molecules have quantum yields that approach zero. Fluorescence mainly occurs in compounds that have  $\pi \rightarrow \pi^*$  transitions because they have much higher molar absorptivities that result in shorter fluorescence lifetimes and because the deactivation processes that compete with fluorescence are minimized.

Compounds that contain aromatic functional groups with low energy  $\pi \rightarrow \pi^*$  transition levels, highly conjugated double bond structures, or aliphatic and alicyclic carbonyl structures exhibit fluorescence. Substitution of the carbonyl or carboxylic acid groups on an aromatic ring prevents fluorescence. Solvents or solutes that contain heavy atoms and halogen substitution on an aromatic ring cause the heavy atom effect which increases the probability of intersystem crossing and decreases the fluorescence intensity as the molecular weight of the halogen increases. Other factors that affect the quantum yield of a molecule include temperature, pH, paramagnetism, and concentration.

### 1.4 Structural Properties of Quantum Dots

Quantum dots (QDs) are small, spherical, fluorescent semiconductor nanocrystals composed of periodic groups of II–VI (CdS, CdSe, CdTe, ZnO, ZnSe), III–V (InP, InAs, GaN, GaP, GaAs), or IV–VI (PbS, PbSe, PbTe) materials. These nanocrystals range from 2 to 10 nanometers in

diameter and can contain hundreds to thousands of atoms. QDs approach the size of the exciton Bohr radius and differ from bulk semiconductors in that they are characterized by discrete atomic-like states with bandgap energies that are determined by the QD radius. This is called the quantum-size effect which can be described by the spherical quantum box model:

$$E_g(\text{QD}) \sim E_{g0} + (\hbar^2 \pi^2 / 2m_{eh}R^2) \quad (1)$$

where  $E_g(\text{QD})$  is the QD energy gap,  $\hbar$  is Planck's constant,  $R$  is the radius of the quantum dot and  $m_{eh}$  is the effective electron mass and effective electron hole mass. Quantum confinement leads to increased stress on the exciton, which results in increased energy of the emitted photon. The smaller the quantum dots, the less room for exciton separation, and more energy is required to form the exciton.

Bulk semiconductors are characterized by continuous energy levels with a fixed bandgap energy. Because of quantum confinement in QDs, a blue shift in the bandgap energy is produced and causes a collapse of continuous energy levels of a bulk semiconductor into discrete atomic-like energy levels.<sup>3</sup>

#### **1.4.1 Optical Properties of Quantum Dots**

QDs undergo a process that is fundamentally the same as conventional fluorescence: in semiconductors, the electron in the valence band can be excited by photon absorption and promoted to the conduction band, creating a "hole" in the valence band. The excited electron relaxes back to the valence band, fills the hole, and emits light. Because of the quantum confinement effect, QDs have unique optical properties that offer several advantages over

conventional fluorophores. These advantages include a broad absorption spectrum, a narrow emission spectrum, high photostability, high emission quantum yield, large molar extinction coefficient, longer fluorescence lifetime, a large Stokes shift, and size dependent emission wavelength tunability. The surface of QDs influences their photoluminescent properties. The QD surface has defects called trap states that cause nonradiative electron energy transitions at the surface. This results in a low quantum yield.<sup>4</sup> The trap states are caused by vacancies, dangling bonds, or adsorbates at the surface. To reduce the effects the defects have on the photoluminescence, QDs are coated with a shell that is a higher bandgap semiconductor. This process is known as surface passivation. The shell is usually made of ZnS and greatly enhances the quantum yield, chemical stability and photostability of the QDs.<sup>5-9</sup>

#### **1.4.2 Synthesis of Quantum Dots**

Size tuning of QDs is done by controlling the relative concentrations, rates of addition, duration, temperature, and ligand molecules used in their synthesis. QDs can be made as colloidal solutions or grown on solid substrates.<sup>4</sup> To make colloidal solutions, precursors of the material are reacted in the presence of a stabilizing agent that will restrict the growth of the particle and keep it within the quantum confinement limits. CdX (X= S, Se, Te) quantum dots are the most widely used because of their emission in the UV-VIS-NIR region of the electromagnetic spectrum. CdSe is the most popular choice of quantum dot material because it has absorption energies that are tunable throughout the visible region, its precursors are available, and its crystallization is simple. The most common procedure to synthesize CdSe quantum dots is pyrolysis of organometallic precursors where dimethylcadmium Cd (CH<sub>3</sub>)<sub>2</sub> is

reacted with a selenium reagent in the presence of a phosphine oxide surfactant at high temperature. This procedure was first reported in 1993 by Murray et al. and was later modified by Peng et al. who replaced the extremely toxic cadmium precursor  $\text{Cd}(\text{CH}_3)_2$  with  $\text{CdO}$ ,  $\text{Cd}(\text{Ac})_2$  and  $\text{CdCO}_3$ .<sup>10, 11</sup> Other techniques to synthesize QDs include lipid bilayers, reverse micelles, zeolites, porous glasses, vapor deposition reactions of precursors on solid substrates, and hollow biological macromolecules.<sup>12-17</sup>

Over the years, QDs have been extensively used as fluorescent labels and probes. Some biological applications involving QDs include biosensing<sup>18</sup>, cellular imaging<sup>19</sup>, in situ hybridization<sup>20</sup>, and immunoassays.<sup>21</sup>

Despite being well studied and their high fluorescence quantum yields,  $\text{CdSe/ZnS}$  quantum dots have little future in the biomedical field.  $\text{CdSe/ZnS}$  have many advantages over typical fluorophores, but they are toxic and are environmentally restricted.<sup>22, 23</sup> Quantum dots made from III-V compounds, such as  $\text{InP}$ , are very desirable because they have very low toxicity and are expected to have even greater quantum size effects.<sup>22, 24-27</sup>  $\text{InP/ZnS}$  core/shell quantum dots can be synthesized to emit into the near infrared region. This is ideal for in vivo applications. Although  $\text{InP/ZnS}$  quantum dots show a promising future, the use and information on these quantum dots is very limited. Another limitation is that  $\text{InP/ZnS}$  quantum dots have poor quantum yields. The best quantum yield achieved for  $\text{InP/ZnS}$  to date is 40% compared to >75% for  $\text{CdSe/ZnS}$  quantum dots.<sup>23, 28</sup> Other limitations of  $\text{InP/ZnS}$  quantum dots include poor control of size distribution, poor size tunability, poor stability, and complicated synthesis.<sup>23</sup>

In a typical procedure to synthesize  $\text{InP}$  quantum dots, the reaction would take several days and the mixture must be pumped under a vacuum with temperatures above 250 °C.<sup>29, 30</sup> Other methods such as etching, developed by Weller and coworkers, involved the use of

dangerous HF solutions to etch the InP nanocrystals.<sup>22, 26</sup> In the past couple of years, Peng and coworkers developed a simple one pot synthetic scheme to synthesize InP/ZnS quantum dots. The synthesis was similar to that for CdSe quantum dots. The synthesis used relatively low reaction temperatures below 200 °C and used In(AC)<sub>3</sub> and myristic acid as precursors.<sup>23</sup>

### 1.4.3 Surface Modification of Quantum Dots

High quality quantum dots are typically synthesized and dispersed in organic solvents. Three major limitations of having quantum dots stored in organic solvents are that the QDs are insoluble in water, non-biocompatible and do not contain functional groups for bioconjugation. In order for QDs to be used in aqueous biological systems, the hydrophobic trioctyl phosphine oxide (TOPO) molecules that serve as capping ligands of luminescent quantum dots must be replaced with bifunctional hydrophilic capping ligands or overcoated with an amphiphilic protective layer in order to become water soluble and have functional groups that allow for bioconjugation. The most common and well studied methods to prepare water soluble quantum dots include ligand exchange, silica encapsulation, and coating with amphiphilic polymers and phospholipids. Ligand exchange involves the replacement of hydrophobic ligands with bifunctional ligands in which one end binds to the inorganic QD surface and the other end provides hydrophilicity. Thiol (-SH) groups are often used to bind to the ZnS surface via metal affinity coordination. The TOPO capping ligands are often exchanged with thiol functionalized compounds such as mercaptoacetic acid (MAA)<sup>31</sup>, 11-mercaptoundecanoic acid (MUA)<sup>32</sup>, 16-mercaptohexadecanoic acid (MHDA)<sup>33</sup>, dihydrolipoic acid (DHLLA)<sup>34</sup>, and dithiothreitol (DTT).<sup>35</sup> The bond between thiol and ZnS is not very strong and as a result quantum dots will aggregate over time. This is one limitation of capping quantum dots with thiol containing

ligands.<sup>36</sup> The displacement of TOPO molecules alters the chemical and physical state of the surface atoms of quantum dot and reduces quantum efficiency.<sup>37</sup> High silica encapsulation involves the growth of a silica layer on the surface of quantum dots. Also, functional groups such as  $-SH$  and  $-NH_2$  on the organosilane molecules are on the surface and enable bioconjugation.<sup>38-41</sup> The silica coated quantum dots are extremely stable because the silica layer is highly cross-linked. However, the method is very laborious, difficult to reproduce, and the silica layer may be hydrolyzed.<sup>42</sup> Coating QDs with an amphiphilic polymer and phospholipids is achieved by forming the layer on the QD surface via hydrophobic interactions with the hydrophobic TOPO ligands. The hydrophilic exterior of the polymer enables the quantum dot to be soluble in aqueous solutions.<sup>43</sup> The TOPO ligands are not displaced from the surface; therefore, the quantum dots retain their high quantum yield and are protected from the external environment. However, the final size of quantum dots is larger, which could limit many biological applications such as FRET measurements and endocytosis.<sup>42</sup> There are several methods for developing water-soluble, biocompatible quantum dots. Each method has its advantages and limitations. Synthesizing stable, high quality water-soluble quantum dots remains in high demand in the area of quantum dot based nanobiotechnology.

#### **1.4.4 Quantum Dots in Multiplexed Imuunoassays**

One objective of this project was to encode mesoporous silica with quantum dots to develop a fluoroimmunoassay that can simultaneously identify multiple breast cancer markers. One of the great advantages of quantum dots is their narrow emission and broad absorption spectra. This allows multicolored QDs that have different emission wavelengths to be excited at

a single wavelength. This technique is called multiplexing. Multicolored QDs were incorporated into mesoporous silica microparticles and labeled with antibodies specific for three breast cancer antigens. These antibody labeled silica particles were used to detect different concentrations of breast cancer antigens. Utilization of these particles for multiplexing was also achieved.

An advantage of mesoporous silica is that the pores can be easily functionalized.<sup>44-46</sup> Lin and coworkers have done extensive research on synthesizing and functionalizing the pores using a co-condensation method based on sodium hydroxide catalyzed reaction of tetraethoxysilane (TEOS) with various organoalkoxysilanes in the presence of a low concentration of cetyltrimethylammonium bromide (CTAB) surfactant.<sup>46</sup> For example, fluorescein functionalized Mobil Crystalline of Materials (MCM-41) type mesoporous silica nanoparticles (diameter: 150 nm, pore: 2.4 nm) containing 3-aminopropyl and *N*-folate-3-aminopropyl surface functional groups were used to measure the endocytosis of the particles by human cervical cancer cells.<sup>47</sup> Thiol functionalized MCM-41 type mesoporous silica nanoparticles (diameter: 150 nm, pore: 2.4 nm) with a poly(lactic-acid) coating were used to develop a fluorescence probe for the detection of amino containing neurotransmitters.<sup>46</sup> 2-(propyl)disulfanyl ethylamine functionalized MCM-41 type mesoporous silica nanoparticles (diameter: 200 nm, pore: 2.3 nm) were used to measure the stimuli-responsive controlled release of neurotransmitters and drug molecules.<sup>48</sup>

Several research groups have reported the use of quantum dots in multiplexed immunoassays. Wilson et al. used a layer by layer technique to create magnetic microspheres encoded with photoluminescent quantum dots for the multiplexed detection of three different explosives.<sup>49</sup> Gao et al. described encapsulating luminescent quantum dots in ABC tri-block copolymer to perform *in vivo* targeting and imaging of human prostate cancer cells growing in

mice.<sup>19</sup> Yezhelyev et al. used a hetero-bifunctional crosslinker to covalently attach multicolored QDs to antibodies. These QD-antibody conjugates were used to perform in situ molecular profiling of five different breast cancer biomarkers.<sup>20</sup>

## **1.5 Preparation of Human Serum Albumin Nanoparticles**

Human serum albumin (HSA) is the most abundant blood plasma protein (molecular weight 65 kDa) that has a wide variety functions which will be discussed in more detail in chapter 5. HSA has a blood concentration of 50 mg/mL and contains 585 amino acids. There are 35 cysteine residues which form 17 disulfide bridges and one free thiol. HSA can form dimers and aggregates that can be used to prepare nanoparticles. The preparation of HSA nanoparticles and microparticles was first proposed in 1972 by Scheffel and coworkers.<sup>50</sup> It was based on an emulsion method which was later modified by Gao and coworkers.<sup>51</sup> An aqueous human serum albumin solution is emulsified at room temperature by the addition of cotton seed oil. The emulsion is then homogenized at high speed and added drop wise to a high volume of oil which is pre-heated above 120°C. The water will be rapidly evaporated and albumin nanoparticles will form. The major disadvantage of the emulsion method is the need for high volumes of organic solvents which need to be properly removed for bioapplications.

An alternative desolvation method which eliminates the need for insoluble oils and high temperatures was first suggested in 1978 by Marty and coworkers.<sup>52</sup> This method involves using salts or alcohols to unfold the tertiary structure of albumin which will cause aggregates to form. A crosslinking agent such as glutaraldehyde is then added to link the amino groups, and albumin nanoparticles are formed.

Langer and coworkers have done extensive research to optimize the preparation conditions of HSA nanoparticles using the desolvation method.<sup>53, 54</sup> They found that the rate of ethanol addition greatly influenced particle diameter and polydispersity. The optimal rate of addition was between 1 and 2 ml/min to achieve monodisperse particles with an average diameter around 150 nm. The pH of the HSA solution prior to the addition of ethanol also affected particle size. The particle diameter and yield significantly decreased with  $\text{pH} > 7$ . No reproducible particle formation was achieved at  $\text{pH} < 7$ . The use of buffers in the desolvation process interfered with glutaraldehyde crosslinking, formed large HSA aggregates, or precipitation of the buffer salts. Therefore, NaCl is used for pH adjustment. The optimal salt concentration to form monodisperse nanoparticles is 10 mM NaCl at pH 8.2.

## 1.6 References

1. Lakowicz, J. R., *Principles of Fluorescence Spectroscopy, Third Edition*. Springer: 2006.
2. Skoog, D. A.; Holler, F. J.; Nieman, T. A., *Principles of Instrumental Analysis, Fifth Edition*. Saunders College Publishing: 1997.
3. Klimov, V. I., Nanocrystal Quantum Dots From fundamental photophysics to multicolor lasing. *Los Alamos Science* **2003**, 28, 214-220.
4. Murphy, C. J., Optical Sensing with Quantum Dots. *Analytical Chemistry* **2002**, 520A-526A.
5. Hines, M. A.; Guyot-Sionnest, P., *J. Phys. Chem. B* **1996**, 100, 468-471.
6. Dabbousi, B. O.; Rodriguez-Viejo, J.; Mikulec, F. V.; Heine, J. R.; Mattoussi, H.; Ober, R.; Jensen, K. F.; Bawendi, M. G., *J. Phys. Chem. B* **1997**, 101, 9463-9475.
7. Li, J. J.; Wang, Y. A.; Guo, W.; Keay, J. C.; Mishima, T. D.; Johnson, M. B.; Peng, X., *J. Am. Chem. Soc.* **2003**, 125, 12567-12575.
8. Mekis, I.; Talapin, D. V.; Kornowski, A.; Haase, M.; Weller, H., *J. Phys. Chem. B* **2003**, 107, 7454-7564.
9. Malik, M. A.; O'Brien, P.; Revaprasadu, N., *Chem. Mater.* **2002**, 14, 2004-2010.
10. Murray, C. B.; Norris, D. J.; Bawendi, M. G., *J. Am. Chem. Soc.* **1993**, 115, 8701-8715.
11. Yu, W. W.; Qu, L.; Guo, W.; Peng, X., Experimental Determination of the Extinction Coefficient of CdTe, CdSe, and CdS Nanocrystals. *Chemistry of Materials* **2003**, 15, (14), 2854-2860.
12. Choi, K. M.; Shea, K. J., *J. Phys. Chem. B* **1994**, 98, 3207.
13. Pileni, M. P.; Motte, L.; Petit, C., *Chem. Mater.* **1992**, 4, 338.
14. Urquhart, R. S.; Furlong, D. N.; Gengenbach, T.; J., G. N.; Grieser, F., *Langmuir* **1995**, 11.
15. Wong, K. K. W.; Mann, S., *Adv. Mater* **1996**, 8.
16. Shenton, W.; Douglas, T.; Young, M.; Stubbs, G.; Mann, S., *Adv. Mater.* **1999**, 11.
17. Heath, J. R., *J. Phys. Chem.* **1996**, 100.
18. Medintz, I. L.; Berti, L.; Pons, T.; Grimes, A. F.; English, D. S.; Alessandrini, A.; Facci,

- P.; Mattoussi, H., A reactive peptidic linker for self-assembling hybrid quantum dot-DNA bioconjugates. *Nano Letters* **2007**, *7*, (6), 1741-1748.
19. Gao, X. H.; Yang, L.; Petrosos, J. A.; Marshall, F. F.; Simons, J. W.; Nie, S. M., In vivo molecular and cellular imaging with quantum dots. *Curr. Opin. Biotechnol.* **2005**, *16*, 63-72.
  20. Yezhelyev, M. V.; Al-Hajj, A.; Morris, C.; Marcus, A. I.; Liu, T.; Lewis, M.; Cohen, C.; Zrazhevskiy, P.; Simons, J. W.; Rogatko, A.; Nie, S.; Gao, X.; O'Regan, R. M., In Situ Molecular Profiling of Breast Cancer Biomarkers with Multicolor Quantum Dots. *Advanced Materials* **2007**, *19*, 3146-3151.
  21. Gao, X.; Nie, S., Quantum Dot-Encoded Mesoporous Beads with High Brightness and Uniformity: Rapid Readout Using Flow Cytometry. *Analytical Chemistry* **2004**, *76*, (8), 2406-2410.
  22. Talapin, D.; Gaponik, N.; Borchert, H.; Rogach, A.; Hasse, M.; Weller, H., *J. Phys. Chem. B* **2002**, *106*, 12659-12663.
  23. Xie, R.; Battaglia, D.; Peng, X., *J. Am. Chem. Soc.* **2007**, *129*, 15432-15433.
  24. Lucey, D. W.; MacRae, D. J.; Furis, M.; Sahoo, Y.; Cartwright, A. N.; Prasad, P. N., *Chem. Mater.* **2005**, *17*, 3754-3762.
  25. Bharali, D. J.; Lucey, D. W.; Jayakumar, H.; Pudavar, H. E.; Prasad, P. N., *J. Am. Chem. Soc.* **2005**, *127*, 11264-11371.
  26. Borchert, H.; Haubold, S.; Haase, M.; Weller, H., *Nano Letters* **2002**, *2*.
  27. Yong, K.-T.; Ding, H.; Roy, I.; Law, W.-C.; Bergey, E. J.; Maitra, A.; Prasad, P. N., *ACS Nano* **2009**, *3*, 502-510.
  28. Xie, R.; Peng, X., *J. Am. Chem. Soc.* **2009**, *131*, 10645-10651.
  29. Micic, O. I.; Sprague, J. R.; Curtis, C. J.; Jones, K.; Machol, J. L.; Nozik, A. J., **1995**, *99*, 7754-7759.
  30. Guzelian, A. A.; Katari, J.; Kadavanich, A.; Banin, U.; Hamad, K.; Juban, E.; Alvisatos, A. P., *J. Phys. Chem.* **1996**, *100*, 7212-7219.
  31. Chan, W. C.; Nie, S. M., *Science* **1998**, *281*, 2016-2018.
  32. Qian, J.; Yong, K.-T.; Roy, I.; Ohulchanskyy, T. Y.; Bergey, E. J.; Lee, H. H.; Trampusch, K. M.; He, S.; Maitra, A.; Prasad, P. N., Imaging Pancreatic Cancer Using Surface-Functionalized Quantum Dots. *The Journal of Physical Chemistry B* **2007**, *111*, 6969-6972.

33. Chen, D.; Wang, G.; Li, J., *The Journal of Physical Chemistry C* **2007**, *111*, 2351-2367.
34. Mattoussi, H.; Mauro, J. M.; Goldman, E. R.; Anderson, G. P.; Sundar, V. C.; Mikulec, F. V.; Bawendi, M. G., *J. Am. Chem. Soc.* **2000**, *122*, 12142-12150.
35. Pathak, S.; Choi, S. K.; Arnheim, N.; Thompson, M. E., *J. Am. Chem. Soc.* **2001**, *123*, 4103-4104.
36. Aldana, J.; Wang, Y. A.; Peng, S., *J. Am. Chem. Soc.* **2001**, *123*, 8844-8850.
37. Yu, W. W.; Chang, E.; Drezek, R.; Colvin, V. L., *Biochem. Biophys. Res. Commun.* **2006**, *348*, 781-786.
38. Mulvaney, P.; Liz-Marzan, L. M.; Giersig, M.; Ung, T., *J. Mater. Chem* **2000**, *10*, 1259-1270.
39. Gerion, D.; Pinaud, F.; Williams, S. C.; Parak, W. J.; Zanchet, D.; Weiss, S.; Alivisatos, A. P., *J. Phys. Chem. B* **2001**, *105*, 8861-8871.
40. Nann, T.; Mulvaney, P.; , *Angew. Chem. Int. Ed.* **2004**, *43*, 5393-5396.
41. Rogach, A. L.; Nagesha, D.; Ostrander, J. W.; Giersig, M.; Kotov, N. A., *Chem. Mater.* **2000**, *12*, 2676-2685.
42. Alivisatos, A. P.; Gu, W. W.; Larabell, C., *Annu. Rev. Biomed. Eng.* **2005**, *7*, 55-76.
43. Pellegrino, T.; Manna, L.; Kudera, S.; Liedl, T.; Koktysh, D.; Rogach, A. L.; Keller, S.; Raedler, J.; Natile, G.; Parak, W. J., *Nano. Lett.* **2004**, *4*, 703-707.
44. Huh, S.; Wiench, J. W.; Yoo, J.-C.; Pruski, M.; Lin, V. S. Y., Organic Functionalization and Morphology Control of Mesoporous Silicas via a Co-Condensation Synthesis Method. *Chemistry of Materials* **2003**, *15*, (22), 4247-4256.
45. Slowing, I. I.; Trewyn, B. G.; Lin, V. S. Y., Mesoporous Silica Nanoparticles for Intracellular Delivery of Membrane-Impermeable Proteins. *Journal of the American Chemical Society* **2007**, *129*, (28), 8845-8849.
46. Radu, D. R.; Lai, C.-Y.; Wiench, J. W.; Pruski, M.; Lin, V. S. Y., Gatekeeping Layer Effect: A Poly(lactic acid)-coated Mesoporous Silica Nanosphere-Based Fluorescence Probe for Detection of Amino-Containing Neurotransmitters. *Journal of the American Chemical Society* **2004**, *126*, (6), 1640-1641.
47. Slowing, I.; Trewyn, B. G.; Lin, V. S. Y., Effect of Surface Functionalization of MCM-41-Type Mesoporous Silica Nanoparticles on the Endocytosis by Human Cancer Cells. *Journal of the American Chemical Society* **2006**, *128*, (46), 14792-14793.

48. Lai, C.-Y.; Trewyn, B. G.; Jęftinija, D. M.; Jęftinija, K.; Xu, S.; Jęftinija, S.; Lin, V. S. Y., A Mesoporous Silica Nanosphere-Based Carrier System with Chemically Removable CdS Nanoparticle Caps for Stimuli-Responsive Controlled Release of Neurotransmitters and Drug Molecules. *Journal of the American Chemical Society* **2003**, *125*, (15), 4451-4459.
49. Wilson, R.; Spiller, D. G.; Prior, I. A.; Bhatt, R.; Hutchinson, A., Magnetic microspheres encoded with photoluminescent quantum dots for multiplexed detection. *Journal of Materials Chemistry* **2007**, *17*, 4400-4406.
50. Scheffel, U.; Rhodes, B. A.; Natarajan, T. K.; Wagner, H. N., Jr., Albumin Microspheres for Study of the Reticuloendothelial System. In 1972; Vol. *13*, pp 498-503.
51. Gao, Z.-h.; Crowley, W. R.; Shukla, A. J.; Johnson, J. R.; Reger, J. F., Controlled Release of Contraceptive Steroids from Biodegradable and Injectable Gel Formulations: In Vivo Evaluation. *Pharmaceutical Research* **1995**, *12*, (6), 864-868.
52. Marty JJ, Oppenheim RC, Speiser P., Nanoparticles - a new colloidal drug delivery system. *Pharm Acta. Helv* **1978** *53*(1): 17-23.
53. Langer, K.; Balthasar, S.; Vogel, V.; Dinauer, N.; von Briesen, H.; Schubert, D., Optimization of the preparation process for human serum albumin (HSA) nanoparticles. *International Journal of Pharmaceutics* **2003**, *257*, (1-2), 169-180.
54. Dreis, S.; Rothweiler, F.; Michaelis, M.; Cinatl Jr, J.; Kreuter, J.; Langer, K., Preparation, characterisation and maintenance of drug efficacy of doxorubicin-loaded human serum albumin (HSA) nanoparticles. *International Journal of Pharmaceutics* **2007**, *341*, (1-2), 207-214.

## Chapter 2

### Experimental

This chapter describes the general experimental information. This section includes chemicals, supplies, and instrumentation for characterization. More detailed experimental procedures will be discussed in subsequent chapters.

#### 2.1 Chemicals and supplies

Cadmium oxide (CdO), lauric acid, trioctylphosphine (TOP), trioctylphosphine oxide (TOPO), diethylzinc ( $\text{Zn}(\text{Et})_2$ ), hexadecylamine (HDA), hexamethyldisilathiane ( $(\text{TMS})_2\text{S}$ ), selenium powder, chloroform, methanol, bovine serum albumin (BSA), human serum albumin (HSA) (3-mercaptopropyl)trimethoxysilane (MPTMS), 1-butanol, trizma base, and streptavidin-maleimide were all purchased from Sigma. Glass bottom well plates were purchased from MatTek. Three micron mesoporous silica particles with 32nm  $\text{C}_{18}$  modified pores were purchased from Phenomenex. Superblock T20 PBS buffer and 20x PBS with Tween 20 was purchased from Pierce. HER2/neu protein was purchased from Invitrogen. Human HER2/neu affinity purified biotinylated polyclonal antibody was purchased from R&D Systems. Estrogen Receptor  $\alpha$  (ER  $\alpha$ ) and Progesterone receptor (PR) protein were purchased from Abcam. BODIPY-vinblastine was purchased from Invitrogen. Ten nanometer diameter PEG coated iron oxide particles were purchased from Ocean Nanotech. All aqueous solutions were prepared with

18 MO deionized water produced by a water purification system (Barnstead Thermolyne Nanopure). All chemicals were used as received without further purification.

## **2.2 Characterization**

### **2.2.1 Fluorescence emission spectra**

Fluorescence emission measurements were performed using a SpectraMax M2 microplate reader (Molecular Devices, Inc.) equipped with a Xenon flash lamp source and a photomultiplier (R-3896) detector. Microplate readers are multi-detection systems with a double monochromator and dual-mode cuvette ports. The system is equipped with a spectrophotometer for absorbance measurements and a spectrofluorometer for fluorescence measurements.

The microplate reader has an excitation monochromator and an emission monochromator for separating different wavelengths. In this device, the output of a xenon flash lamp light source is directed to a concave holographic grating for tuning the different excitation wavelengths. Holographic gratings are a type of diffraction grating that exhibit less scattered light than other grating types.<sup>1</sup> They are composed of a polished substrate coated with a photoresist to reduce astigmatism at multiple angles. The excitation light travels through 1 mm fiber optic bundles to cuvette ports and microplates. In the cuvette mode, the incident light is reflected by an elliptical mirror and directed to the cuvette. When in fluorescence mode, the fluorescence emission of fluorescent probes is focused on an elliptical mirror and directed to a concave holographic grating. The light then reaches the photomultiplier tube. For microplate mode, the light passes through the second fiber optic to a focusing elliptical mirror. The light beam penetrates the top

of the microplates and passes through the sample. The fluorescence light is collected and directed to the second wavelength isolation module and then to the photomultiplier tube.

### **2.2.2 Photomultiplier tubes**

Photomultiplier tubes (PMTs) are very sensitive to UV/Vis radiation. Advantages of using PMTs as detectors include their fast response times and their ability to amplify low intensity light signals. Disadvantages include dark current interferences and damage if the PMT is exposed to high power radiation.<sup>2</sup> The dark current interferences can be minimized by cooling the system. The photocathode generates electrons upon being struck by light. The dynodes are held at a more positive potential than the cathode which causes the electrons to be accelerated toward the dynodes. Each dynode is at a more positive potential than the previous dynode. Each photoelectron produces several additional electrons upon striking the dynode. This causes the current from each incident photon to be multiplied by  $10^6$ . The photocathode is covered by a quartz envelope.

### **2.2.3 Digital fluorescence imaging microscopy**

Fluorescence images were taken using a digital fluorescence imaging microscopy system that contained an Olympus IX71 inverted fluorescence microscope equipped with a 100 W mercury lamp as a light source and a high performance color charge coupled device camera (CCD) (Olympus DP 70). The fluorescence images were obtained through a 20x microscope objective using a filter cube containing a  $425 \pm 20$  nm band-pass excitation filter, a 465 nm

dichroic mirror, and a 475nm long pass emission filter. The exposure time was 20 ms and numerical aperture was 0.5. Numerical aperture is the range of angles over which the system can emit light. The software Image-pro Plus and DP Controller were used for image analysis. The microscope contains a trinocular observation head that is coupled to a CCD camera system, and has two illumination sources, one for transmitted light and the other for episcopic observations.<sup>4</sup> Fluorescence microscopy demonstrates the properties of fluorescence emission of molecules upon specific excitation and gives information about their spatial distribution with direct application in biological experiments. The output of the lamp passes through collecting optics to a filter cube that contains a set of excitation and emission filters and a dichroic mirror. The fluorescence produced after excitation of the sample is collected by the objective and directed through different paths to the CCD and eyepiece.

Microscope objectives are designed to focus excitation light on a sample and to collect emission light from the sample. When excitation and emission light travel through the same objective it is called epifluorescence microscopy. Epifluorescence separates excitation and emission light. The spatial resolution,  $R$ , of a microscope is defined as the minimum separation distance between two distinguishable points in a field:

$$R = 1.22\lambda/2(\text{NA}) \quad (1)$$

$$\text{NA} = n \sin \alpha \quad (2)$$

where NA is the numerical aperture of the objective,  $n$  is the refractive index of the medium surrounding the lens,  $\alpha$  is the angular aperture which is the angle between the microscope optical axis and the oblique light rays captured by the objective, and  $\lambda$  is the wavelength.<sup>4</sup> How bright the image will be depends on the light gathering power of the objective. The light gathering

power,  $F$ , of the objective is directly proportional to the square of the numerical aperture (NA) and magnification ( $M$ ):

$$F = 10^4 \cdot (NA/M)^2 \quad (3)$$

Excitation and emission filters are placed in front and underneath the dichroic mirror. The excitation filters are located in front of the dichroic mirror and select the desired excitation wavelength. Reflection losses take place at the boundary of the excitation filter due to changes in the refractive index. Emission filters placed underneath the dichroic mirror select the desired emission wavelength and eliminate residual excitation light. A dichroic mirror is a color filter which separates the excitation and emission paths. The surface of the mirror is coated with a thin layer of metal. The thickness and type of coating control the percent of reflectivity and transmission of incident light. The values below the transition wavelength are reflected into the objective, while the ones above the value are transmitted. The excitation light reflected by dichroic mirrors is directed through the objective to excite the fluorescent probes.

#### **2.2.4 Charge-coupled device**

A CCD camera has a great sensitivity to low light levels and contains a thin silicon wafer divided into an array of several light-sensitive regions that capture and store image information in the form of localized electrical charge that depends on the incident light intensity. The electronic signal that corresponds with each pixel of the detector has an output as an intensity value for the corresponding image location. After the values are digitized, the image can be reconstructed and displayed on a computer monitor very rapidly.<sup>6</sup>

The pixel is made from p-type silicon and the electrons formed by the absorbed radiation collect in the well below the electrode. The holes move away from the n-type layer toward the substrate.<sup>2</sup> The accumulated charge is measured by a three phase clock circuit that shifts the charge. The charges are transferred to a preamplifier and finally read out.

## 2.3 References

1. Strobel, H. A.; Heineman, W. R., *Chemical Instrumentation: A Systematic approach: Monochromators and Polychromators*. John Wiley & Sons: 1989.
2. Skoog, D. A.; Holler, F. J.; Nieman, T. A., *Principles of Instrumental Analysis, Fifth Edition*. Saunders College Publishing: 1997.
3. Photomultiplier Tubes  
<http://micro.magnet.fsu.edu/primer/digitalimaging/concepts/photomultipliers.html>  
Date accessed: June 2009
4. Anatomy of a Fluorescence Microscope  
[www.olympusmicro.com](http://www.olympusmicro.com)  
Date accessed: March 2009
5. Strobel, H. A.; Heineman, W. R., *Chemical Instrumentation*. John Wiley and Sons: 1989.
6. CCD Sense Element (Pixel) Structure  
[www.microscopyu.com](http://www.microscopyu.com)  
Date accessed: March 2009

## Chapter 3

### Dual Emission quantum dot-labeled silica particles for Bioanalytical Assays

#### 3.1 Abstract

Chapter 3 discusses the preparation and characterization of mesoporous silica particles encoded with highly fluorescent CdSe/ZnS quantum dots for the detection of breast cancer markers. A rapid and simple method for encoding mesoporous silica particles with quantum dots (SiQDs) for the simultaneous detection of multiple analytes in complex mixtures is described. The assay was based on the use of quantum dot-containing mesoporous silica particles as signal transducers. To prepare the composite particles CdSe/ZnS quantum dots were incorporated into mesoporous silica particles of 3  $\mu\text{m}$  diameter and 35 nm pore size. The incorporation of the quantum dots into the mesoporous silica spheres was completed in 30 minutes. By using this simple and efficient incorporation method, it was possible to stably encapsulate quantum dots of different diameter (and emission color) in the silica particles. It was also possible to incorporate mixtures of quantum dots of different emission color and precisely control the ratio between quantum dots of different emission colors in the silica particles. This could facilitate the use of the quantum dot-silica composites in luminescence assays of multiple analytes in which composite silica particles of different emission colors are used to identify and quantify specific analytes in a complex mixture. To demonstrate the capabilities of the quantum dot-silica

composite particles, the composite particles were applied for the analysis of multiple breast cancer markers.

### **3.2 Introduction**

Fluorescent microparticles have been widely used in bioanalytical assays as fluorescent tags primarily due to their high fluorescence intensity and ability to label biomolecules with a relatively simple coupling chemistry<sup>1-8</sup>. Silica and polystyrene fluorescent particles are typical examples of fluorescent particle technology. They are commonly prepared by incorporating organic dye molecules into the particles during or following their synthesis. Nie and coworkers reported the synthesis and application of semiconductor quantum dots (QD) into polystyrene particles<sup>9,10</sup>. Multiple DNA targets were detected by labeling multicolored QD encoded polystyrene with probe DNA strands. QD are particularly attractive because of their unique optical properties that offer several advantages over conventional fluorophores. These include broad absorption spectra, narrow emission peaks, high photostability, high emission quantum yields, large molar extinction coefficients, relatively long fluorescence lifetimes, large Stokes shifts, and size dependent emission wavelength tunability<sup>11-17</sup>. These advantages make quantum dots well suited for multiplex analysis. High quality quantum dots are typically synthesized and dispersed in organic solvents. Three major limitations of having quantum dots stored in organic solvents are that the QDs are insoluble in water, are not biocompatible and do not contain functional groups for bioconjugation. In order for QDs to be used in aqueous biological systems, the hydrophobic TOPO molecules that serve as capping ligands of luminescent quantum dots must be replaced with bifunctional hydrophilic capping ligands or overcoated with an

amphiphilic protective layer in order to become water soluble and have functional groups that allow for bioconjugation. Polystyrene and silica encapsulation are two of the most common and well studied methods to prepare water soluble quantum dots. The polystyrene microparticles were prepared using microemulsion and the luminescent QD were loaded after swelling the polystyrene with an organic solvent. Nie and coworkers demonstrated that it is possible to control the ratio between QD of different emission color in the polystyrene particles with high precision<sup>9,10</sup>. In our laboratory we have carried out similar experiments and encountered difficulties in loading large amounts of QD into polystyrene particles, which often resulted in their structural deformation. We therefore directed our attention to the more rigid silica particles and focused on mesoporous silica particles since we already demonstrated the incorporation of ruthenium complexes into silica particles using a one-step Stöber synthesis method<sup>18-20</sup>. Unlike the microemulsion method, the Stöber technique does not involve the use of potentially toxic organic solvents and surfactants<sup>21-23</sup>. Conjugation of biomolecules to the particles is easier because there is no need to repetitively and thoroughly wash surfactant molecules from the particles.

In addition, it has already been shown by Lin and coworkers that QD could be successfully incorporated into mesoporous silica particles without altering their structural morphology<sup>24</sup>. Lin and coworkers have also done extensive research on synthesizing and functionalizing the mesopores using a co-condensation method based on sodium hydroxide catalyzed reaction of tetraethoxysilane (TEOS) with various organoalkoxysilanes in the presence of a low concentration of cetyltrimethylammonium bromide (CTAB) surfactant<sup>25</sup>. For example, fluorescein functionalized Mobil Crystalline Materials (MCM-41) type mesoporous silica nanoparticles (diameter: 150 nm, pore: 2.4 nm) containing 3-aminopropyl and *N*-folate 3-

aminopropyl surface functional groups were used to measure the endocytosis of the particles by human cervical cancer cells<sup>26</sup>. Thiol functionalized MCM-41 type mesoporous silica nanoparticles (diameter: 150 nm, pore: 2.4 nm) with a poly(lactic-acid) coating were used to develop a fluorescence probe for the detection of amino containing neurotransmitters<sup>25</sup>. 2-(propyldisulfanyl)ethylamine functionalized MCM-41 type mesoporous silica nanoparticles (diameter: 200 nm, pore: 2.3 nm) were used to measure the stimuli-responsive controlled release of neurotransmitters and drug molecules<sup>27</sup>.

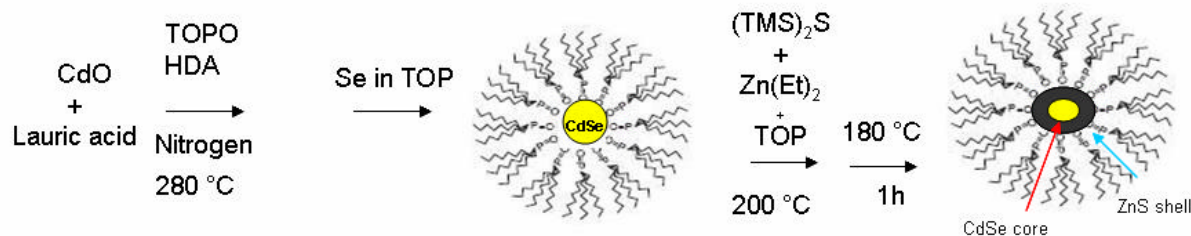
In this paper, we describe the preparation and characterization of QD-incorporating mesoporous silica particles and demonstrate their application for the analysis of breast cancer markers in solution.

### **3.3 Experimental**

#### **3.3.1 Synthesis of TOPO coated quantum dots**

TOPO coated CdSe/ZnS quantum dots were prepared by a method developed by Peng with slight modifications<sup>15, 16</sup>. Briefly, 12.7 mg cadmium oxide (CdO) and 160 mg lauric acid were mixed in a 3-neck flask under nitrogen and heated to >200 °C until the CdO was dissolved in the lauric acid. A clear, colorless solution was formed. Then, 1.9 g of trioctylphosphine oxide (TOPO) and 1.9 g hexadecylamine (HDA) were added to the solution under stirring and the temperature was increased to 280°C for 10 min. Next, 80 mg selenium powder was dissolved in 2mL of trioctylphosphine (TOP) and was rapidly injected into the solution under vigorous stirring. The mixture was cooled to ~200 °C and kept at this temperature for 3 minutes. When

the quantum dots reached the desired color, a ZnS shell was added as follows: a 2 mL of TOP solution containing 250  $\mu\text{L}$  hexamethyldisilathiane ( $(\text{TMS})_2\text{S}$ ) were mixed with 1 mL diethylzinc ( $\text{Zn}(\text{Et})_2$ ) was premixed well under nitrogen and then slowly injected into the solution. The reaction mixture was kept at 180  $^\circ\text{C}$  for one hour. The solution was then cooled to room temperature and the resulting TOPO coated CdSe/ZnS quantum dots were washed three times with methanol and re-dispersed in chloroform. Scheme 3.1 shows the synthesis of CdSe/ZnS quantum dots.



Scheme 3.1. Schematic representation of the synthesis of CdSe/ZnS core/shell quantum dots

### 3.3.2 Preparation of mesoporous and thiol-modified fluorescent silica microparticles

Mesoporous fluorescent silica microparticles were prepared by dispersing 2mg of mesoporous silica particles, averaging 3  $\mu\text{m}$  in diameter with 32 nm  $\text{C}_{18}$  modified pores in 1 mL butanol. Two hundred microliters of 1  $\mu\text{M}$  green emitting TOPO capped CdSe/ZnS QD ( $\lambda_{\text{em}} = 545 \text{ nm}$ ) or red emitting CdSe/ZnS QD ( $\lambda_{\text{em}} = 655 \text{ nm}$ ) or a mixture of green and red emitting QD were added to the solution. The mixture was incubated for 30 minutes and then washed three times with ethanol. Thiol-modified fluorescent mesoporous silica microparticles were prepared according to a previously described method<sup>18, 19</sup>. Briefly, 2mg of fluorescent QD

loaded silica particles were dispersed in 10 ml of butanol. Five hundred microliters of 3-mercaptopropyltrimethoxysilane (MPTMS) were added to the solution. The mixture was incubated for 30 minutes and washed three times with ethanol. The particles were then re-dispersed in 4mL of phosphate buffer (PB) containing 0.1% BSA at pH 7.4.

### **3.3.3 Preparation of streptavidin-modified fluorescent mesoporous silica beads –**

Streptavidin-modified fluorescent mesoporous silica beads were prepared according to a previously described method<sup>19</sup>. Briefly, 1 mL of thiol-modified fluorescent mesoporous silica stock solution was added to 2mg streptavidin-maleimide in 5mL PB containing 0.1% BSA at pH 7.4. The mixture was incubated under gentle stirring for three hours at room temperature. The streptavidin-labeled beads were separated by centrifugation (5500 rpm, 10min) and washed three times with PB. The streptavidin-labeled fluorescent mesoporous silica beads were re-dispersed in 4 mL PB and used immediately for biotin-avidin assays.

### **3.3.4 Preparation of anti HER2/neu labeled fluorescent mesoporous silica beads –**

Anti-HER2/neu labeled fluorescent mesoporous silica particles were prepared by mixing 1mL streptavidin modified silica particles with 50 µg of biotinylated anti-HER2/neu in 1 mL PBS. The anti-HER2/neu labeled particles were incubated at room temperature for two hours. The anti-HER2/neu labeled particles were separated by centrifugation (5500 rpm, 10min) and washed three times with PBS at pH 7.4. The particles were then re-dispersed in 4 mL PBS at pH 7.4 and immediately used for binding assays.

### **3.3.5 Preparation of HER2/neu coated 96-well plate –**

A glass bottom 96-well plate was coated with HER2/neu protein through nonspecific adsorption by adding 100  $\mu\text{L}$  HER 2 protein at concentrations of 10  $\mu\text{g}/\text{mL}$ , 5  $\mu\text{g}/\text{mL}$ , 2  $\mu\text{g}/\text{mL}$ , 0.1  $\mu\text{g}/\text{mL}$ , 85  $\text{ng}/\text{mL}$  and 65  $\text{ng}/\text{mL}$ . Each concentration of protein was added to three wells. The plate was incubated for 20 hrs at 4°C. Unoccupied sites were blocked by adding 300  $\mu\text{L}$  of Superblock T20 PBS buffer. One hundred microliters of anti HER2/neu labeled silica particles were added and incubated for 2 hours. The plate was washed with PBS containing 0.05% Tween-20 and dried under a stream of nitrogen.

### **3.3.6 Characterization of particles by TEM and SEM –**

SEM images were taken on a Hitachi S-4800 Field Emission SEM at 3kV without coating. SEM images were taken at a magnification of 20, 000 x. TEM images were taken on a JEOL 2011 TEM at 200kV. TEM images were taken at a magnification of 6, 000 x.

## **3.4 Results and Discussion**

### **3.4.1 Fluorescence properties of fluorescent mesoporous silica beads –**

Three micron fluorescent mesoporous silica microparticles were prepared as described in the experimental section. Figure 3.1 shows fluorescence microscopy images and corresponding spectra of mesoporous silica particles that contain only green emitting QD (a), only red emitting QD (b) and mixtures of QD with 1:5 (c), 1:1 (d), and 3:1 (e) ratios. It can be clearly seen that the emission properties of the silica microspheres could be controlled and that the green and red emission peaks are baseline separated. The particles in figure 3.1 c have a 1:5 loading of green to red QD. The particles appear reddish yellow. The yellowish color is a result of the combination of both green and red emitting QD. The particles in c appear to be more red than green because there are five times more red QD than green (see spectrum). The particles in figure 3.1 d have a 1:1 loading of green to red QD in the silica. There is a more homogenous yellow color than in c because of the even loading of green and red QD. The particles in figure 3.1 e appear green because there are three times more green QD than red. The emission properties of the fluorescent mesoporous silica beads were similar to the emission properties of green and red emitting QDs (data not shown).

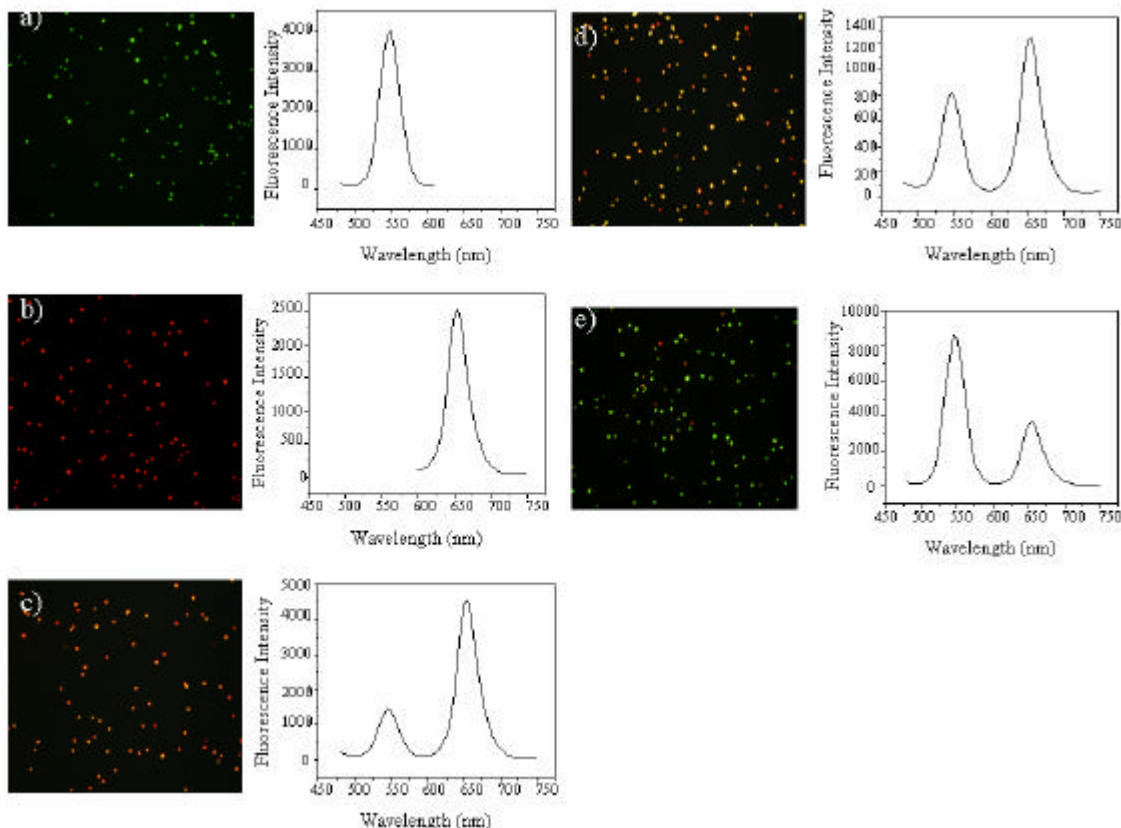


**Figure 3.1** - Digital fluorescence microscope images and fluorescence spectra ( $\lambda_{\text{ex}} = 400 \text{ nm}$ ) of (a)  $3 \mu\text{m}$  mesoporous silica particles that contain 545 nm green emitting CdSe/ZnS QD, (b) 655 nm red emitting CdSe/ZnS QD, (c) and green and red emitting QD mixtures with 1:2, (d) 1:1, and (e) 3:1 ratios. A typical exposure time was 150 msec.

### 3.4.2 Characterization of fluorescent mesoporous silica beads

Figure 3.2 shows microtome TEM and SEM images along with EDS spectra of mesoporous silica particles with and without QD. The microtome TEM samples were cut to have a 70 nm thickness. The incorporation of QD did not affect the morphology of the silica particles. EDS shows both Cd and S peaks indicating the presence of QD in the pores; whereas, there are no Cd or S peaks for mesoporous silica without QD.

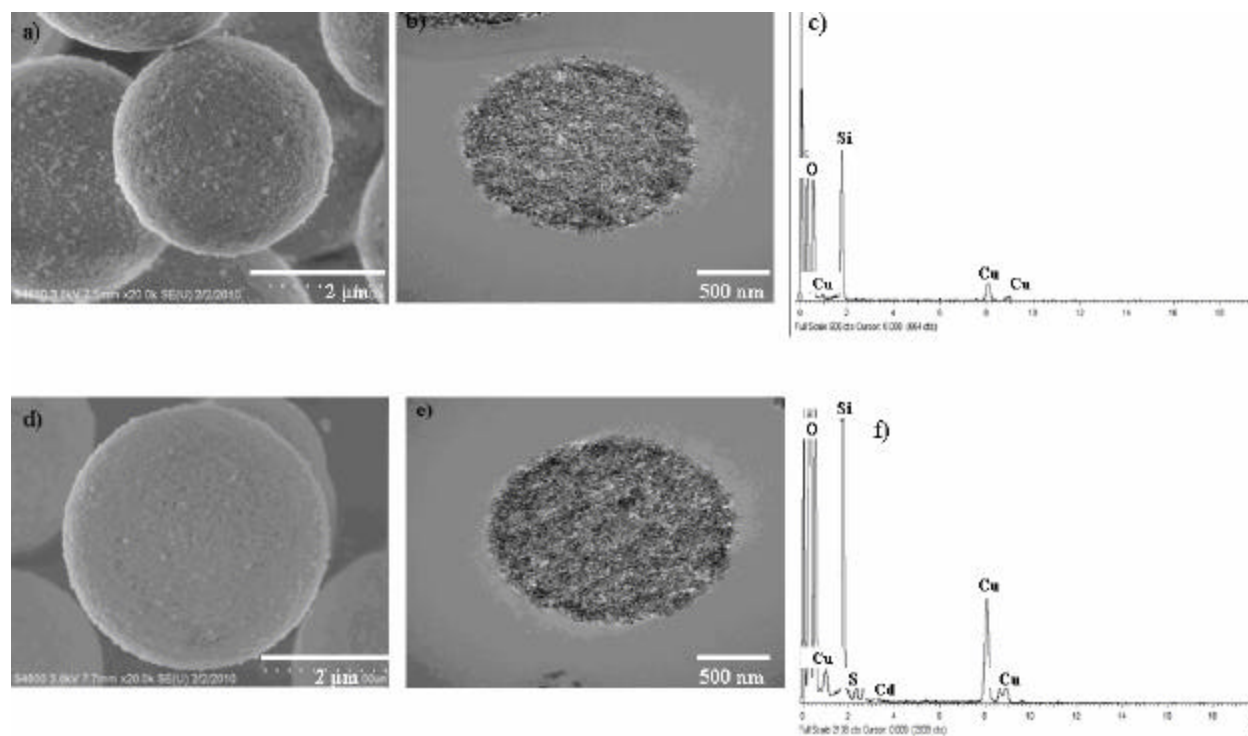


**Figure 3.2** – Characterization of mesoporous silica (a) SEM image of mesoporous silica particles without quantum dots, (b) microtomeTEM image of mesoporous silica particles without quantum dots, (c) EDS spectrum of mesoporous silica particles without quantum dots, (d) SEM image of mesoporous silica particles with quantum dots, (e) microtomeTEM image of mesoporous silica particles with quantum dots, and (f) EDS spectrum of mesoporous silica particles with quantum dots

### 3.4.3 Luminescence properties of fluorescent mesoporous silica beads

Figure 3.3 compares the photostability of mesoporous silica loaded with 1:1 545 nm and 655 nm emitting CdSe/ZnS QD, 545 nm and 655 nm emitting QD, and mesoporous silica loaded with fluorescein DHPE (1,2-dihexadecanoyl-sn-glycero-3-phosphoethanolamine), and rhodamine DHPE. All solutions were illuminated continuously for 2 hours using a 100W mercury lamp. It can be clearly seen that the QD-containing silica microparticles exhibit higher photostability than free QD and significantly higher photostability than fluorescein and rhodamine DHPE. The fluorescence intensity of 545 nm or 655 nm QD-containing silica

microparticles decreased by 45% and 30% respectively over 2 hours of illumination compared to their original intensity. The fluorescence intensity of green and red-emitting QD solutions decreased by 60% and 55% compared to their original intensities. The fluorescence intensity of solutions of rhodamine and fluorescein-containing mesoporous silica particles decreased by 80% and 85% compared to their original intensity under the same illumination conditions.

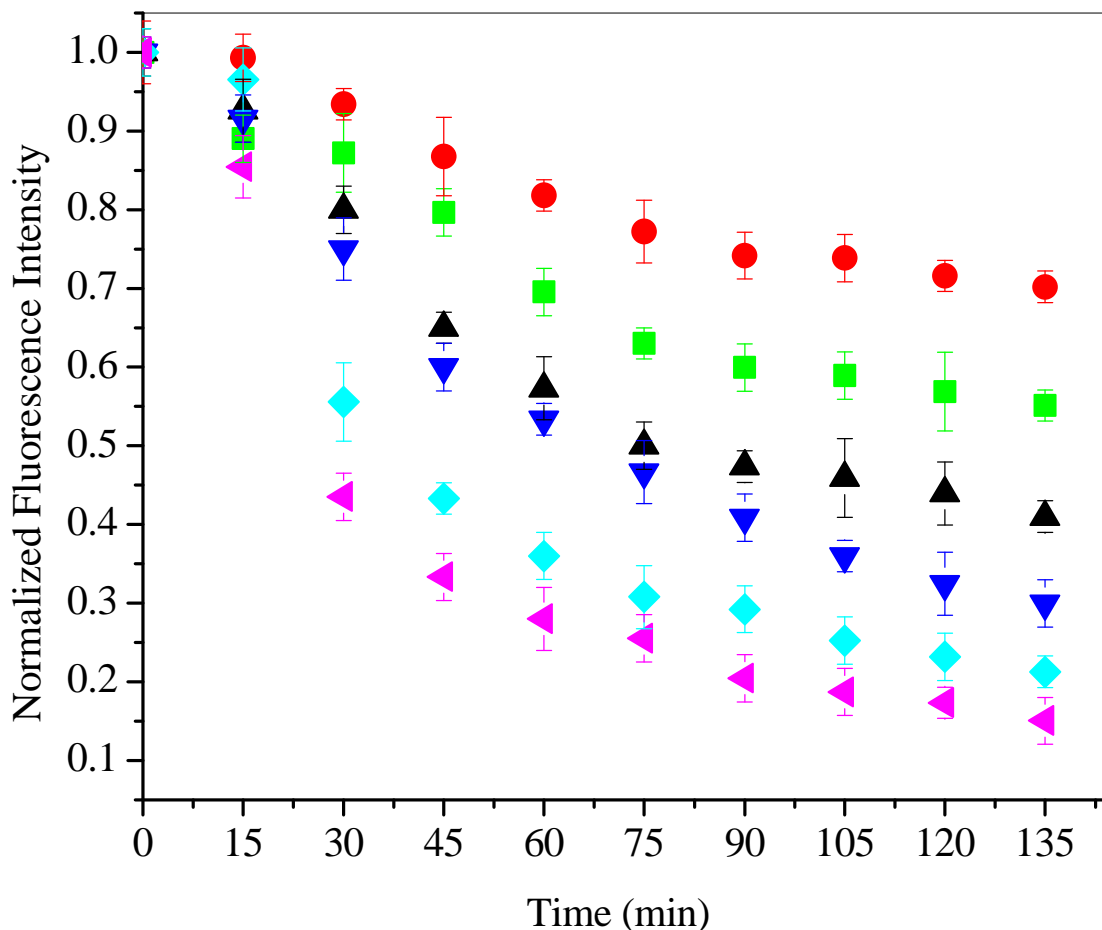


**Figure 3.3** - Photostability measurements of ● mesoporous silica particles with 655 nm quantum dots, ■ mesoporous silica particles with 545 nm quantum dots, ▲ free 545 nm quantum dots ▼ free 655 nm quantum dots, ◆ mesoporous silica with rhodamine DHPE, and ▼ mesoporous silica with fluorescein DHPE.

It is interesting to note that the emission intensity of QD and QD-containing mesoporous silica microparticles did decrease during illumination although to a significantly lesser extent than the fluorescence decrease for molecular organic fluorophores. While the fluorescence of organic fluorophores decreased due to photobleaching, the decrease in the emission of the QD is attributed to surface photo-oxidation or photo-corrosion<sup>28</sup>. It appears that encapsulation of QD in mesoporous silica microparticles decreases their rate of photo-oxidation, which is a significant advantage over the use of free QD or organic fluorophores.

#### **3.4.4 Leakage of quantum dots from mesoporous silica**

Leakage of QD from the mesoporous silica microparticles is a significant concern since the QD were loaded into the mesoporous silica microparticles and could conceivably leak out of the particles to the solution. Leakage of QD, fluorescein DHPE, and rhodamine DHPE from the silica particles was monitored for 10 days by adding the loaded mesoporous silica microparticles to butanol and measuring the fluorescence intensity of supernatant samples daily. Figure 3.4 shows that supernatants of solutions of green and red emitting QD-containing mesoporous silica microparticles did not show a measurable fluorescence signal during 10 days of observation.

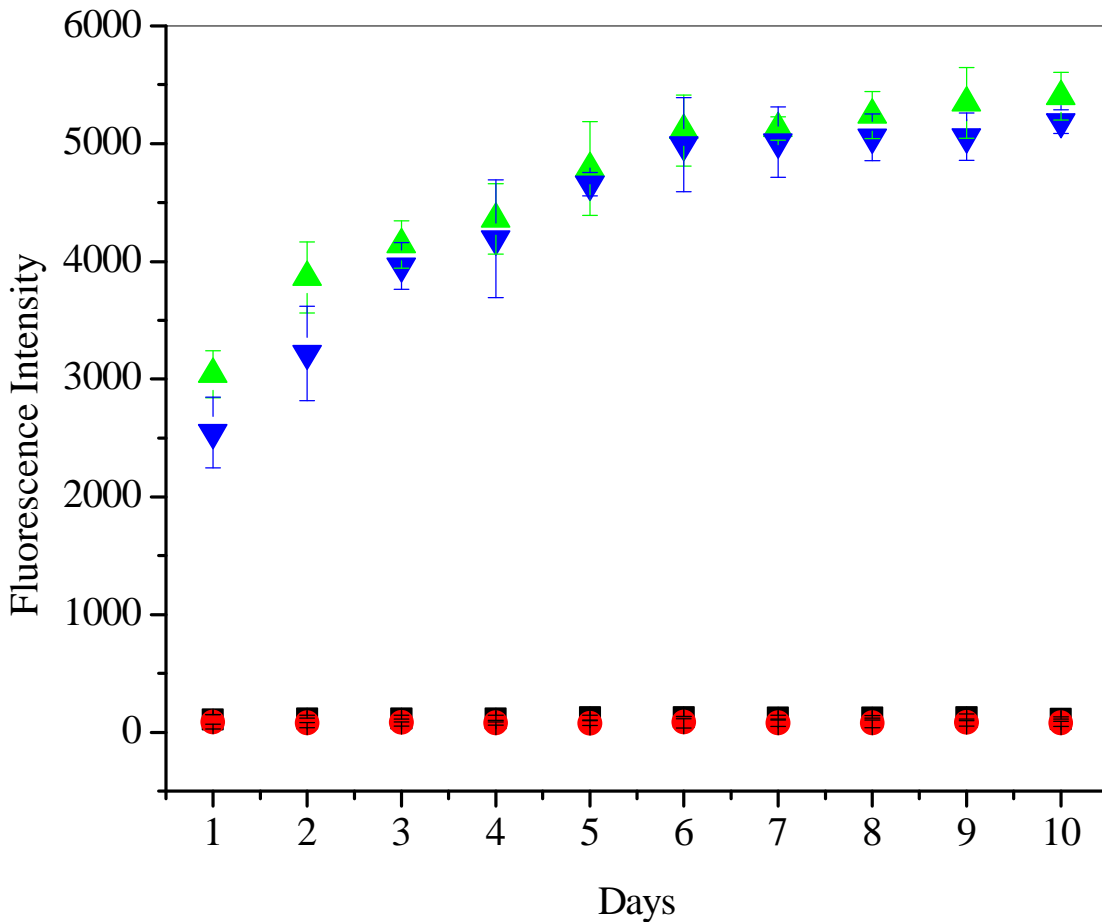
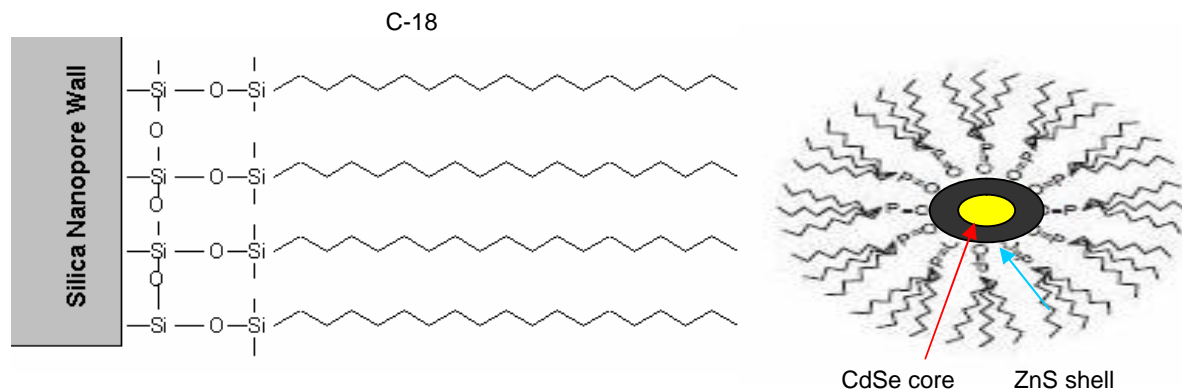


**Figure 3.4** - Fluorescence intensity measurements of supernatant samples collected daily from solutions of mesoporous silica microparticles loaded with fluorescein-DHPE ▲, rhodamine-DHPE ▼, green emitting ( $\lambda_{exc}$  = 400 nm,  $\lambda_{em}$  = 545 nm) QD ■ and red-emitting ( $\lambda_{exc}$  = 400 nm,  $\lambda_{em}$  = 655 nm) QD ●

This minimal leakage of QD from the mesoporous silica microparticles is attributed to strong hydrophobic interactions between the hydrocarbon molecules of the pore walls and the TOPO molecules on the quantum dot surface. In contrast, the fluorescence intensity of the supernatant collected from solutions of fluorescein DHPE and rhodamine DHPE-containing mesoporous silica microparticles had an increase in intensity during the first day of observation. The fast leakage during the first day may be attributed to the release of fluorescein-DHPE and rhodamine-

DHPE that were loosely attached to the particle surface. This was followed by a slower leakage component of fluorescein-DHPE and rhodamine-DHPE molecules that were incorporated into the pores but leaked out over time to the solution due to their amphiphilic nature.



Scheme 3.2. Schematic representation of the interaction between the C-18 hydrocarbon chain of the pore wall and the TOPO molecules on the quantum dot surface.

### 3.4.5 Effect of temperature on the fluorescence intensity of the silica-quantum dot composites

Figure 3.5 shows the effects of temperature on the fluorescence intensity of the particles. The particles have the highest fluorescence intensity at room temperature and decreases as the temperature is increased. The greatest decrease in fluorescence intensity was at 100 °C. This is expected because of the deactivation process caused by the increased frequency of collisions at higher temperatures.

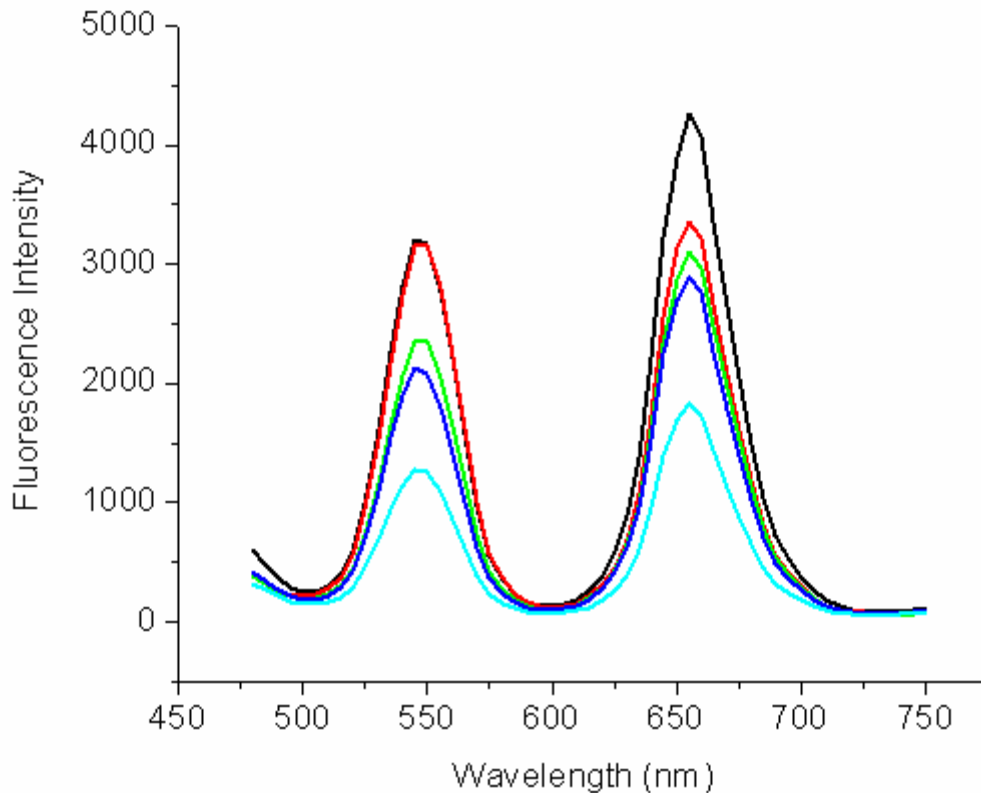


**Figure 3.5** - Effect of temperature on the stability of the silica-quantum dot composites. — 25 °C, — 50 °C, — 75 °C, — 85 °C, and — 100 °C.

### 3.4.6 Stability of quantum dots in mesoporous silica microparticles

In order to protect the quantum dots in the silica pores, MPTMS was added which polymerizes upon addition of water. Fluorescence measurements were taken of SiQDs with MPTMS and without MPTMS for ten days to monitor the effects of photo oxidation on the fluorescent microparticles. Particles with MPTMS were more stable than those without. The particles were loaded with a 1:1 ratio of 545 nm and 655 nm quantum dots. The composite particles were separated into four categories: a) particles deoxygenated argon that were stored in the dark, b) particles deoxygenated by argon that were stored in room light, c) particles with no argon stored in the dark, and d) particles with no argon stored in room light. Figure 3.6

demonstrates a negligible change in the fluorescence intensities of mesoporous silica particles containing argon that were stored in the dark. For particles stored in the dark without argon, there was a 4% decrease in fluorescence intensity for SiQDs with MPTMS and a 38% decrease for particles without MPTMS. There was a 13% decrease in fluorescence intensity for SiQDs with MPTMS stored under argon in room light and a 50% decrease in fluorescence intensity for particles without MPTMS stored with argon stored in room light. The fluorescence intensity of particles with no argon stored in room light with MPTMS had a decrease of 28% and 81% for particles without MPTMS.

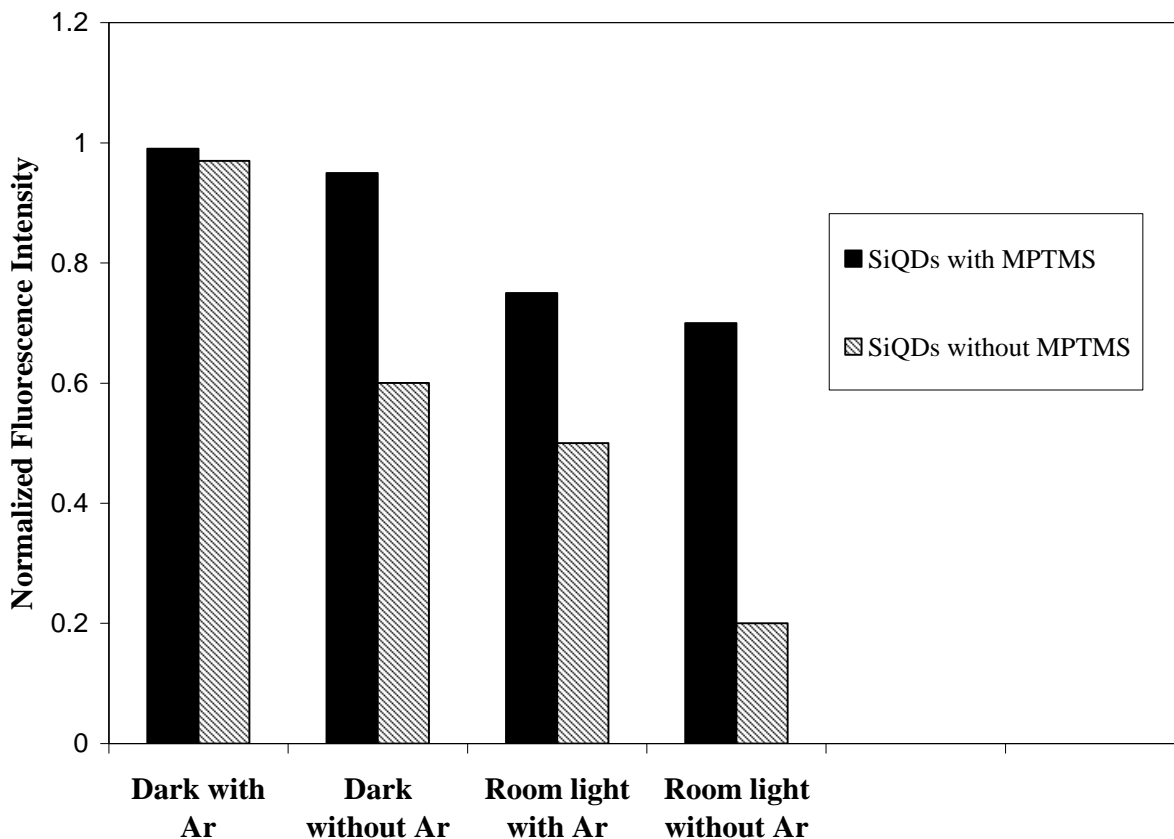


**Figure 3.6** - Stability of quantum dots in mesoporous silica with and without MPTMS. a) particles deoxygenated by argon that were stored in the dark, b) particles deoxygenated by argon that were stored in room light, c) particles with no argon stored in the dark, and d) particles with no argon stored in room light.

### **3.4.7 Direct assay for the detection of the breast cancer marker HER2/neu –**

The surface of the 3 $\mu$ m mesoporous silica particles were functionalized with thiol groups because thiol is a reactive functional group that allows the covalent coupling of maleimide modified biomolecules through the formation of thio-ether bonds. Maleimide-streptavidin was attached to the surface of the fluorescent mesoporous silica particles in order to couple the biotin labeled anti-HER2/neu through streptavidin-biotin interactions. A direct detection assay was developed by nonspecifically adsorbing the HER2/neu protein to the surface of the glass well plate, adding the anti-HER2 labeled fluorescent silica particles to the plate, washing, and measuring the fluorescence intensities of the individual wells. The glass 96-well plate was incubated with HER2/neu solutions ranging from 0 to 10  $\mu$ g/mL in PBS buffer at pH 7.4 for 20 hours at 4°C. Unoccupied sites were blocked by adding 300  $\mu$ L of Superblock T20 PBS buffer. 100  $\mu$ L of anti HER2/neu labeled silica particles were added and incubated for 2 hours. The plate was washed with PBS containing 0.05% Tween-20 and dried under a stream of nitrogen before taking measurements. Figures 3.7 and 3.8 demonstrate the dependence of the binding of the fluorescent anti-HER2/neu labeled particles (containing 1:1 of 545 nm and 655 nm QD) on the concentration of HER2/neu. At concentrations of 0 and 65 ng/mL, there was no measureable fluorescence signal. The fluorescence intensity continued to increase when the concentration of HER2/neu increased from 85 ng/mL to 10  $\mu$ g/mL. There were also no fluorescence signals for unlabeled particles with 10  $\mu$ g/mL HER2/neu nor with anti-HER2/neu labeled particles added to 50  $\mu$ g/mL and 10  $\mu$ g/mL of ERa and PR, respectively. No fluorescence signal for unlabeled particles with HER2/neu indicates that there is no nonspecific binding which eliminates any false positives. No fluorescence signal for anti-HER2/neu labeled particles in the presence of ERa

and PR indicate that there is no cross reactivity between the anti-HER2/neu labeled particles and ERa and PR. The cutoff level for HER2/neu in serum is 10 ng/mL. The limit of detection of the direct assay was 85 ng/mL HER2/neu. The limit of detection values were determined by measuring the fluorescence intensity as a function of HER2/neu concentration. This assay was very reproducible yielding similar results for three separate experiments. A more detailed explanation of the significance of the limit of detection values and comparison to other methods will be given in Chapter 4.

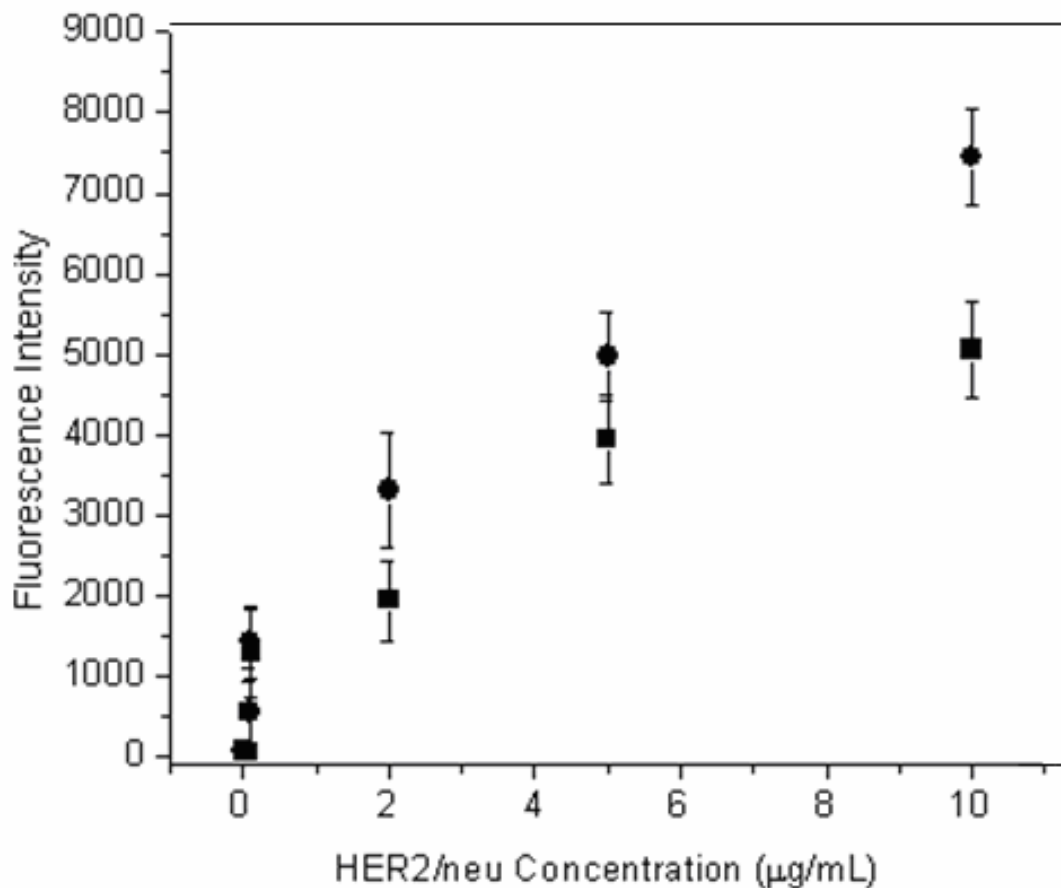


**Figure 3.7** - Dependence of the binding of the fluorescent anti-HER2/neu labeled particles on the concentration of HER2/neu: Plot of fluorescence intensity versus HER2/neu concentration of 545 nm ● and 655 nm SiQDs ■.

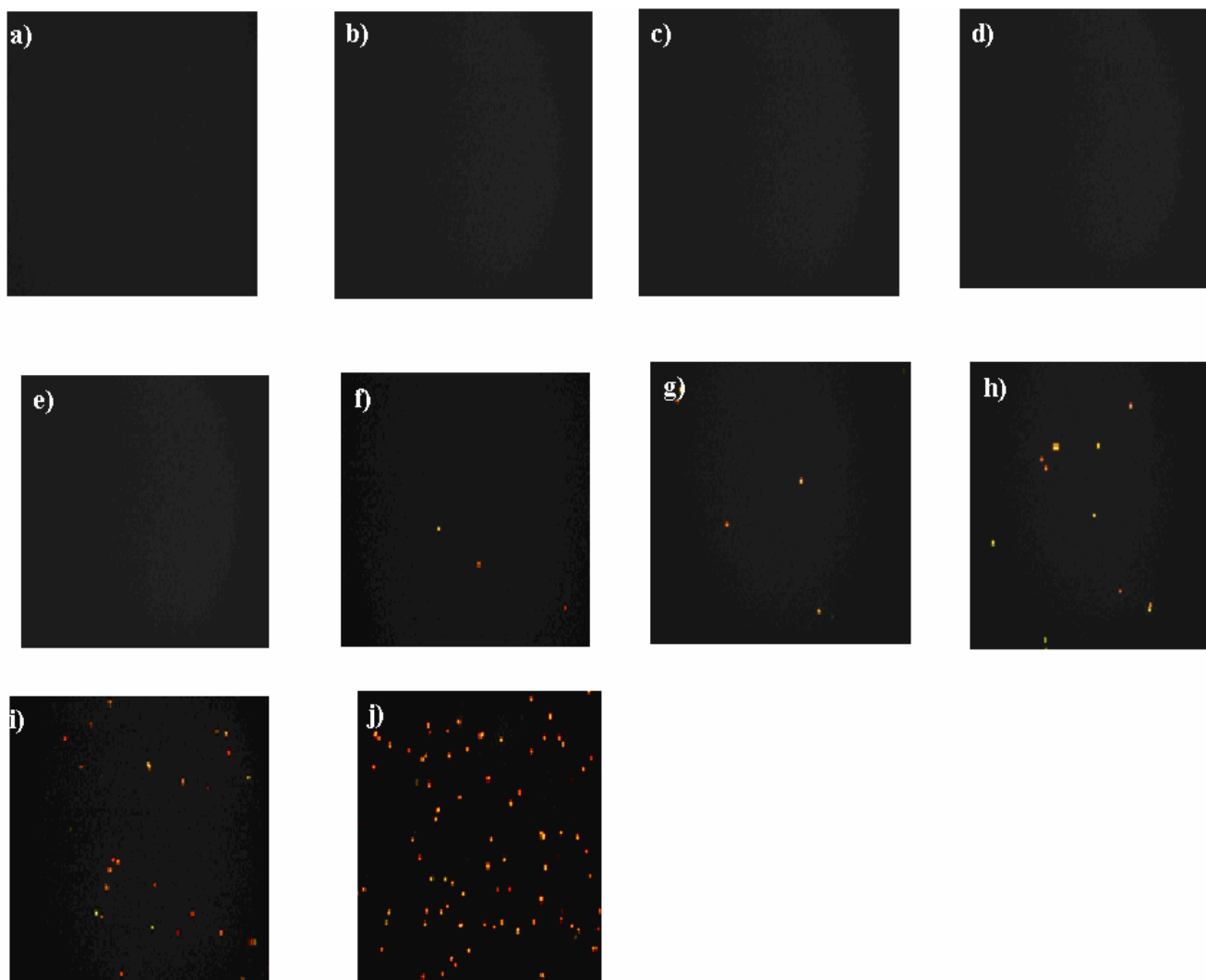


**Figure 3.8** - Digital fluorescence microscopy images of (a) Unlabeled anti-HER2 silica with 10  $\mu\text{g/mL}$  HER2/neu, (b) 0  $\mu\text{g/mL}$  HER2/neu, (c) 50  $\mu\text{g/mL}$  ER, (d) 10  $\mu\text{g/mL}$  PR, (e) 65 ng/mL HER2/neu, (f) 85 ng/mL HER2/neu, (g) 0.1  $\mu\text{g/mL}$  HER2/neu, (h) 2  $\mu\text{g/mL}$  HER2/neu, (i) 5  $\mu\text{g/mL}$  HER2/neu, and (j) 10  $\mu\text{g/mL}$  HER2/neu.

### 3.5 Summary and Conclusions

Some previously used methods for preparing fluorescent microparticles include the incorporation of organic dyes and lanthanide oxides into beads by microemulsion and spray pyrolysis, respectively. These methods can be both costly and laborious. Neither organic dyes nor lanthanide oxides have high photostability, rapid and simple incorporation techniques, or the ability to multiplex. It is impossible to precisely control the ratios of the fluorescent molecules into the microparticles by the microemulsion and spray pyrolysis methods. The inability to multiplex and the self-quenching effect of organic dyes are major disadvantages when considering the use of these fluorescent microparticles in biological applications. The method used in this study for preparing the fluorescent silica particles was rapid and simple. Unlike polystyrene microparticles, the rigid silica particles were resistant to structural deformation. 545 nm, 655 nm, and several precisely controlled ratios of 545 nm and 655 nm quantum dot – silica composites were prepared. QDs have several advantages over conventional fluorophores including high photostability, high emission quantum yield, and size dependent emission wavelength tunability. The use of quantum dots is ideal for multiplexing. The SiQDs showed high photostability compared to dye labeled mesoporous silica particles and free quantum dots. The quantum dot encapsulated particles showed very high stability to leakage compared to particles loaded with fluorescein DHPE and rhodamine DHPE. The particles were very stable when stored under argon in the dark and SiQDs containing MPTMS were much more stable than unmodified particles. The composite particles were applied for the analysis of the HER2/neu breast cancer marker. The anti-HER2/neu was biotinylated which made attachment to the streptavidin modified particles easy. The direct detection method used in this study was simple

and straightforward. Normal levels of HER2/neu in serum are < 10 ng/mL. The HER2/neu assay had a limit of detection of 85 ng/mL and was only able to detect abnormal levels of HER2/neu. We are currently developing a more sensitive assay that can rapidly and reliably detect multiple breast cancer markers for potential use in clinical and academic laboratories.

### **3.6 Acknowledgements**

This study was funded by the Louisiana Board of Regents LEQSF(2007-12)-ENH-PKSFI-PRS-04 and the National Science Foundation CHE-0717526.

### 3.6 References

1. Corrie, S. R.; Lawrie, G. A.; Trau, M., Quantitative Analysis and Characterization of Biofunctionalized Fluorescent Silica Particles. *Langmuir* **2006**, 22, (6), 2731-2737.
2. Wang, J.; Wang, X.; Ren, L.; Wang, Q.; Li, L.; Liu, W.; Wan, Z.; Yang, L.; Sun, P.; Ren, L.; Li, M.; Wu, H.; Wang, J.; Zhang, L., Conjugation of Biomolecules with Magnetic Protein Microspheres for the Assay of Early Biomarkers Associated with Acute Myocardial Infarction. *Analytical Chemistry* **2009**, 81, (15), 6210-6217.
3. Alexander, L. M.; Sanchez-Martin, R. M.; Bradley, M., Knocking (Anti)-Sense into Cells: The Microsphere Approach to Gene Silencing. *Bioconjugate Chemistry* **2009**, 20, (3), 422-426.
4. Blin, J. L.; Gerardin, C.; Carteret, C.; Rodehuser, L.; Selve, C.; Stebe, M. J., Direct One-Step Immobilization of Glucose Oxidase in Well-Ordered Mesostructured Silica Using a Nonionic Fluorinated Surfactant. *Chemistry of Materials* **2005**, 17, (6), 1479-1486.
5. Huh, S.; Wiench, J. W.; Yoo, J.-C.; Pruski, M.; Lin, V. S. Y., Organic Functionalization and Morphology Control of Mesoporous Silicas via a Co-Condensation Synthesis Method. *Chemistry of Materials* **2003**, 15, (22), 4247-4256.
6. Zhao, Y.; Ye, M.; Chao, Q.; Jia, N.; Ge, Y.; Shen, H., Simultaneous Detection of Multifood-Borne Pathogenic Bacteria Based on Functionalized Quantum Dots Coupled with Immunomagnetic Separation in Food Samples. *Journal of Agricultural and Food Chemistry* **2009**, 57, (2), 517-524.
7. Agrawal, A.; Sathe, T.; Nie, S., Single-Bead Immunoassays Using Magnetic Microparticles and Spectral-Shifting Quantum Dots. *Journal of Agricultural and Food Chemistry* **2007**, 55, (10), 3778-3782.
8. Shi, D.; Cho, H. S.; Dong, Z., Fluorescent Polystyrene-Fe<sub>3</sub>O<sub>4</sub> Composite Nanospheres for In vivo Imaging and Hyperthermia. *Adv. Mater* **2009**, 21, 1-4.
9. Han, M.; Gao, X.; Su, J. Z.; Nie, S. M., Quantum-dot-tagged microbeads for multiplexed optical coding of biomolecules. *Nature* **2001**, 19, 631-635.
10. Gao, X.; Nie, S., Quantum Dot-Encoded Mesoporous Beads with High Brightness and Uniformity: Rapid Readout Using Flow Cytometry. *Analytical Chemistry* **2004**, 76, (8), 2406-2410.
11. Wang, D.; He, J.; Rosenzweig, N.; Rosenzweig, Z., Superparamagnetic Fe<sub>2</sub>O<sub>3</sub> Beads CdSe/ZnS Quantum Dots Core Shell Nanocomposite Particles for Cell Separation. *Nano Letters* **2004**, 4, (3), 409-413.
12. Shi, L.; Rosenzweig, N.; Rosenzweig, Z., Luminescent Quantum Dots Fluorescence

- Resonance Energy Transfer-Based Probes for Enzymatic Activity and Enzyme Inhibitors. *Analytical Chemistry* **2006**, 79, (1), 208-214.
13. Chen, Y.; Ji, T.; Rosenzweig, Z., Synthesis of Glyconanospheres Containing Luminescent CdSe ZnS Quantum Dots. *Nano Letters* **2003**, 3, (5), 581-584.
  14. Bawendi, M. G.; Steigerwald, M. L.; Brus, L. E., The Quantum Mechanics of Larger Semiconductor Clusters ("Quantum Dots"). *Annu. Rev. Phys. Chem.* **1990**, 41, 477-496.
  15. Peng, Z. A.; Peng, X., Formation of High-Quality CdTe, CdSe, and CdS Nanocrystals Using CdO as Precursor. *Journal of the American Chemical Society* **2001**, 123, (1), 183-184.
  16. Peng, Z. A.; Peng, X., Mechanisms of the Shape Evolution of CdSe Nanocrystals. *Journal of the American Chemical Society* **2001**, 123, (7), 1389-1395.
  17. Alivisatos, A. P., Semiconductor clusters, nanocrystals, and quantum dots. *Science* **1996**, 271, 933-937.
  18. Rossi, L. M.; Shi, L.; Quina, F. H.; Rosenzweig, Z., Stober Synthesis of Monodispersed Luminescent Silica Nanoparticles for Bioanalytical Assays. *Langmuir* **2005**, 21, (10), 4277-4280.
  19. Rossi, L. M.; Shi, L.; Rosenzweig, N.; Rosenzweig, Z., Fluorescent silica nanospheres for digital counting bioassay of the breast cancer marker HER2/neu. *Biosensors and Bioelectronics* **2006**, 21, 1900-1906.
  20. Wang, L.; Tan, W., Multicolor FRET Silica Nanoparticles by Single Wavelength Excitation. *Nano Letters* **2005**, 6, (1), 84-88.
  21. Bagwe, R. P.; Hilliard, L. R.; Tan, W., Surface Modification of Silica Nanoparticles to Reduce Aggregation and Nonspecific Binding. *Langmuir* **2006**, 22, (9), 4357-4362.
  22. Chen, X.; Estevez, M. C.; Zhu, Z.; Huang, Y.-F.; Chen, Y.; Wang, L.; Tan, W., Using Aptamer-Conjugated Fluorescence Resonance Energy Transfer Nanoparticles for Multiplexed Cancer Cell Monitoring. *Analytical Chemistry* **2009**, 81, (16), 7009-7014.
  23. He, X.; Nie, H.; Wang, K.; Tan, W.; Wu, X.; Zhang, P., In Vivo Study of Biodistribution and Urinary Excretion of Surface-Modified Silica Nanoparticles. *Analytical Chemistry* **2008**, 80, (24), 9597-9603.
  24. Slowing, I. I.; Trewyn, B. G.; Lin, V. S. Y., Mesoporous Silica Nanoparticles for Intracellular Delivery of Membrane-Impermeable Proteins. *Journal of the American Chemical Society* **2007**, 129, (28), 8845-8849.
  25. Radu, D. R.; Lai, C.-Y.; Wiench, J. W.; Pruski, M.; Lin, V. S. Y., Gatekeeping Layer Effect: A Poly(lactic acid)-coated Mesoporous Silica Nanosphere-Based

- Fluorescence Probe for Detection of Amino-Containing Neurotransmitters. *Journal of the American Chemical Society* **2004**, 126, (6), 1640-1641.
26. Slowing, I.; Trewyn, B. G.; Lin, V. S. Y., Effect of Surface Functionalization of MCM-41-Type Mesoporous Silica Nanoparticles on the Endocytosis by Human Cancer Cells. *Journal of the American Chemical Society* **2006**, 128, (46), 14792-14793.
27. Lai, C.-Y.; Trewyn, B. G.; Jęftinija, D. M.; Jęftinija, K.; Xu, S.; Jęftinija, S.; Lin, V. S. Y., A Mesoporous Silica Nanosphere-Based Carrier System with Chemically Removable CdS Nanoparticle Caps for Stimuli-Responsive Controlled Release of Neurotransmitters and Drug Molecules. *Journal of the American Chemical Society* **2003**, 125, (15), 4451-4459.
28. Van Sark, Wilfried; Gerritsen, Hans; Meijerink, Andries., Photooxidation and Photobleaching of Single CdSe/ZnS Quantum Dots Probed by Room-Temperature Time-Resolved Spectroscopy. *Journal of Physical Chemistry B* **2001**, 105, (35), 8281-8284.

## Chapter 4

### Quantum Dot-Mesoporous Silica Microcomposites for Biomarker Analysis

#### 4.1 Abstract

Chapter 4 discusses the preparation and application of mesoporous silica particles encoded with highly fluorescent CdSe/ZnS quantum dots as signal transducers for the simultaneous detection of three different breast cancer markers. Breast cancer is the most commonly diagnosed cancer in women. Early diagnosis of this disease has great prognostic value, allows for patients to receive the correct treatment, and is particularly important for breast cancer recovery and survival. The ability to screen for multiple biomarkers simultaneously greatly reduces cost, diagnosis time, and improves prognosis. The current gold standards for detecting breast cancer are fluorescence in situ hybridization (FISH) and immunohistochemistry (IHC), neither of which can identify multiple biomarkers simultaneously. Both FISH and IHC are invasive because they require a biopsy in order to provide a sample for analysis. The use of quantum dot-mesoporous silica composite particles (SiQDs) to detect breast cancer proteins offers several advantages over FISH and IHC. A rapid and simple method for encoding mesoporous silica particles with quantum dots for the minimally invasive, simultaneous detection of the three most common breast cancer markers HER2/neu, ER $\alpha$ , and PR in bovine serum is described. The method using SiQD is minimally invasive in that it requires a serum sample that can be obtained by inserting a needle in the vein compared to removing breast tissue via biopsy. The assay is based on the use of quantum dot-containing mesoporous silica particles

as signal transducers. The normal level for HER2/neu in serum is < 10 ng/mL and <15 ng/mL for ERa and PR. A direct detection and sandwich assay were employed to measure the levels of breast cancer proteins in bovine serum. The direct detection method was the simpler of the two and involves the nonspecific adsorption of protein to a glass well plate. This method was only able to measure abnormal levels of protein. The HER2/neu assay had a limit of detection of 85 ng/mL. The ERa assay had a limit of detection of 100 ng/mL, and the PR assay had a limit of detection of 200 ng/mL. The sandwich assay had approximately a 20 to 30-fold improvement in detection and was able to detect both normal and abnormal levels of protein. The sandwich assay was performed by covalently binding a capture antibody to the glass plate and using the antibody labeled SiQDs as the detection. The HER2/neu sandwich assay was able to measure as low as 3 ng/mL, 6ng/mL for ERa, and 11 ng/mL for PR. Multiplexed detection for the lowest detectable levels for the sandwich assay was achieved. InP/ZnS quantum dots were also used to detect the breast cancer markers. Multiplexed detection was achieved using the InP/ZnS encoded particles. The limits of detection of HER2/neu, ERa, and PR were 17 ng/mL, 25 ng/mL, and 32 ng/mL, respectively. The use of SiQDs as signal transducers could potentially be used in the early diagnosis of breast cancer and can possibly be used to either replace or complement FISH and IHC.

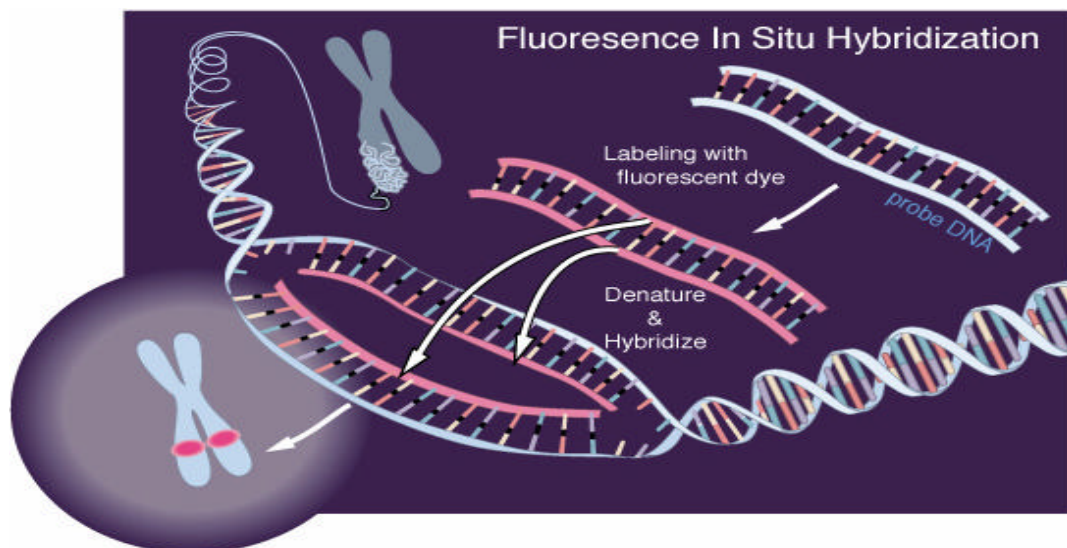
## **4.2 Introduction**

In the United States one in eight women have breast cancer, and approximately 192,000 new cases of invasive breast cancer and 67,800 of noninvasive breast cancer will be diagnosed this year.<sup>1,2</sup> Besides lung cancer, breast cancer death rates are higher than those for any other cancer. An estimated 40,500 women are expected to die from breast cancer this year.<sup>1, 2</sup> Over

the past two decades, death rates have decreased, and the outcome of patients with breast cancer has improved. This improvement is due to advances in treatment and early diagnosis. Early diagnosis is of great prognostic value and is particularly important for breast cancer recovery and survival. Human epidermal growth factor receptor 2 (HER2/neu) and the steroid hormone receptors estrogen receptor (ER) and progesterone receptor (PR) are the most commonly amplified and overexpressed proteins in breast cancer. Detection of elevated HER2/neu, ER, and PR expression can greatly improve the treatment and prognosis of breast cancer. It is essential to be able to screen for all three breast cancer markers simultaneously. Their simultaneous detection greatly reduces time and cost, thus increasing the chances of early diagnosis, improving prognosis, and providing information about the proper treatment. The current gold standards for detecting breast cancer are fluorescence in situ hybridization (FISH) and immunohistochemistry (IHC). Although FISH and IHC are most commonly used, both of these methods have limitations including rapid photobleaching of the fluorophore, the inability to screen for multiple breast cancer markers simultaneously, and invasiveness. These techniques are also time consuming, labor intensive, and costly.<sup>3-8</sup>

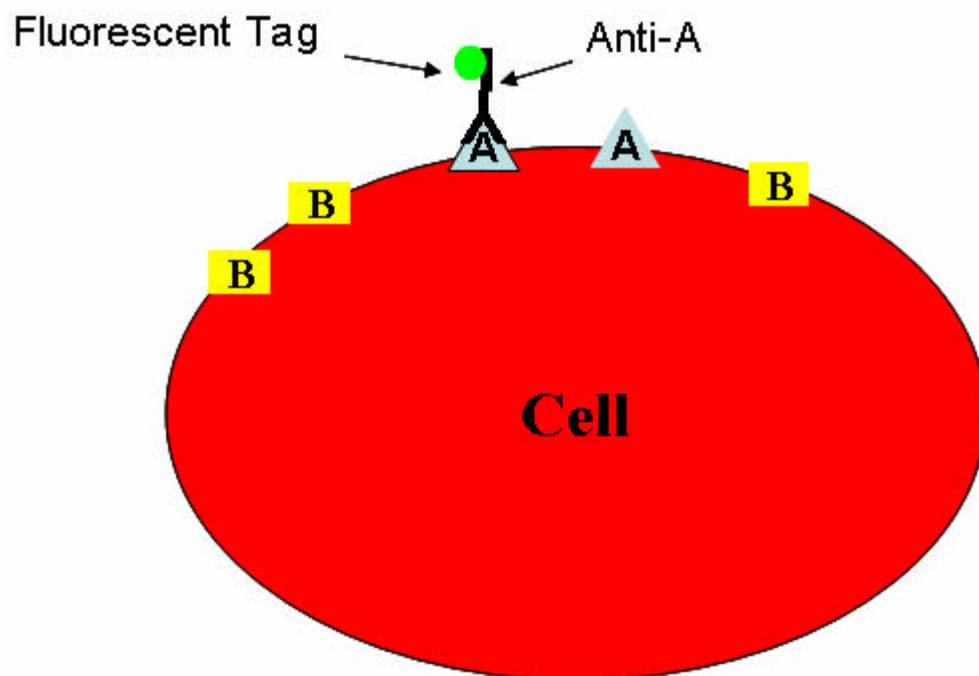
FISH uses fluorescent probes that only hybridize to the region of the chromosome that shows a highly similar sequence to the probe. A DNA probe is fluorescently labeled, denatured, and then hybridized to specific DNA sequences on chromosomes. Scheme 4.1 shows the general process of FISH. FISH is very accurate and highly sensitive with a limit of detection down to the fmol/mg protein range. There are also some disadvantages. FISH is labor intensive and takes days to complete.<sup>9-11</sup> FISH analysis is expensive and requires highly skilled technicians.<sup>11</sup> Another limitation is that the permeability of the tissue or cells of interest must be increased without destroying the structural integrity of the cell or tissue. FISH uses fluorophores which are

susceptible to rapid photobleaching, have various excitation wavelengths, and overlapping emission peaks. The spectral overlap of the fluorophores does not allow simultaneous detection of multiple fluorescent probes.



Scheme 4.1. General scheme of FISH. [www.genome.gov](http://www.genome.gov)

IHC uses fluorescently labeled antibodies to directly locate proteins in the cells of tissue. The fluorescently labeled antibody specifically binds to the antigen of interest and can be visualized using fluorescence microscopy. Scheme 4.2 shows the scheme of IHC. IHC has a limit of detection comparable to that of FISH. It is also inexpensive and can be done easily with simple training.<sup>12-14</sup> Some limitations are that IHC is invasive, the fluorophores used are subject to photobleaching, and simultaneous detection of antigens in the tissue section is not possible.



Scheme 4.2. Scheme of IHC.

The minimally invasive application of quantum dot encoded mesoporous silica particles as signal transducers in a multiplexed assay of the breast cancer markers HER2/neu, ERa, and PR is described. QDs have unique optical properties that offer several advantages over conventional fluorophores including broad absorption spectra, narrow emission peaks, high photostabilities, high emission quantum yields, large molar extinction coefficients, longer fluorescence lifetimes, large Stokes shifts, and size dependent emission wavelength tunability.<sup>15-</sup>  
<sup>26</sup> The levels of HER2/neu in serum are < 10 ng/mL in normal patients and > 10ng/mL in breast cancer patients.<sup>27, 28</sup> The levels of ERa and PR in serum are > 15ng/mL in breast cancer patients. It is essential to have a sensitive assay that can rapidly and reliably measure the levels of the HER2/neu, ERa, and PR protein and gene in order to issue an accurate prognosis for treatment. This rapid, simple, multiplexed technique offers several advantages to the gold standard methods

and can possibly be used to either replace or complement the FISH and IHC. The multiplexed detection of HER2/neu, ER $\alpha$ , and PR with SiQD entails immobilizing the antigen with a capture antibody and adding antibody labeled SiQD to serve as the signal transducer.

## 4.3 Experimental

### 4.3.1 Synthesis of TOPO coated quantum dots

TOPO coated CdSe/ZnS quantum dots were prepared by a method developed by Peng with slight modifications. Briefly, 12.7 mg cadmium oxide (CdO) and 160 mg lauric acid were mixed in a 3-neck flask under nitrogen and heated to  $>200\text{ }^{\circ}\text{C}$  until the CdO was dissolved in the lauric acid. A clear, colorless solution was formed. Then, 1.9 g of trioctylphosphine oxide (TOPO) and 1.9 g hexadecylamine (HDA) were added to the solution under stirring and the temperature was increased to  $280^{\circ}\text{C}$  for 10 min. Next, 80 mg selenium powder was dissolved in 2 mL solution of trioctylphosphine (TOP) and was rapidly injected into the solution under vigorous stirring. The mixture was cooled to  $\sim 200\text{ }^{\circ}\text{C}$  and kept at this temperature for 3 minutes. When the quantum dots reached the desired color, a ZnS shell was added as follows: a 2 mL TOP solution containing 250  $\mu\text{L}$  hexamethyldisilathiane ( $(\text{TMS})_2\text{S}$ ) were mixed with 1 mL diethylzinc ( $\text{Zn}(\text{Et})_2$ ) under nitrogen and then slowly injected into the solution. The reaction mixture was kept at  $180\text{ }^{\circ}\text{C}$  for one hour. The solution was then cooled to room temperature and the resulting TOPO coated CdSe/ZnS quantum dots were washed three times with methanol and re-dissolved in chloroform.

### 4.3.2 Synthesis of myristic acid coated quantum dots

**Injection solution preparation:** 0.3 mmol (87 $\mu$ L) of tris(trimethylsilyl)phosphine and 2.4 mmol (397 $\mu$ L) of 1-octylamine were dissolved in 1016  $\mu$ L octadecene (ODE) (1.5mL total volume) in a glove box.

**Synthesis Procedure:** 0.6 mmol (0.1752g) of indium acetate, 1.8 mmol (0.4111g) of myristic acid, and 5mL of ODE were loaded into a three-neck flask. The mixture was heated to 180 °C under argon flow, for 30 min. Then, the P(TMS)<sub>3</sub>/amine solution made in glove box was injected rapidly into the hot reaction mixture and allowed to react for 60 min. For the growth of ZnS shell, the reaction solution was cooled down to 150 °C. Zinc stearate (0.1 M in ODE) and sulfur (0.1 M in ODE) precursors (1.2 mL each) were added consecutively to the reaction flask with the InP nano crystals, waiting for 10 min between each injection at 150 °C. After that, the temperature was increased to 230 °C for 20 min to allow the growth of the ZnS shell. The reaction was cooled down to room temperature. For purification, the nanocrystals were precipitated with methanol and centrifuged. The precipitate was redissolved in chloroform.

### 4.3.3 Preparation of fluorescent mesoporous silica beads

Fluorescent silica particles were prepared by dispersing 2mg of C<sub>18</sub> modified silica in 1 mL 1- butanol. Two hundred microliters of 1  $\mu$ M 495 nm, 560 nm, or 655 nm quantum dots were added to the solution. The mixture was incubated for 30 minutes, centrifuged (5500 rpm, 10min), and washed three times with ethanol.

### 4.3.4 Preparation of thiol-modified fluorescent mesoporous silica beads

Thiol-modified fluorescent mesoporous silica beads were prepared according to a previously described method.<sup>29, 30, 31, 33</sup> Briefly, two milligrams of fluorescent silica particles were dispersed in 10 mL 1-butanol. To prepare thiol modified particles, 500  $\mu$ L 3-mercaptopropyl trimethoxysilane (MPTMS) were added to the solution. The particles were separated by centrifugation (5500 rpm, 10min) and washed three times with ethanol. The particles were then re-dispersed in 4 mL of phosphate buffer (PB) containing 0.1% BSA at pH 7.4.

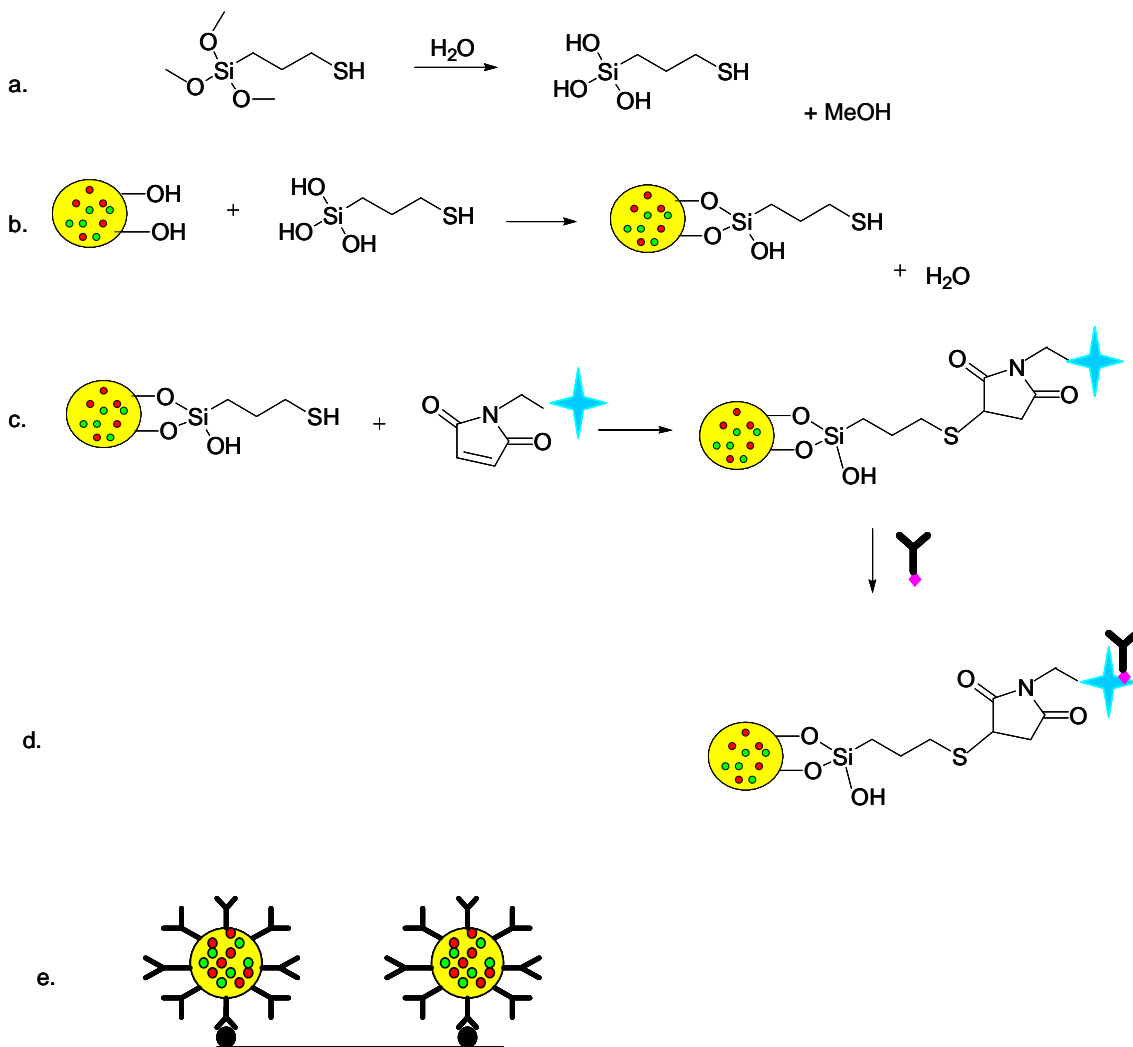
#### **4.3.5 Preparation of streptavidin-modified fluorescent mesoporous silica beads**

Streptavidin-modified fluorescent mesoporous silica beads were prepared according to a previously described method.<sup>32</sup> One milliliter of thiol-modified fluorescent mesoporous silica stock solution was added to 2mg streptavidin-maleimide in 5mL PB containing 0.1% BSA at pH 7.4. The mixture was incubated under gentle stirring for three hours at room temperature. The streptavidin-labeled beads were separated by centrifugation (5500 rpm, 10min) and washed three times with PB. The streptavidin-labeled fluorescent mesoporous silica beads were re-dispersed in 4 mL PB and used immediately for biotin-avidin assays.

#### **4.3.6 Preparation of anti- HER2/neu, anti-ERa, and anti-PR labeled fluorescent mesoporous silica beads**

Antibody labeled fluorescent mesoporous silica particles were prepared by mixing 1mL streptavidin modified silica particles with 50  $\mu$ g of biotinylated anti-HER2/neu, anti-ERa, and

anti-PR per milliliter PBS, separately. The antibody labeled particles were incubated at room temperature for two hours. The particles were separated by centrifugation (5500 rpm, 10min) and washed three times with PBS at pH 7.4. The particles were then re-dispersed in 4 mL of PBS at pH 7.4 and immediately used for binding assays. Figure 4.1 is the schematic of the preparation of antibody labeled particles used for direct detection.



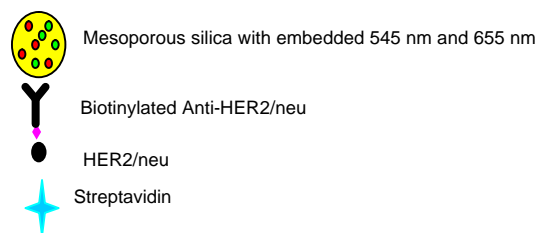


Figure 4.1. Anti-HER2/neu modified fluorescent silica particles for detection of HER2/neu. (a) the reactive methoxy groups are hydrolyzed upon addition of water, (b) condensation covalently links the silane to the oxide surface of quantum dot encoded mesoporous silica particles, (c) streptavidin is covalently bound to the silica particles via thiol-maleimide chemistry, (d) biotinylated HER2/neu is added and bound to streptavidin modified particles, and (e) direct detection assay performed.

#### 4.3.7 Preparation of HER2/neu, ERa, and PR coated 96-well plate

For direct detection, a glass bottom 96-well plate was coated separately with HER2/neu, ERa, and PR protein through nonspecific adsorption by adding 100  $\mu\text{L}$  HER2/neu, ERa, and PR protein in serum in PBS at varying concentrations. For sandwich detection, carboxylic acid modified plates were incubated separately with 300  $\mu\text{L}$  of a PBS solution containing 40mM 1-Ethyl-3-[3-dimethylaminopropyl]carbodiimide hydrochloride (EDC)/5mM *N* – hydroxysulfosuccinimide (sulfo-NHS) and 100  $\mu\text{L}$  of 6  $\mu\text{g}/\text{mL}$  anti-HER2/neu, anti-ERa, and anti-PR capture antibodies. Each concentration of protein was added to three wells. The plate was incubated for 20 hrs at 4°C. Unoccupied sites were blocked by adding 300  $\mu\text{L}$  of Superblock T20 PBS buffer. Separately, one hundred microliters of anti- HER2/neu, anti-ERa, and anti-PR labeled silica particles were added and incubated for 2 hours. The plate was washed with PBS containing 0.05% Tween-20 and dried under a stream of nitrogen.

#### 4.3.8 Characterization of the fluorescent mesoporous silica particles in solution and attached to the 96-well glass plate:

#### **4.3.8.1 Fluorescence emission spectra**

Fluorescence emission measurements were performed using a SpectraMax M2 microplate reader (Molecular Devices, Inc.) equipped with a Xenon flash lamp source and a photomultiplier (R-3896) detector.

#### **4.3.8.2 Digital fluorescence imaging microscopy**

Fluorescence images of the silica particles in solution and attached to the glass plate were taken using a digital fluorescence imaging microscopy system that contained an Olympus IX71 inverted fluorescence microscope equipped with a 100 W mercury lamp as a light source and a high performance color CCD camera (Olympus DP 70). The fluorescence images were obtained through a 20x microscope objective using a filter cube containing a 425  $\pm$ 20 nm band-pass excitation filter, a 465 nm dichroic mirror, and a 475nm long pass emission filter. The software DP controller was used for image analysis.

### **4.4 Results and Discussion**

#### **4.4.1 Direct assay for the detection of the breast cancer marker HER2/neu**

The surface of the 3 $\mu$ m mesoporous silica particles were functionalized with thiol groups because thiol is a reactive functional group that allows the covalent coupling of maleimide modified biomolecules through the formation of thio-ether bonds. Maleimide-streptavidin was attached to the surface of the fluorescent mesoporous silica particles in order to couple the biotin labeled anti-HER2/neu through streptavidin-biotin interactions. A direct detection assay was developed by nonspecifically adsorbing the HER2/neu protein to the surface of the glass well plate, adding the anti-HER2 labeled fluorescent silica particles to the plate, and averaging the number of fluorescent particles in 20 randomly selected fields of view. Figures 4.2 and 4.3 demonstrate the dependence of the binding of the fluorescent anti-HER2/neu labeled particles on the concentration of HER2/neu. At concentrations of 0  $\mu$ g/mL and 65 ng/mL, there were no particles attached to the glass slide. There were also no particles for unlabeled particles with 10  $\mu$ g/mL HER2/neu nor with anti-HER2/neu labeled particles added to 50  $\mu$ g/mL and 10  $\mu$ g/mL of ERa and PR, respectively. The number of particles attached to the glass plate increased from  $11 \pm 8$  to  $70 \pm 11$  when the concentration of HER2/neu increased from 85 ng/mL to 10  $\mu$ g/mL. The limit of detection for this direct assay was 85 ng/ml and the response was linear over the range of HER2/neu concentrations studied (85 ng/mL and 10  $\mu$ g/mL). This assay was very reproducible yielding similar results for three separate experiments.

To test the reproducibility of the assay when multiple wells are prepared in advance, seven wells of the microplate were incubated with 10  $\mu$ g/mL of HER2/neu. Measurements were taken for seven days. For each day, one well of the HER2/neu coated glass plate was incubated with anti-HER2/neu labeled fluorescent mesoporous silica particles. The standard procedure to perform the assay was carried out and measurements were taken. Figure 4.4 shows that from day 1 to day 7 the fluorescence intensity decreased by 80%. The decrease in fluorescence intensity

indicates that although the fluorescent silica beads are stable, HER2/neu adsorbed to the plate loses activity daily when the plates are prepared in advanced. The direct assay should be performed immediately after the plate preparation in order to achieve the optimal fluorescence signal. The assay was highly reproducible when new plates are prepared.

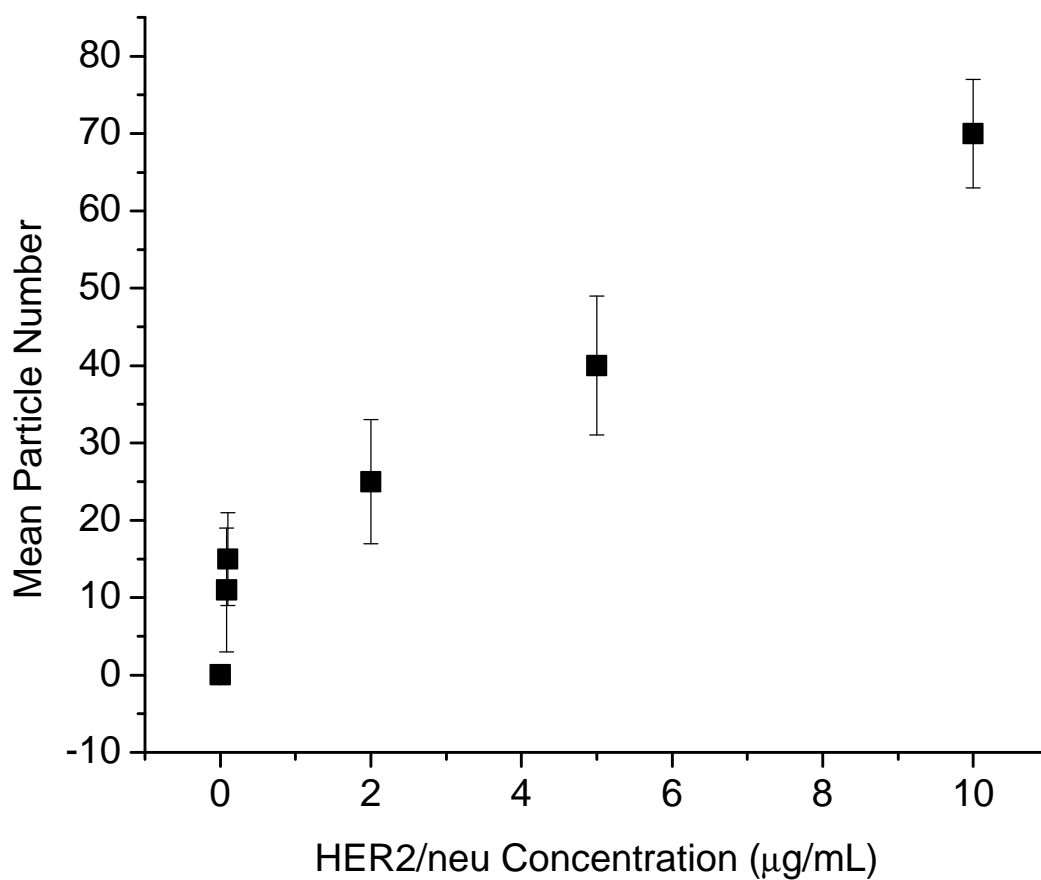


Figure 4.2. Dependence of the binding of the fluorescent anti-HER2/neu labeled particles on the concentration of HER2/neu exposed to the glass well plate before addition of the antibody labeled beads: plot of mean number of particles attached to glass versus HER2/neu concentration.

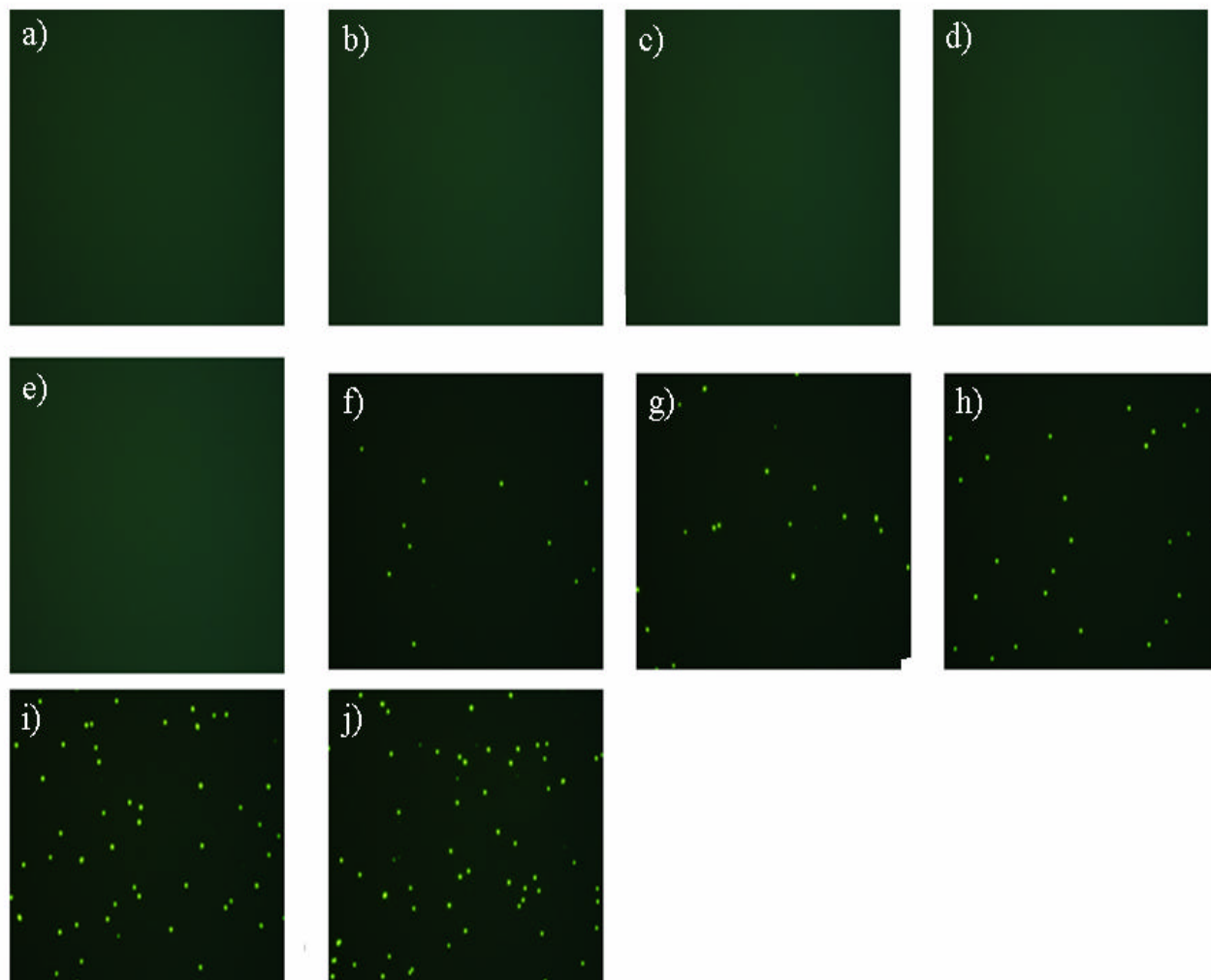


Figure 4.3. Dependence of the binding of the fluorescent anti-HER2/neu labeled particles on the concentration of HER2/neu exposed to the glass well plate before addition of the antibody labeled beads: (a) digital fluorescence microscopy images of unlabeled anti-HER2 silica with 10  $\mu\text{g/mL}$  HER2/neu, (b) 0  $\mu\text{g/mL}$  HER2/neu, (c) 10  $\mu\text{g/mL}$  PR, (d) 50  $\mu\text{g/mL}$  ERa, (e) 65 ng/mL HER2/neu, (f) 85 ng/mL HER2/neu, (g) 0.1  $\mu\text{g/mL}$  HER2/neu, (h) 2  $\mu\text{g/mL}$  HER2/neu, (i) 5  $\mu\text{g/mL}$  HER2/neu, and (j) 10  $\mu\text{g/mL}$  HER2/neu.

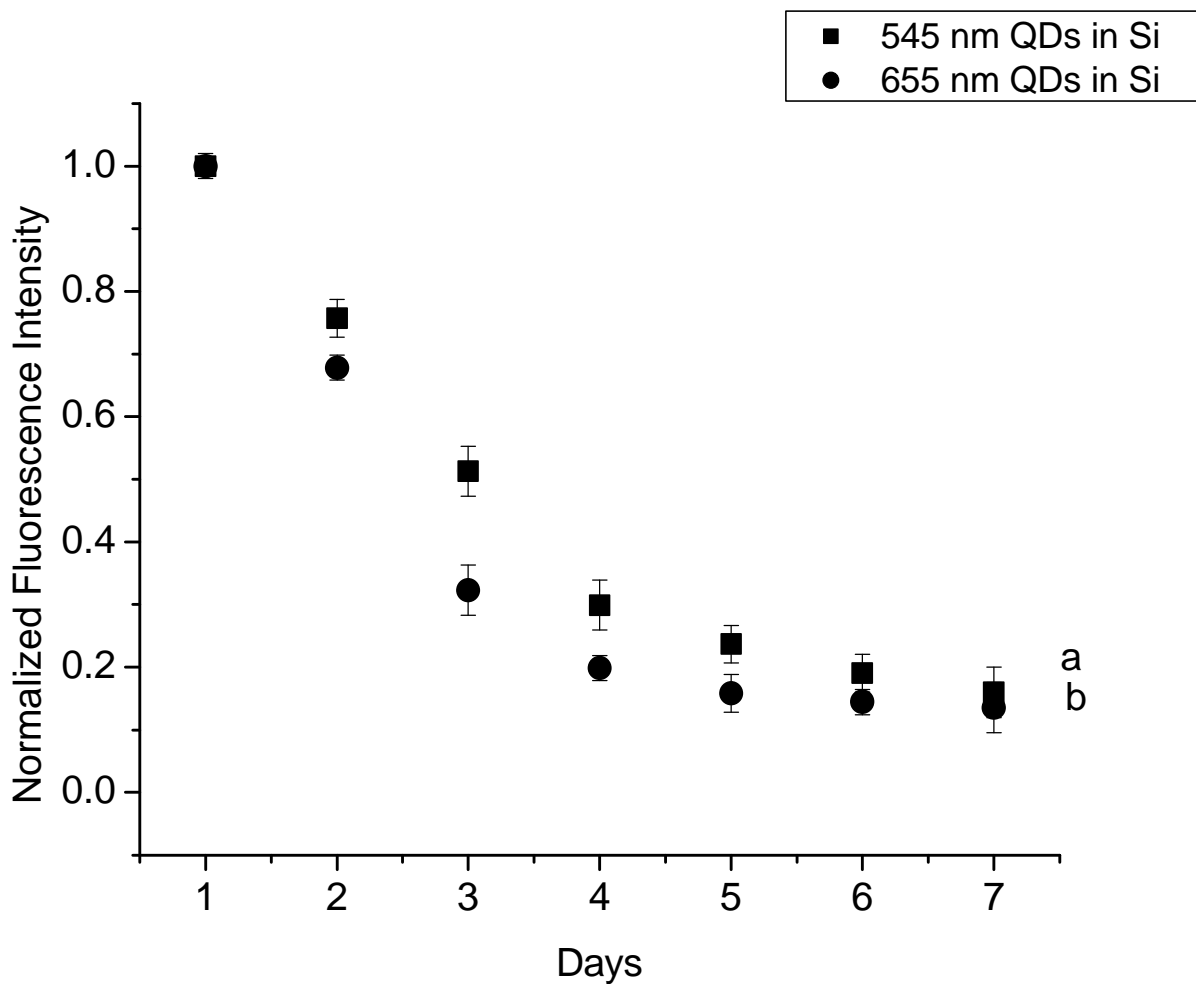


Figure 4.4. Stability of HER2/neu plate prepared in advance (a) 545 nm quantum dots in silica and (b) 655 nm quantum dots in silica.

#### 4.4.2 Detection of ERa

The assay was performed using the same approach as for the HER2/neu assay but uses 496 nm QD instead of 560 nm. The limit of detection for ERa was 100 ng/mL, and the response was linear over the range of HER2/neu concentrations studied (100 ng/mL and 50  $\mu$ g/mL).

Figures 4.5 and 4.6 show the increase of the number of particles attached to the glass bottom plate with increasing ER $\alpha$  concentration. ER $\alpha$  was first added to the plate, the plate was then washed, and then the anti- ER $\alpha$  labeled beads were added. At concentrations of 0  $\mu\text{g/mL}$  and 85 ng/mL, there were no particles attached. There were also no particles for unlabeled particles with 50  $\mu\text{g/mL}$  ER $\alpha$ , nor with anti-ER $\alpha$  labeled particles added to 10  $\mu\text{g/mL}$  and 10  $\mu\text{g/mL}$  of HER2/neu and PR, respectively. The number of particles attached to the glass per image increased from  $10 \pm 9$  to  $88 \pm 6$  when the concentration of ER $\alpha$  increased from 100 ng/mL to 50  $\mu\text{g/mL}$ .

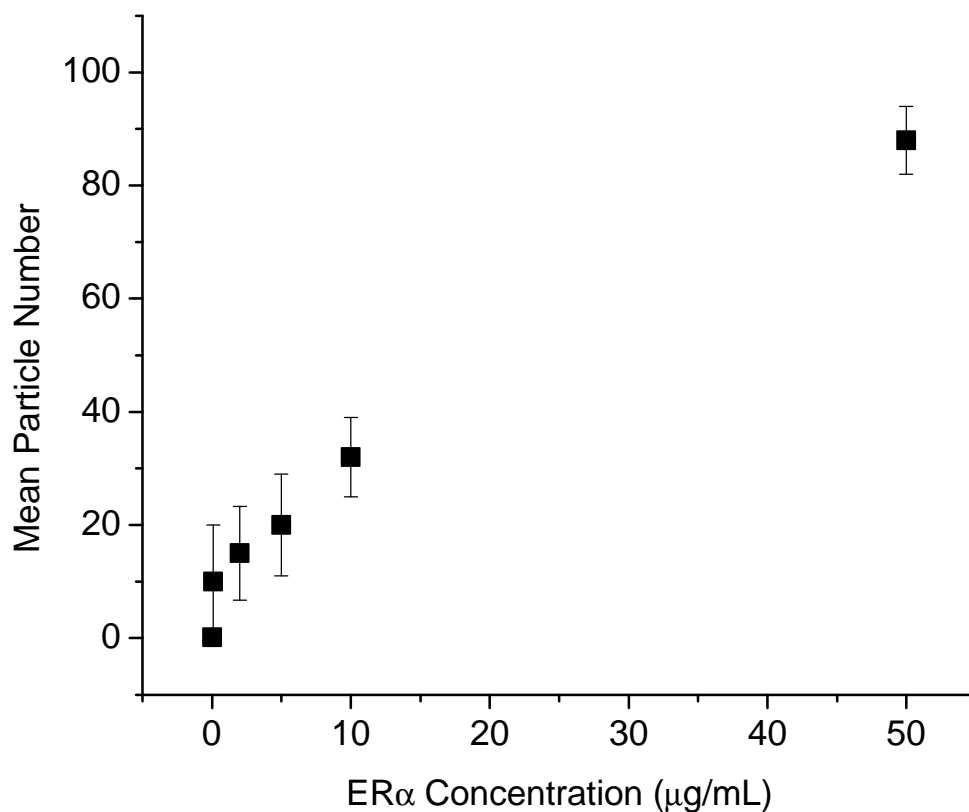


Figure 4.5. Dependence of the binding of the fluorescent anti-ER $\alpha$  labeled particles on the concentration of ER $\alpha$  exposed to the glass well plate before addition of the antibody labeled beads: plot of mean number of particles attached to glass versus ER $\alpha$  concentration.

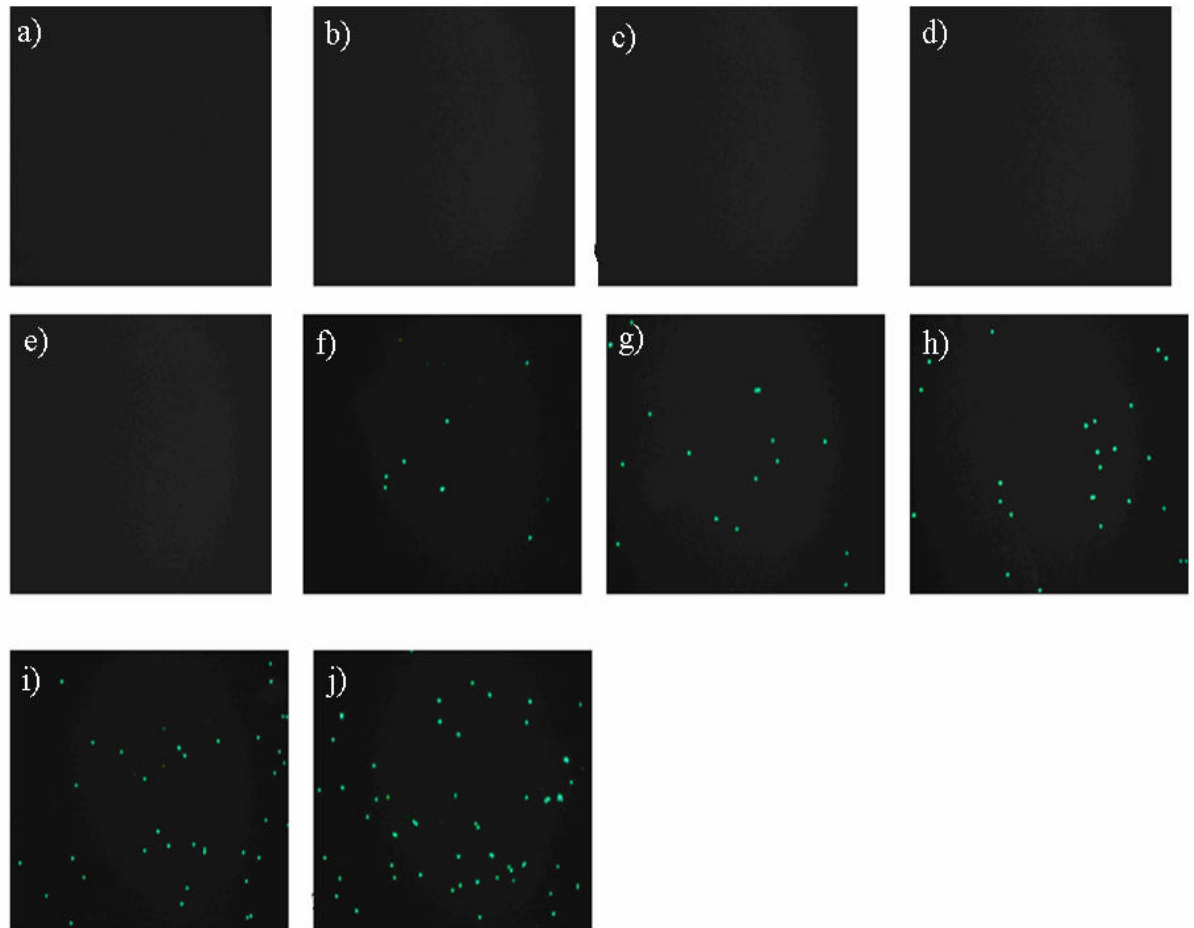


Figure 4.6. Dependence of the binding of the fluorescent anti-ERa labeled particles on the concentration of ERa (a) digital fluorescence microscopy images of unlabeled anti- ERa silica with 50  $\mu\text{g/ml}$  ERa, (b) 0  $\mu\text{g/ml}$  ERa, (c) 85  $\text{ng/ml}$  ERa, (d) 10  $\mu\text{g/ml}$  HER2/neu, (e) 10  $\mu\text{g/ml}$  PR, (f) 100  $\text{ng/ml}$  ERa, (g) 2  $\mu\text{g/ml}$  ERa, (h) 5  $\mu\text{g/ml}$  ERa, and (i) 10  $\mu\text{g/ml}$  ERa, and (j) 50  $\mu\text{g/ml}$  ERa.

#### 4.4.3 Detection of PR

The limit of detection for PR was 200 ng/mL, and the response was linear over the range of HER2/neu concentrations studied (200 ng/mL and 10  $\mu$ g/mL). The emission wavelength of QD was 655 nm. Figures 4.7 and 4.8 show an increase of the number of particles attached with increasing PR concentration exposed to the glass. At concentrations of 0  $\mu$ g/mL and 100 ng/mL, there were no particles attached. There were also no particles attached for unlabeled particles with 10  $\mu$ g/mL PR, nor with anti-PR labeled particles added to 50  $\mu$ g/mL and 10  $\mu$ g/mL of ERa and HER2/neu, respectively. The number of particles attached to the glass increased from  $10 \pm 4$  to  $60 \pm 9$  when the concentration of ERa increased from 200 ng/mL to 10  $\mu$ g/mL.

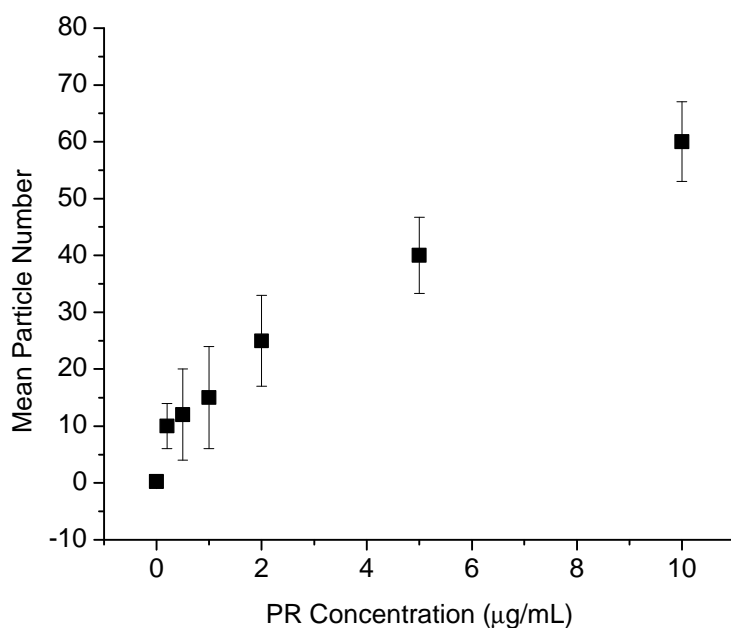


Figure 4.7. Dependence of the binding of the fluorescent anti-PR labeled particles on the concentration of PR exposed to the glass well plate before addition of the antibody labeled beads: plot of mean number of particles attached to glass versus PR concentration.

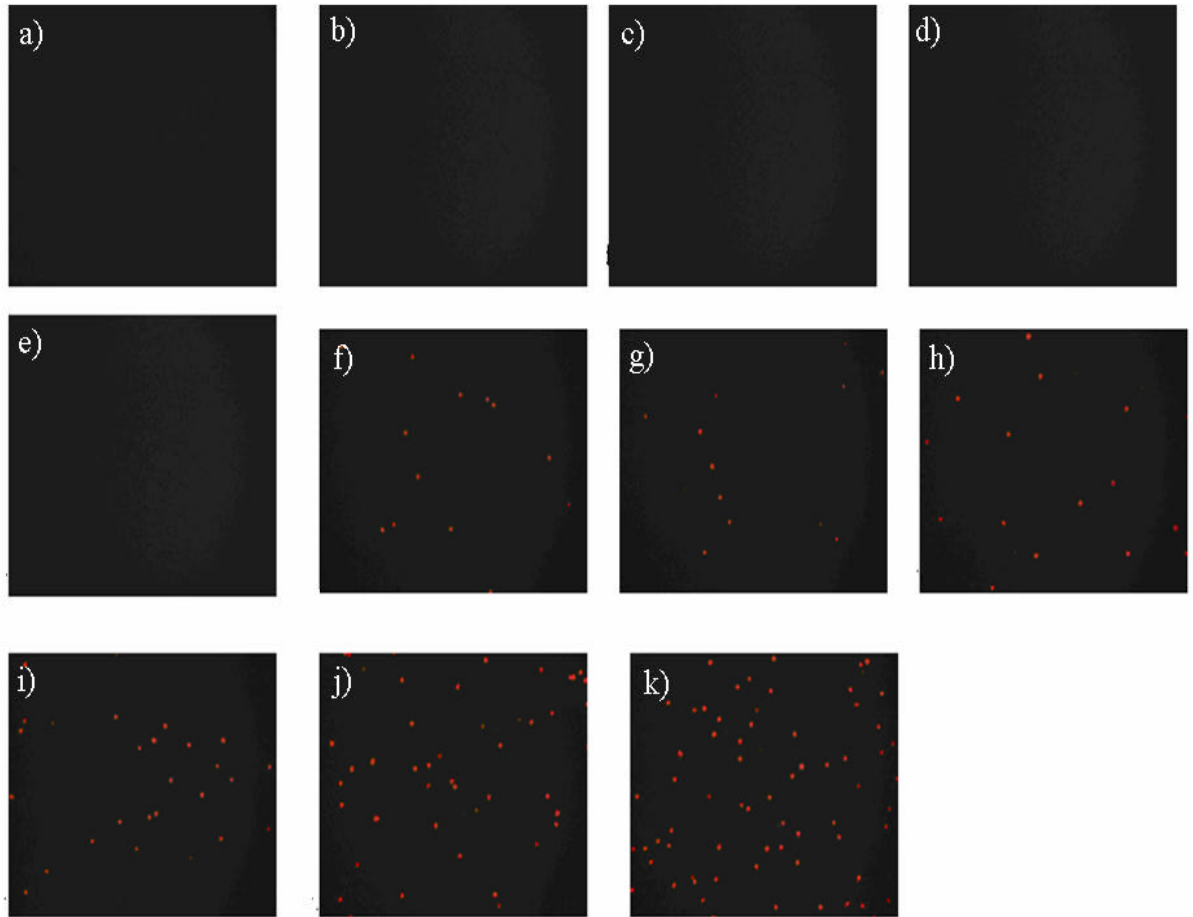


Figure 4.8. Dependence of the binding of the fluorescent anti-PR labeled particles on the concentration of PR: (a) digital fluorescence microscopy images of unlabeled anti- PR silica with 10  $\mu\text{g/ml}$  PR, (b) 0  $\mu\text{g/ml}$  PR, (c) 100  $\text{ng/ml}$  ERa, (d) 10  $\mu\text{g/ml}$  HER2/neu, (e) 50  $\mu\text{g/ml}$  ERa, (f) 200  $\text{ng/ml}$  PR, (g) 500  $\text{ng/mL}$ , (h) 1  $\mu\text{g/ml}$  PR, (ij) 2  $\mu\text{g/ml}$  PR, (j) 5  $\mu\text{g/ml}$  PR, and (k) 10  $\mu\text{g/ml}$  PR.

#### 4.4.4 Sandwich Detection of HER2/neu, ERa, and PR

The sandwich detection assay was performed in order to improve the limit of detection of the breast cancer markers. The sandwich technique is more sensitive in that it involves the use of two antibodies to detect the antigen. The capture antibody was covalently bound to a carboxylic acid modified glass plate via EDC/sulfo-NHS chemistry. Using both EDC and sulfo-NHS produces a more stable amide bond than using EDC alone. EDC reacts with a carboxyl to form an unstable amine-reactive *o*-acylisourea intermediate. If this intermediate does not encounter an amine, it will hydrolyze and regenerate the carboxyl group. In the presence of sulfo-NHS, EDC can be used to convert carboxyl groups to amine-reactive sulfo-NHS esters. This is accomplished by mixing the EDC with the carboxyl containing glass plate, adding Sulfo-NHS, and the capture antibody. Separately, varying concentrations of HER2/neu, ERa, and PR were then added and allowed to bind to the capture antibodies on the plate. The plate was then washed and the antibody labeled SiQDs were added. Figure 4.9 shows the fluorescence microscope images of the bound anti-HER2/neu modified beads after the activation of the HER2/neu capture antibody with EDC/sulfo-NHS to bind to amino-modified plates and the activation of a carboxylic acid- modified plate with EDC/sulfo-NHS to bind to the capture antibody. The concentration of HER2/neu was 10 $\mu$ g/mL. The image where the capture antibody is bound to the amino-modified plate shows a high degree of aggregation; whereas, the image of the capture antibody bound to the carboxylic modified plate showed substantially less aggregation. The aggregation in Figure 4.9a is due to the cross-linking of the –NH<sub>2</sub> groups of one antibody to the –COOH groups of a neighboring antibody. Aggregation is reduced by activating the plate instead of the antibody to eliminate any cross-linking. Figure 4.10 shows

that the sandwich assay yields approximately 100 times more captured particles than the direct detection assay under the same conditions.

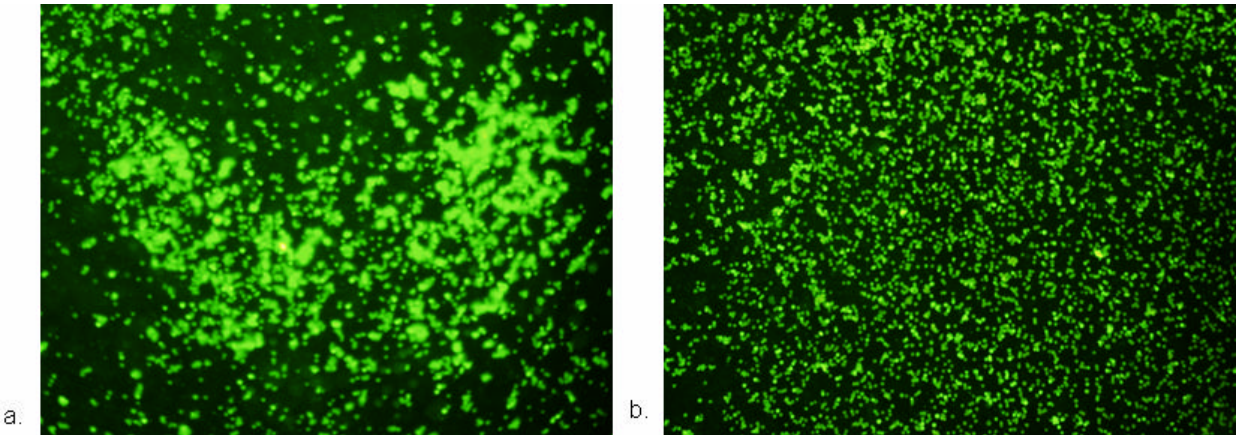


Figure 4.9. Fluorescence microscope images of a) EDC/sulfo-NHS activated capture HER2/neu antibody bound to amino-modified glass plate and b) EDC/sulfo-NHS activated carboxylic acid modified glass plate bound to amino groups of capture HER2/neu antibody.

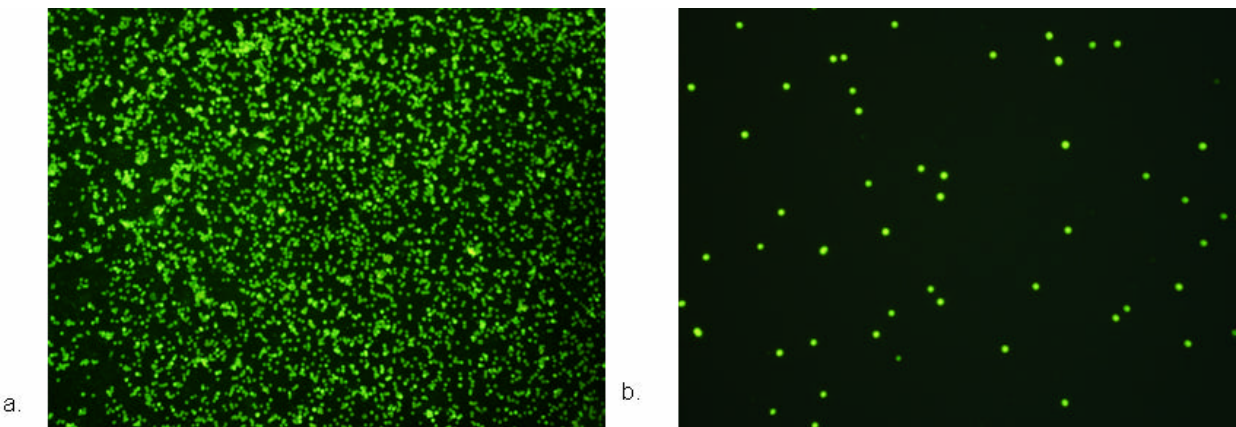


Figure 4.10. Fluorescence microscope images of a) sandwich assay with 10 $\mu$ g/mL HER2/neu and b) direct detection assay with 10 $\mu$ g/mL HER2/neu.

The normal levels for HER2/neu in serum is < 10 ng/mL and < 15 ng/mL for ERa and PR. The direct assay was only able to detect abnormal levels of breast cancer proteins. It is essential to be able to detect both normal and abnormal levels of breast cancer proteins for

diagnostic and prognostic reasons. The negative controls (data not shown) were the same as those for the direct detection and showed no particles attached to the glass plate. Figures 4.11 and 4.12 show the number of attached particles observed per image as a function of antigen concentration exposed to the well. The highest concentrations used for the sandwich assay were the limit of detection values for the direct assay. The average number of particles attached to the glass plate increased from  $12 \pm 2$  to  $150 \pm 8$  when the concentration of HER2/neu increased from 3 ng/mL to 85 ng/mL. The limit of detection of the direct assay was 3 ng/mL.

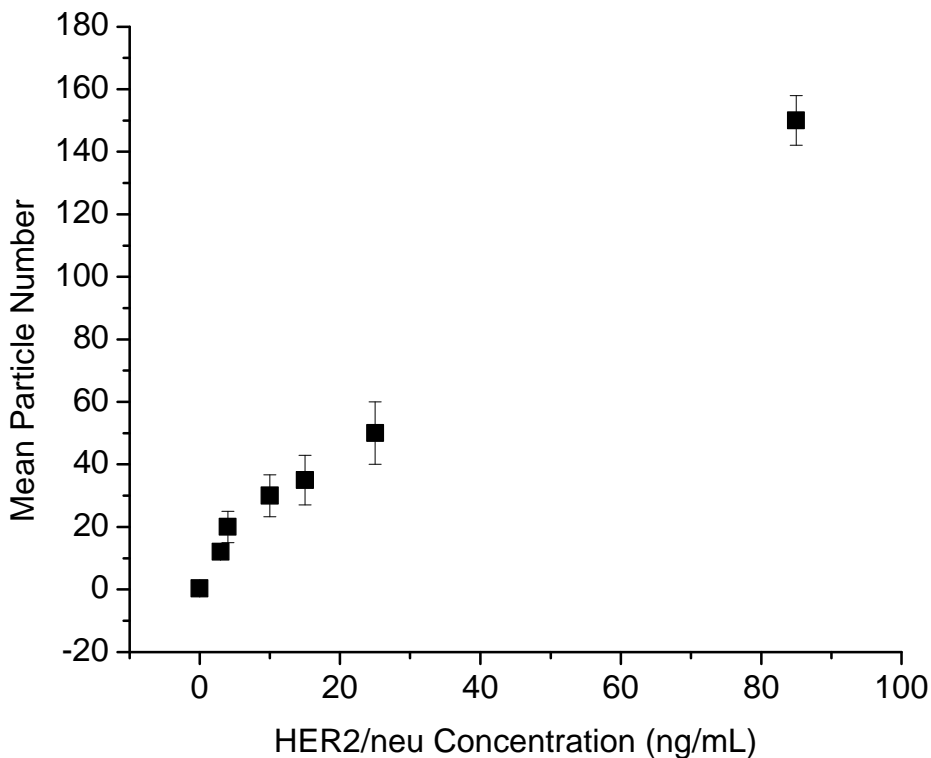


Figure 4.11. Dependence of the binding of the fluorescent anti-HER2/neu labeled particles on the concentration of HER2/neu: plot of mean number of particles attached to glass versus HER2/neu concentration.

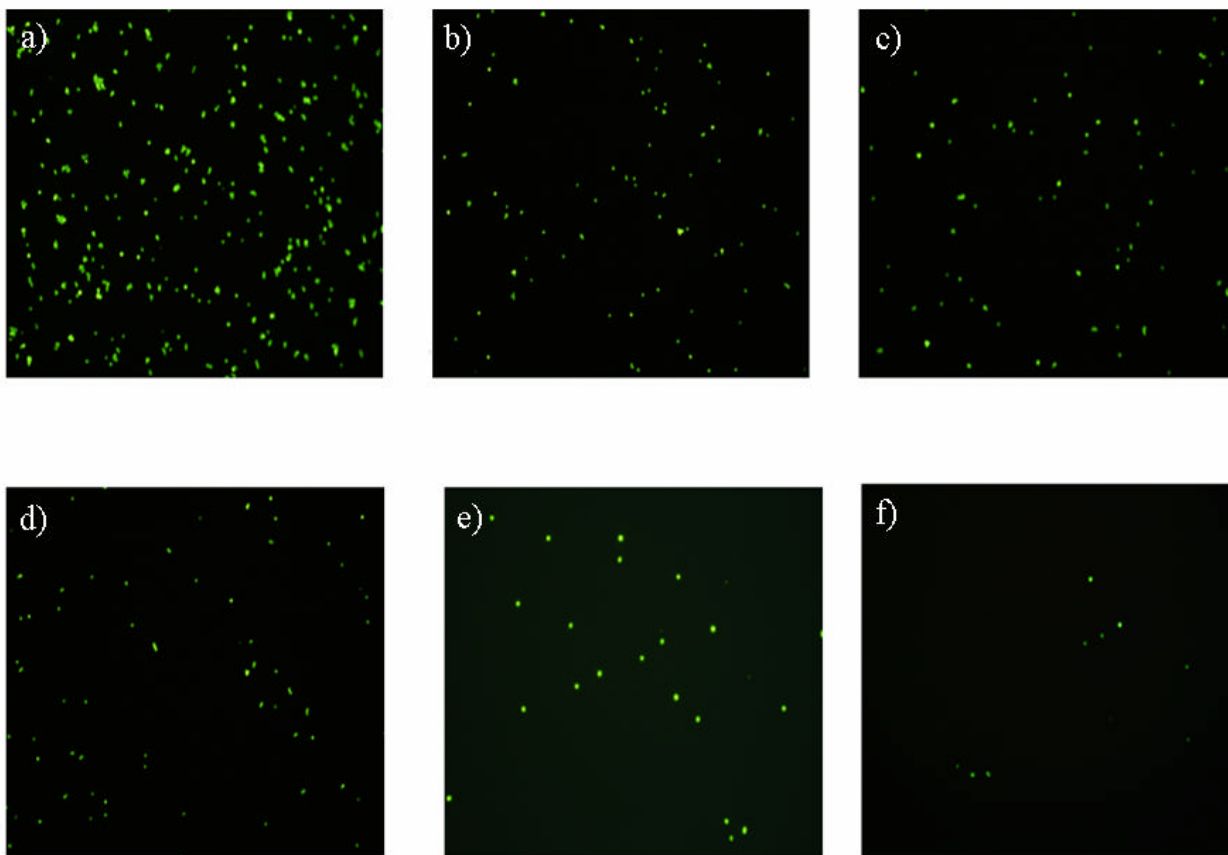


Figure 4.12. Dependence of the binding of the fluorescent anti-HER2/neu labeled particles on the concentration of HER2/neu: (a) digital fluorescence microscopy images of anti-HER2 silica with 85 ng/mL HER2/neu, (b) 25ng/mL HER2/neu, (c) 15 ng/mL HER2/neu, (d) 10 ng/mL HER2/neu, (e) 4 ng/mL HER2/neu, and (f) 3 ng/mL HER2/neu.

The limit of detection for ERa was 6 ng/mL. Figures 4.13 and 4.14 show the increase of the number of particles attached to the glass bottom plate with increasing ERa concentration. The number of particles attached to the glass increased from  $14 \pm 8$  to  $210 \pm 11$  when the concentration of ERa increased from 6 ng/mL to 100 ng/mL.

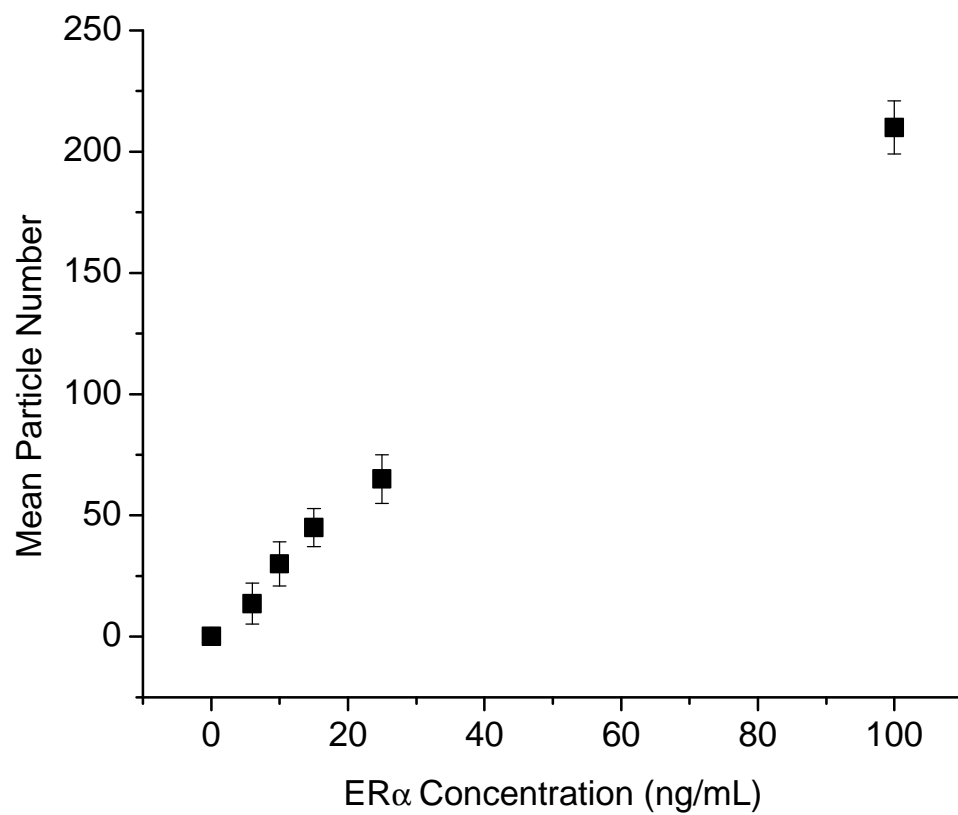


Figure 4.13. Dependence of the binding of the fluorescent anti-ER $\alpha$  labeled particles on the concentration of ER $\alpha$ : plot of mean number of particles attached to glass versus ER $\alpha$  concentration.

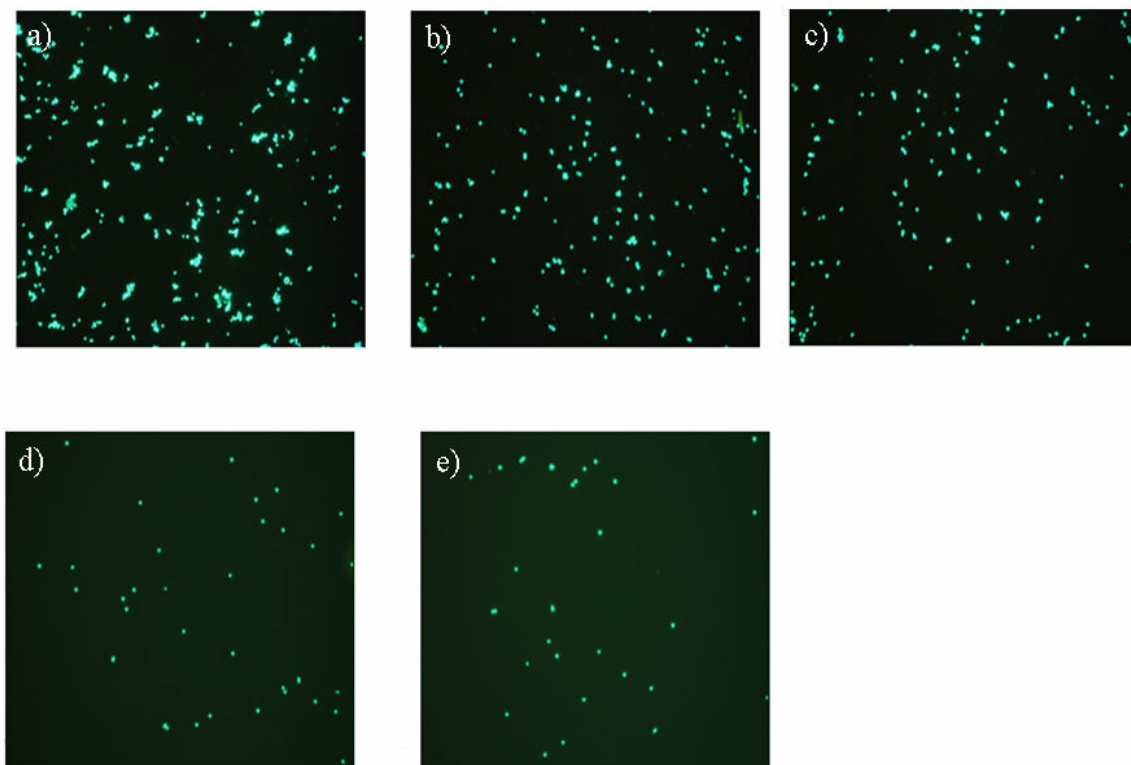


Figure 4.14. Dependence of the binding of the fluorescent anti-ERA labeled particles on the concentration of ERA: (a) digital fluorescence microscopy images of anti- ERA silica with 100 ng/mL ERA, (b) 25 ng/mL ERA, (c) 15 ng/mL ERA, (d) 10 ng/mL ERA, and (e) 6 ng/mL ERA.

The limit of detection for PR was 11 ng/mL. Figures 4.15 and 4.16 show an increase of the number of particles attached with increasing PR concentration. The number of particles attached to the glass increased from  $11 \pm 6$  to  $195 \pm 8$  when the concentration of ERA increased from 11 ng/mL to 200 ng/mL. The sandwich assay had approximately a 20 to 30-fold

improvement in detection limit compared to the direct detection method and was able to detect both normal and abnormal levels of protein.

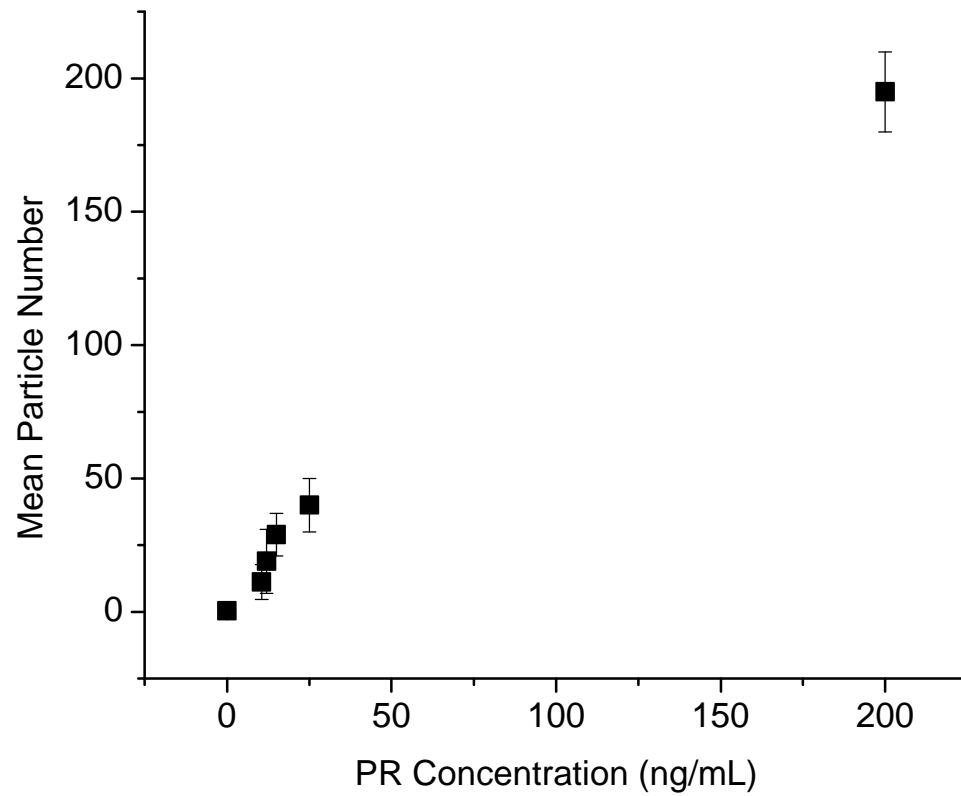


Figure 4.15. Dependence of the binding of the fluorescent anti-PR labeled particles on the concentration of PR: plot of mean number of particles attached to glass versus PR concentration.

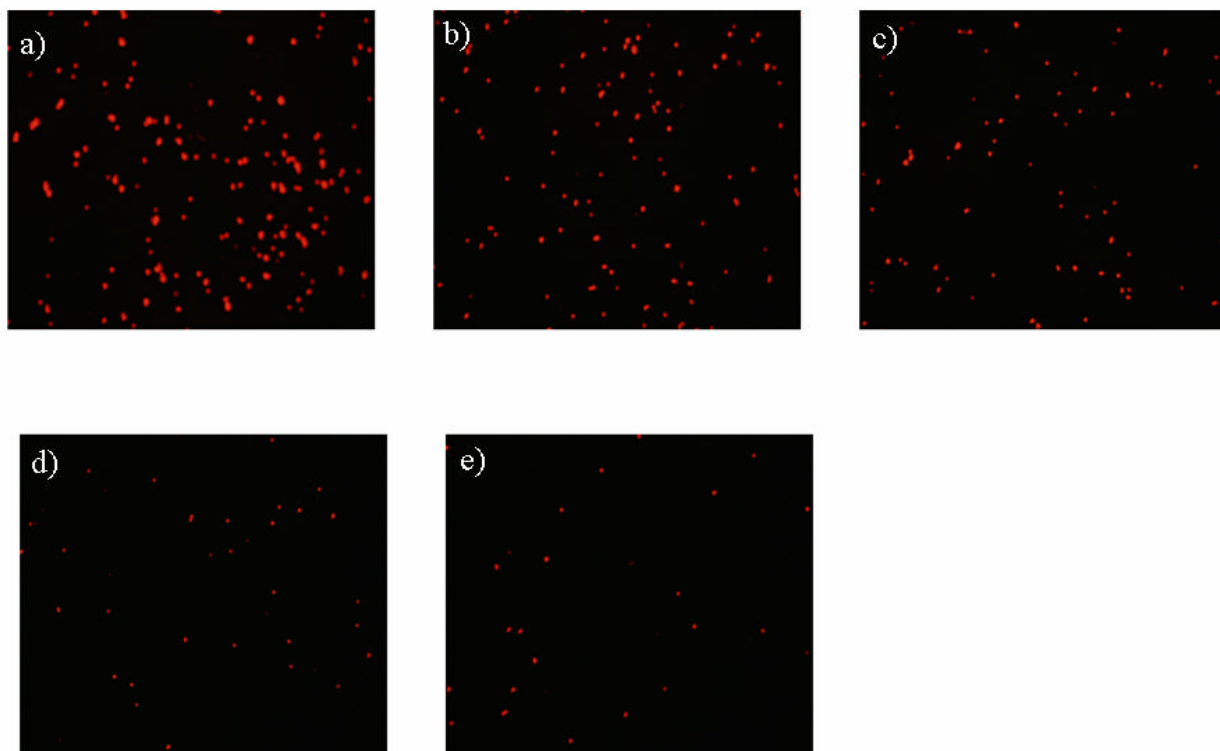


Figure 4.16. Dependence of the binding of the fluorescent anti-PR labeled particles on the concentration of PR: (a) digital fluorescence microscopy images of anti-PR silica with 200 ng/mL PR, (b) 25 ng/mL PR, (c) 15 ng/mL PR, (d) 12 ng/mL PR, and (e) 11 ng/mL PR.

#### 4.4.5 Multiplexed Analysis of HER2/neu, ERa, and PR

For the multiplexed analysis of HER2/neu, ERa, and PR, a mixture of the biomarkers were added to the well plate and the assay was performed like the individual sandwich assays. The limit of detection concentrations from the individual assays were used in the multiplexed analysis. One hundred microliters each of 4 ng/mL HER2/neu, 6 ng/mL ERa, and 11 ng/mL PR

were added. One hundred microliters of each antibody labeled silica particle were then added and the plate was analyzed as described previously. Figure 4.17 shows the fluorescence microscope images of a mixture of HER2/neu, ERa, and PR and the fluorescence spectrum of the emission wavelengths of all three fluorescently labeled silica particles in a mixture. The presence of biomarkers can easily be determined by the different colors corresponding to the particular antigens. The simultaneous detection of all three biomarkers using the SiQD is advantageous over FISH and IHC because neither method can multiplex.

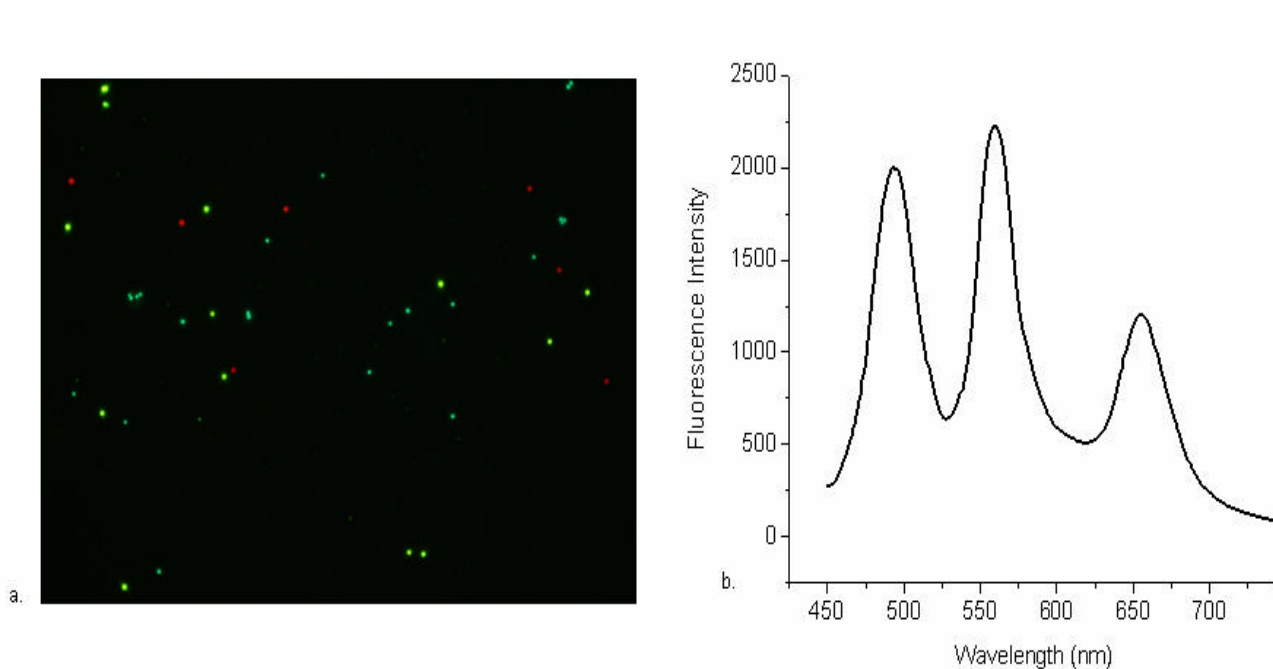


Figure 4.17. Multiplexed detection of (a) 3 ng/mL HER2/neu, 6 ng/mL ERa, and 11 ng/mL PR and (b) the fluorescence spectrum of 495 nm, 560 nm, and 655 nm SiQDs.

#### 4.4.6 Sandwich assay with InP/ZnS quantum dots

As mentioned in Section 1.4.2, CdSe/ZnS quantum dots have limited use in biological applications because of their toxicity and are environmentally restricted. InP/ZnS have low toxicity and would be a good alternative to use in biological and environmental applications. Therefore, 485 nm, 550 nm, and 620 nm InP/ZnS have been incorporated into mesoporous silica particles to demonstrate their capabilities as signal transducers for the individual and multiplexed detection of HER2/neu, ERa, and PR, respectively. The limit of detection for HER2/neu was 17 ng/mL. Figure 4.18 shows the fluorescence microscope images of the increase of the number of particles attached to the glass plate with increasing HER2/neu concentration. The limit of detection for ERa was 25 ng/mL. Figure 4.19 shows the fluorescence microscope images of the increase of the number of particles attached to the glass plate with increasing ERa concentration. The limit of detection for PR was 32 ng/mL. Figure 4.20 shows the fluorescence microscope images of the increase of the number of particles attached to the glass bottom plate with increasing PR concentration. Figure 4.21 shows the fluorescence microscope images of a mixture of HER2/neu, ERa, and PR. The mixture contained the limit of detection concentrations of 17 ng/mL HER2/neu, 25 ng/mL ERa, and 32 ng/mL PR. The limits of detection for the sandwich assay using the InP/ZnS quantum dots were inferior to that of CdSe/ZnS. The InP/ZnS encoded silica particles were only able to detect abnormal levels of the breast cancer markers. The higher limits of detection are directly related to the disadvantages of InP/ZnS compared to CdSe/ZnS quantum dots, the most obvious one being poor fluorescence quantum yield. The sandwich assay using InP/ZnS quantum dots was able to detect approximately four times better than the direct assay using the CdSe/ZnS quantum dots. The limits of detection for HER2, ERa,

and PR for the sandwich assay using CdSe/ZnS quantum dots were (3, 6, and 11) ng/mL, respectively; and, (17, 25, and 32) ng/mL for the InP/ZnS quantum dots. CdSe/ZnS typically have quantum yields that are = 75%. To date, the highest quantum yield achieved for InP/ZnS is 40%.

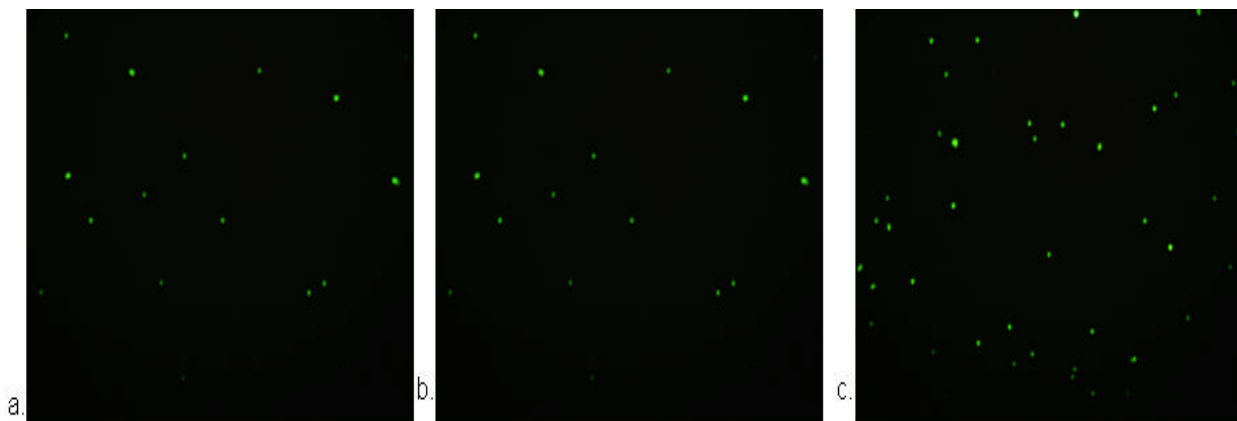


Figure 4.18. Sandwich detection of HER2/neu with InP/ZnS QDs of (a) 17 ng/mL HER2/neu, (b) 25 ng/mL HER2/neu, and (c) 50 ng/mL HER2/neu.

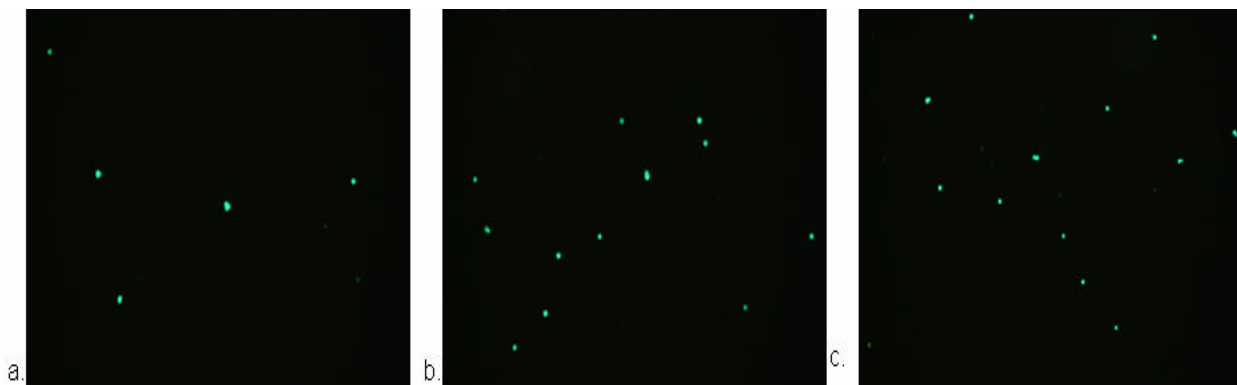


Figure 4.19. Sandwich detection of ERa with InP/ZnS QDs of (a) 25 ng/mL ERa, (b) 40 ng/mL ERa, and (c) 50 ng/mL ERa.

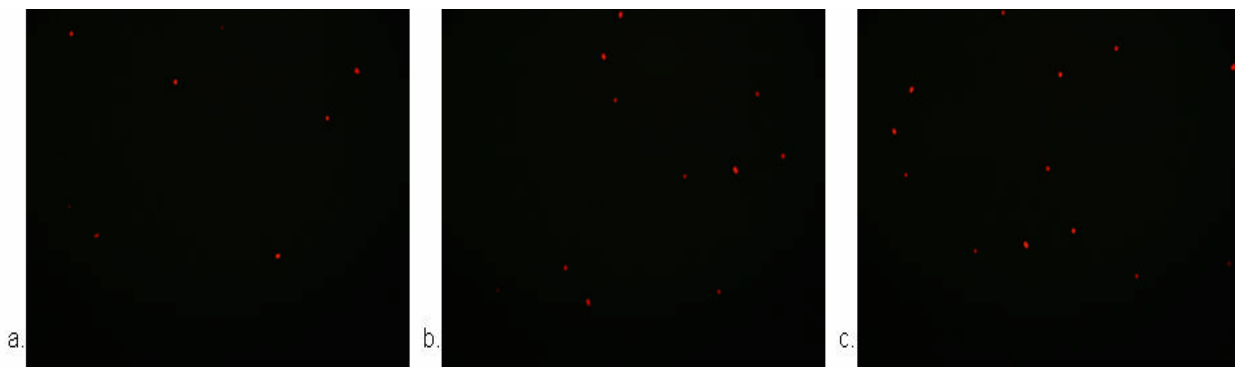


Figure 4.20. Sandwich detection of PR with InP/ZnS QDs of (a) 32 ng/mL PR, (b) 40 ng/mL PR, and (c) 50 ng/mL PR.

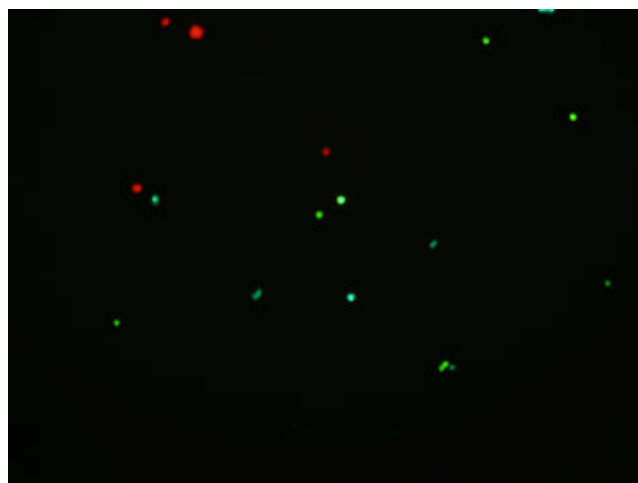


Figure 4.21. Multiplexed detection of (a) 17 ng/mL HER2/neu, 25 ng/mL ERa, and 32 ng/mL PR.

#### 4.5 Summary and Conclusions

The ability to specifically, rapidly, and reliably detect cancer markers is important and in high demand. The assay in this study was based on the use of quantum dot-containing mesoporous silica particles as signal transducers which identified and quantified the amount of HER2/neu, ERa, and PR present. We have successfully prepared anti-HER2/neu, anti-ERa, and anti-PR labeled fluorescent mesoporous silica particles to detect the breast cancer markers in

serum. The antibodies were biotinylated which made attachment to the streptavidin modified particles easy. The direct detection method used in this study was simple but only able to detect abnormal levels of breast cancer markers. The HER2/neu assay had a limit of detection of 85 ng/mL. The ERa assay had a limit of detection of 100 ng/mL, and the PR assay had a limit of detection of 200 ng/mL. Simultaneous detection of the three markers was achieved. The direct assay should be performed immediately after plate preparation in order to achieve the optimal fluorescence signal. The sandwich detection assay was performed in order to improve the limit of detection of the breast cancer markers. The sandwich assay could detect both normal and abnormal levels of breast cancer markers. There was a 20 to 30-fold improvement in the detection of the breast cancer markers with this technique. The detection limits for HER2/neu, ERa, and PR were 3 ng/mL, 6ng/mL and 11 ng/mL, respectively. The sandwich assay using InP/ZnS quantum dots were able to detect (17, 25, and 32) ng/mL of HER2/neu, ERa, and PR, respectively. The higher detection limits are due to the poor quantum yield compared to that of CdSe/ZnS quantum dots. More studies to improve the properties of InP/ZnS quantum dots are needed in order to have optical properties superior to CdSe/ZnS quantum dots. These quantum dot encoded particles could potentially be used in the early detection of HER2/neu, ERa, or PR positive breast cancer. Unlike FISH and IHC, this technique was capable of analyzing all three biomarkers simultaneously which would reduce diagnosis time and improve prognosis. This technique is also a better candidate than FISH and IHC for early diagnosis in that serum levels can be monitored without the presence of a tumor. This is important for the recovery and survival of breast cancer patients. The invasive techniques of FISH and IHC analyze breast tissue samples from regions of interest usually where a tumor has been detected. By the time the tumor is detected, the probability of proliferation or metastasis is increased significantly. By

simply using the minimally invasive technique of collecting serum samples, the use of SiQDs as signal transducers could potentially be used in the early diagnosis of breast cancer and can possibly be used to either replace or complement FISH and IHC.

## 4.6 References

1. National Cancer Institute  
<http://www.nci.nih.gov/cancertopics/types/breast>  
Date accessed: May 2009
2. Breast Cancer  
[www.breastcancer.org](http://www.breastcancer.org)  
Date accessed: May 2009
3. Pernthaler, A.; Pernthaler, J.; Amann, R., Fluorescence In Situ Hybridization and Catalyzed Reporter Deposition for the Identification of Marine Bacteria. *APPLIED AND ENVIRONMENTAL MICROBIOLOGY* **2002**, 68, 3094-3101.
4. Sieben, V. J.; Debes Marun, C. S.; Pilarski, P. M.; . Kaigala, G. V.; Pilarski, L. M.; Backhouse, C. J., FISH and chips: chromosomal analysis on microfluidic platforms. *IET Nanobiotechnology* **2007**, 3, 27-35.
5. Levisky, J. M.; Singer, R. H., Fluorescence in situ hybridization: past, present and future. *Journal of Cell Science* **2003**, 116, 2833-2838.
6. Harari, P. M., Epidermal growth factor receptor inhibition strategies in oncology. *Endocrine-Related Cancer* **2004**, 11, 689-708.
7. Press, M. F., Diagnostic evaluation of HER-2 as a molecular target: an assessment of accuracy and reproducibility of laboratory testing in large, prospective, randomized clinical trials. *Clinical Cancer Research* **2005**, 18, 6598-6607.
8. Jorgensen, J. T.; Vang Nielsen, K.; Ejlersen, B., Pharmacodiagnosics and targeted therapies - a rational approach for individualizing medical anticancer therapy in breast cancer. *The Oncologist* **2007**, 12, 397-405.
9. Klimov, V. I., Nanocrystal Quantum Dots From fundamental photophysics to multicolor lasing. *Los Alamos Science* **2003**, 28, 214-220.
10. Murphy, C. J., Optical Sensing with Quantum Dots. *Analytical Chemistry* **2002**, 520A-526A.
11. Medintz, I. L.; Berti, L.; Pons, T.; Grimes, A. F.; English, D. S.; Alessandrini, A.; Facci, P.; Mattoussi, H., A reactive peptidic linker for self-assembling hybrid quantum dot-DNA bioconjugates. *Nano Letters* **2007**, 7, (6), 1741-1748.
12. Gao, X. H.; Yang, L.; Petrosos, J. A.; Marshall, F. F.; Simons, J. W.; Nie, S. M., In vivo molecular and cellular imaging with quantum dots. *Curr. Opin. Biotechnol.* **2005**, 16, 63-72.

13. Yezhelyev, M. V.; Al-Hajj, A.; Morris, C.; Marcus, A. I.; Liu, T.; Lewis, M.; Cohen, C.; Zrazhevskiy, P.; Simons, J. W.; Rogatko, A.; Nie, S.; Gao, X.; O'Regan, R. M., In Situ Molecular Profiling of Breast Cancer Biomarkers with Multicolor Quantum Dots. *Advanced Materials* **2007**, *19*, 3146-3151.
14. Gao, X.; Nie, S., Quantum Dot-Encoded Mesoporous Beads with High Brightness and Uniformity: Rapid Readout Using Flow Cytometry. *Analytical Chemistry* **2004**, *76*, (8), 2406-2410.
15. Corrie, S. R.; Lawrie, G. A.; Trau, M., Quantitative Analysis and Characterization of Biofunctionalized Fluorescent Silica Particles. *Langmuir* **2006**, *22*, (6), 2731-2737.
16. Lin, V. S. Y., A porous silicon-based optical interferometric biosensor. *Science* **1997**, *278*, 840-843.
17. Descalzo, A.; Marcos, M.; Martinez-Manez, R.; Soto, J.; Beltran, D.; Amoros, P., Anthrylamine functionalized mesoporous silica based materials as hybrid fluorescent chemosensors for ATP. *Journal of Materials Chemistry* **2005**, *15*, 2721-2731.
18. Blin, J. L.; Gerardin, C.; Carteret, C.; Rodehuser, L.; Selve, C.; Stebe, M. J., Direct One-Step Immobilization of Glucose Oxidase in Well-Ordered Mesoporous Silica Using a Nonionic Fluorinated Surfactant. *Chemistry of Materials* **2005**, *17*, (6), 1479-1486.
19. Huh, S.; Wiench, J. W.; Yoo, J.-C.; Pruski, M.; Lin, V. S. Y., Organic Functionalization and Morphology Control of Mesoporous Silicas via a Co-Condensation Synthesis Method. *Chemistry of Materials* **2003**, *15*, (22), 4247-4256.
20. Slowing, I. I.; Trewyn, B. G.; Lin, V. S. Y., Mesoporous Silica Nanoparticles for Intracellular Delivery of Membrane-Impermeable Proteins. *Journal of the American Chemical Society* **2007**, *129*, (28), 8845-8849.
21. Radu, D. R.; Lai, C.-Y.; Wiench, J. W.; Pruski, M.; Lin, V. S. Y., Gatekeeping Layer Effect: A Poly(lactic acid)-coated Mesoporous Silica Nanosphere-Based Fluorescence Probe for Detection of Amino-Containing Neurotransmitters. *Journal of the American Chemical Society* **2004**, *126*, (6), 1640-1641.
22. Slowing, I.; Trewyn, B. G.; Lin, V. S. Y., Effect of Surface Functionalization of MCM-41-Type Mesoporous Silica Nanoparticles on the Endocytosis by Human Cancer Cells. *Journal of the American Chemical Society* **2006**, *128*, (46), 14792-14793.
23. Rossi, L. M.; Shi, L.; Rosenzweig, N.; Rosenzweig, Z., Fluorescent silica nanospheres for digital counting bioassay of the breast cancer marker HER2/neu. *Biosensors and Bioelectronics* **2006**, *21*, 1900-1906.
24. Nichkova, M.; Dosev, D.; Gee, S.; Hammock, B.; Kennedy, I., Multiplexed immunoassays for proteins using magnetic luminescent nanoparticles for internal calibration. *Analytical*

- Biochemistry* **2007**, *369*, 34-40.
25. Gao, X.; Nie, S., Doping Mesoporous Materials with Multicolor Quantum Dots. *The Journal of Physical Chemistry B* **2003**, *107*, (42), 11575-11578.
  26. Sathe, T. R.; Agrawal, A.; Nie, S., Mesoporous Silica Beads Embedded with Semiconductor Quantum Dots and Iron Oxide Nanocrystals: Dual-Function Microcarriers for Optical Encoding and Magnetic Separation. *Analytical Chemistry* **2006**, *78*, (16), 5627-5632.
  27. Qhobosheane, M.; Santra, S.; Zhang, P.; Tan, W., Biochemically functionalized silica nanoparticles. *Analyst* **2001**, *126*, 1274-1278.
  28. Dosev, D.; Nichkova, M.; Dumas, R.; Gee, S.; Hammock, B.; Liu, K.; Kennedy, I., Magnetic luminescent core shell particles synthesized by spray pyrolysis and their application in immunoassays with internal standard. *Nanotechnology* **2007**, *18*, 1-6.
  29. Han, M.; Gao, X.; Su, J. Z.; Nie, S. M., Quantum-dot-tagged microbeads for multiplexed optical coding of biomolecules. *Nature* **2001**, *19*, 631-635.
  30. Peng, Z. A.; Peng, X., Formation of High-Quality CdTe, CdSe, and CdS Nanocrystals Using CdO as Precursor. *Journal of the American Chemical Society* **2001**, *123*, (1), 183-184.
  31. Peng, Z. A.; Peng, X., Mechanisms of the Shape Evolution of CdSe Nanocrystals. *Journal of the American Chemical Society* **2001**, *123*, (7), 1389-1395.
  32. Rossi, L. M.; Shi, L.; Quina, F. H.; Rosenzweig, Z., Stober Synthesis of Monodispersed Luminescent Silica Nanoparticles for Bioanalytical Assays. *Langmuir* **2005**, *21*, (10), 4277-4280.
  33. Halliwell, C. M.; Cass, A. E. G., A Factorial Analysis of Silanization Conditions for the Immobilization of Oligonucleotides on Glass Surfaces. *Analytical Chemistry* **2001**, *73*, (11), 2476-2483.

## **Chapter 5**

### **Enzymatic Release of Fluorescent Drug Analogue from Human Serum Albumin Nanoparticles**

#### **5.1 Abstract**

Chapter 5 discusses the application of magnetic, fluorescent human serum albumin (HSA) nanoparticles that were prepared using the desolvation method. The HSA nanoparticles used in this study had an average diameter of ~ 100 nm. The HSA particles were loaded with 10 nm PEG coated magnetite particles and the fluorescent drug analogue, BOPIPY-vinblastine. This paper describes the effect of matrix metalloproteinase (MMP) concentration on the release of drug analogue from the composite particles. The MMPs used were collagenase and MMP-11. With higher doses of collagenase, the release of the drug was complete within 24 hours; whereas, the release was still not complete after 48 hours with the highest does of MMP-11 studied. These magnetic, fluorescent particles could also potentially be used as a theranostic tool in that the particles can detect the diseased site, image using MRI, release drug upon heating by magnetic field, and magnetic hyperthermia.

#### **5.2 Introduction**

Conventional chemotherapy involves the nonspecific action of the drug on normal tissue which causes toxic, deleterious side effects. The toxic side effects occur because there is no specific targeting of the drug to only diseased tissue. The controlled release and targeting of

drug agents specifically to diseased sites are of major interest in cancer research.<sup>1-5</sup> This approach would allow for smaller doses to be administered and would significantly reduce the toxicity to normal cells. Nanoparticles have the advantages of good stability, high drug loading efficiency, minimal drug leakage, and preferential accumulation in tumors.<sup>6-8</sup> Nanoparticle-based drug delivery systems have exhibited great success at both targeting and controlled release. Recently, Mirkin, Lippard, and coworkers developed a DNA-gold nanoparticle conjugate system to bind to the Pt(IV) prodrug, Cisplatin, to monitor its uptake and efficacy in multiple cancer cell lines.<sup>9</sup> It was shown that the Pt-DNA-gold nanoparticle conjugates were more effective than free cisplatin at killing the cancer cells. Linden and coworkers demonstrated the use of mesoporous silica nanoparticles for the targeted intracellular delivery of hydrophobic model drug fluorophores to cancer cells.<sup>10</sup> The mesoporous silica nanoparticles were able to specifically release two hydrophobic fluorophores into the endosomes of cancer cells. The fluorophores were subsequently released into the cytoplasm which is critical for good drug efficacy. Briesen and coworkers used antibody labeled human serum albumin (HSA) nanoparticles to specifically target and release the anti-cancer drug doxorubicin to HER2 positive breast cancer cells.<sup>11</sup> It was shown that the antibody labeled HSA particles loaded with doxorubicin were significantly more effective at killing the cancer cells than doxorubicin loaded particles labeled with a nonspecific antibody.

HSA is the most abundant blood plasma protein whose functions include transporting hormones<sup>12</sup>, fatty acids<sup>13</sup>, and drugs.<sup>14</sup> HSA is inexpensive, and the preparation of HSA nanoparticles is simple and reproducible. HSA nanoparticles as drug carriers are very attractive because they are biocompatible, biodegradable, nontoxic, nonimmunogenic and contain functional groups on the surface which allow for covalent linkage of biomolecules.<sup>15-18</sup>

Spankuch and coworkers loaded anti-HER2 labeled HSA nanoparticles with antisense oligonucleotides (ASO) to specifically target breast cancer cells.<sup>19</sup> It was found that the ASO labeled particles significantly reduced the gene expression of an overexpressed mitotic regulator. In 2005 the Food and Drug Administration (FDA) approved Abraxane, the first ever drug carrier system based on 130 nm HSA nanoparticles as transporters for the water insoluble chemotherapeutic agent, paclitaxel. Paclitaxel is used to treat breast, ovarian, and lung cancers.<sup>20</sup> HSA nanoparticles show much higher intratumoral concentrations, higher anti-tumor activity, and less adverse side effects than the traditional Cremophor-based paclitaxel delivery.<sup>21-24</sup>

In this paper we describe the preparation and in vitro application of magnetic, fluorescent HSA nanoparticles for the targeting and controlled release (as a function of enzyme concentration) of the fluorescent cancer drug analogue BODIPY vinblastine. Matrix metalloproteinases (MMPs) are a large family of proteolytic enzymes that are responsible for the degradation of the basement membrane and extracellular matrix and play a role in apoptosis and angiogenesis.<sup>35-37</sup> MMP overexpression in tumors is largely responsible for tumor invasion and metastasis.<sup>38-40</sup> MMPs are composed of four main subgroups: the collagenases, gelatinases, stromelysins, and membrane MMPs. In this study, collagenase and MMP-11 (stromelysin-3) were used to study the enzymatic activity on the magnetic, fluorescent HSA nanoparticles.

Collagenase is an enzyme that cleaves peptide bonds in collagen but also has a wide range of proteolytic activity that is not specific to only collagen. MMP-11 is unique from other MMPs in that it does not degrade the extracellular matrix.<sup>41, 42</sup> It cleaves the serine proteinase inhibitor a1-proteinase. MMP-11 is also unique in that it is not expressed in normal tissue, but is present in the majority of the stromal cells which surround the cancer cells in invasive tumors.<sup>43,</sup>

Previously our group has studied the release (as a result of an oscillating magnetic field) of the drug analog, dextran-tetramethylrhodamine, from magnetic collagen gels.<sup>25</sup> We also used iron oxide nanoparticles coated with luminescent quantum dots and labeled with antibodies to detect and separate breast cancer cells in serum.<sup>26</sup> Vinblastine is a plant derived chemotherapy drug used to treat a number of cancers including lymphoma, testicular, non-small cell lung, cervical, and breast cancers.<sup>27, 28</sup> It functions as a mitotic inhibitor that binds to tubulin in the mitotic spindle. Vinblastine inhibits microtubule formation which causes mitotic arrest and death of tumor cells.<sup>29</sup> It also acts to inhibit drug efflux mediated by P-glycoprotein in multidrug - resistant cells.<sup>30</sup> As with several anti-cancer drugs, vinblastine has toxic side effects and poor water solubility. The use of HSA nanoparticles, which preferentially bind hydrophobic drugs, can alleviate these issues. Incorporating magnetic iron oxide nanoparticles offers several advantages. The iron oxide particles can be used to magnetically target the HSA complex to diseased sites<sup>31</sup>, image the drug loaded particles using magnetic resonance imaging (MRI)<sup>32</sup>, and act as a mechanism to kill cancer cells by magnetic hyperthermia.<sup>33</sup> The magnetic, drug-loaded HSA nanoparticles have the potential to revolutionize the future of cancer therapy.

## **5.3 Experimental**

### **5.3.1 Preparation of magnetic BODIPY-Vinblastine encoded HSA nanoparticles**

HSA particles were prepared using a well established desolvation technique.<sup>16, 34</sup> 20 mg of HSA were dissolved in 1 mL of purified water and the pH was adjusted to 8.2 with 10 mM

NaOH. One hundred microliters of 100 nM BODIPY-vinblastine and 25  $\mu\text{L}$  of 1  $\mu\text{M}$  PEG coated  $\text{Fe}_3\text{O}_4$  were added to the HSA solution. The solution was stirred constantly at 650 rpm at room temperature for 2 h. Three milliliters of ethanol were added at a rate of 1 mL/min with a peristaltic pump. 8% glutaraldehyde was added (1.175  $\mu\text{L}/\text{mg}$  HSA) and the solution was stirred constantly for 24 h. The solution was then centrifuged three times at 13,000 g for 12 minutes and redispersed in 1 mL of DI water.

### **5.3.2 Preparation of Anti-PR labeled HSA particles**

Antibody labeled magnetic fluorescent HSA particles were prepared by mixing 1 mL HSA composite particles (prepared as described above) with 50  $\mu\text{g}$  of anti-PR / mL PBS containing 40 mM EDC/5 mM sulfo-NHS. The antibody labeled particles were incubated under gentle stirring at room temperature for two hours. The particles were separated by centrifugation (13,000g, 12min) and washed three times with PBS at pH 7.4. The particles were then re-dispersed in 4 mL of PBS at pH 7.4 and immediately used for binding assays.

### **5.3.3 Direct detection of PR**

For direct detection, a 96-well plate was coated with 100  $\mu\text{L}$  bovine serum spiked with 10  $\mu\text{g}/\text{mL}$  PR protein through nonspecific adsorption. The plate was incubated for 20 hrs at 4°C. Unoccupied sites were blocked by adding 300  $\mu\text{L}$  of Superblock T20 PBS buffer. One hundred microliters of anti-PR labeled HSA composite particles were added and incubated for 2 hours. The plate was washed with PBS containing 0.05% Tween-20 and dried under a stream of nitrogen. To measure the release of BODIPY-vinblastine, 300  $\mu\text{L}$  of PBS buffer pH 7.4 containing varying concentrations of collagenase and MMP-11 were added to the wells. At

different time intervals ranging from 0 hours to 48 hours, 200  $\mu\text{L}$  aliquots of the sample were taken and the fluorescence intensity was measured using a microplate reader.

### 5.3.4 Characterization of unloaded HSA particles

Cryo-TEM images were taken with a JEOL 2011 TEM at 120 kV. The image magnifications were 50,000 x for 1 micron HSA and 12,000 x for 100 nm HSA particles.

## 5.4 Results and Discussion

### 5.4.1 Characterization of unloaded HSA particles

Figure 5.1 shows the cryo-TEM images of a) 1 micron HSA particles and b) 100 nm HSA particles. The particles have a well defined spherical shape and are monodisperse. The scale bar for a) is 20 nm and b) 100 nm.

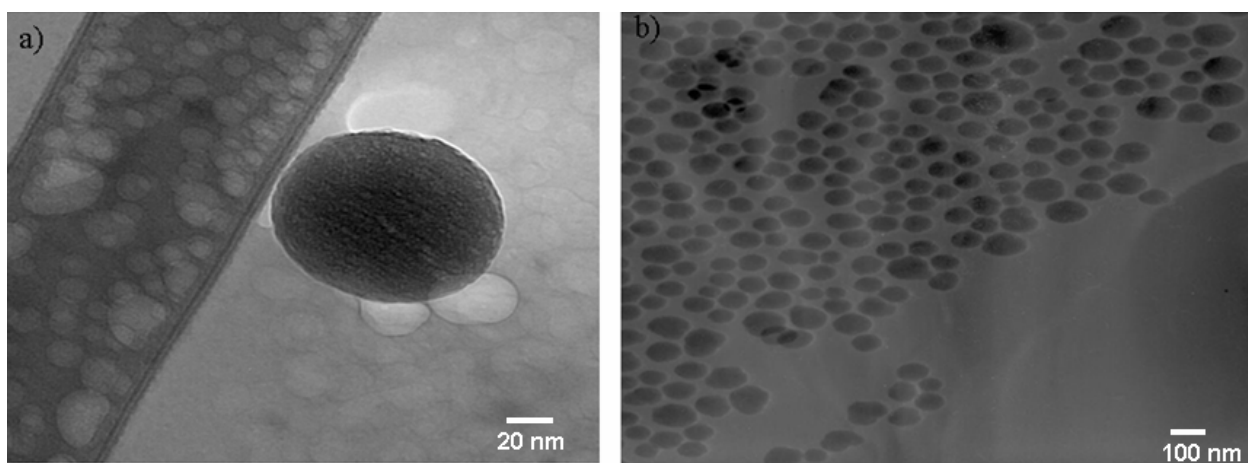


Figure 5.1. Cryo-TEM images of a) 1 micron HSA and b) 100 nm HSA.

Figure 5.2 shows images of 100 nm magnetic BODIPY-Vinblastine encoded HSA particles suspended in aqueous buffer. The percent entrapment of BODIPY-vinblastine and Fe<sub>3</sub>O<sub>4</sub> in HSA was calculated to be 69% and 16%, respectively. The values were calculated using the equation:

$$(C-c)/C \times 100 \quad (1)$$

Where C is the initial concentration of fluorophore and magnetic particles added and c is the concentration of the supernatant after cross linking of HSA.

The images were taken in room light and under UV radiation to show the magnetic and fluorescent properties of the composite particles. The particles were placed in a sample vial and mounted in front of a strong magnet. After 15 minutes, the magnetic/fluorescent HSA particles were completely separated from the solvent.

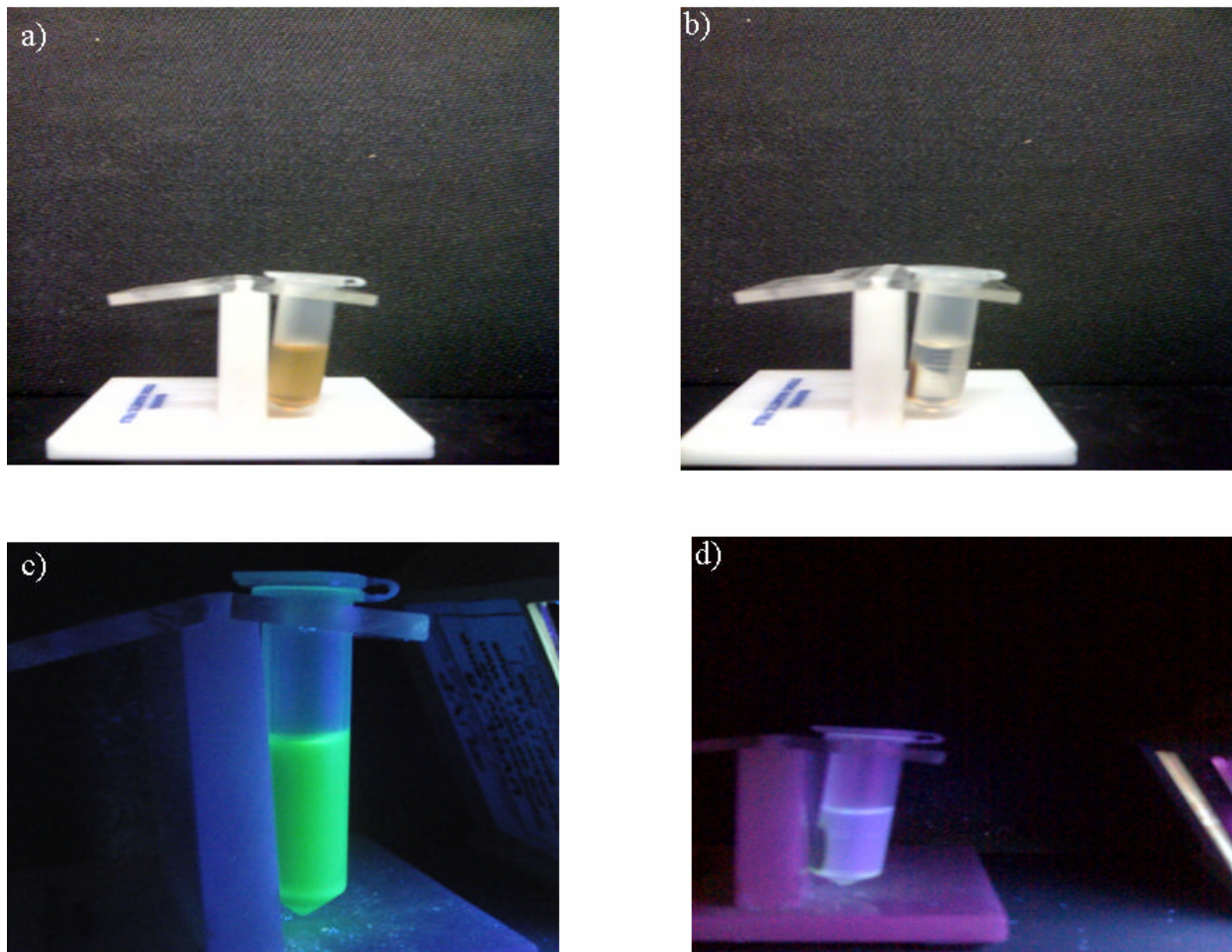


Figure 5.2. Images of a) HSA nanoparticles at  $t = 0$  min in room light, b) HSA nanoparticles at  $t = 15$  min in room light, c) HSA nanoparticles at  $t = 0$  min under UVlight, and d) HSA nanoparticles at  $t = 15$  min under UV light.

#### 5.4.2 Effect of enzyme concentration on the release of BODIPY-Vinblastine from HSA nanoparticles

Figures 5.3 and 5.4 show the release rates of BODIPY-vinblastine in the presence of collagenase and MMP-11. After the anti-PR labeled HSA particles attached to the antigen and the plate was washed, varying concentrations of collagenase and MMP-11 were added. Fluorescence intensity measurements ( $F/F_0$ ) were taken at 0, 2, 6, 8, 24, 32, and 48 hours after addition of the enzyme to the HSA particles. The excitation wavelength was  $\lambda_{ex} = 375$  nm and

the emission wavelength was  $\lambda_{em} = 515$  nm. As the concentration of enzyme increased, the rate of BODIPY-vinblastine release from the HSA nanoparticles increased. Concentrations of collagenase and MMP-11 ranged from 0 to 10  $\mu\text{g/mL}$ . The release of BODIPY-vinblastine was complete within 24 hours with a collagenase concentration of 10  $\mu\text{g/mL}$ . However, the release of BODIPY-vinblastine was not complete within 48 hours with 10  $\mu\text{g/mL}$  MMP-11. The slow proteolytic cleavage with MMP-11 is consistent with reports that MMP-11 has very low proteolytic activity in vitro.<sup>45</sup>

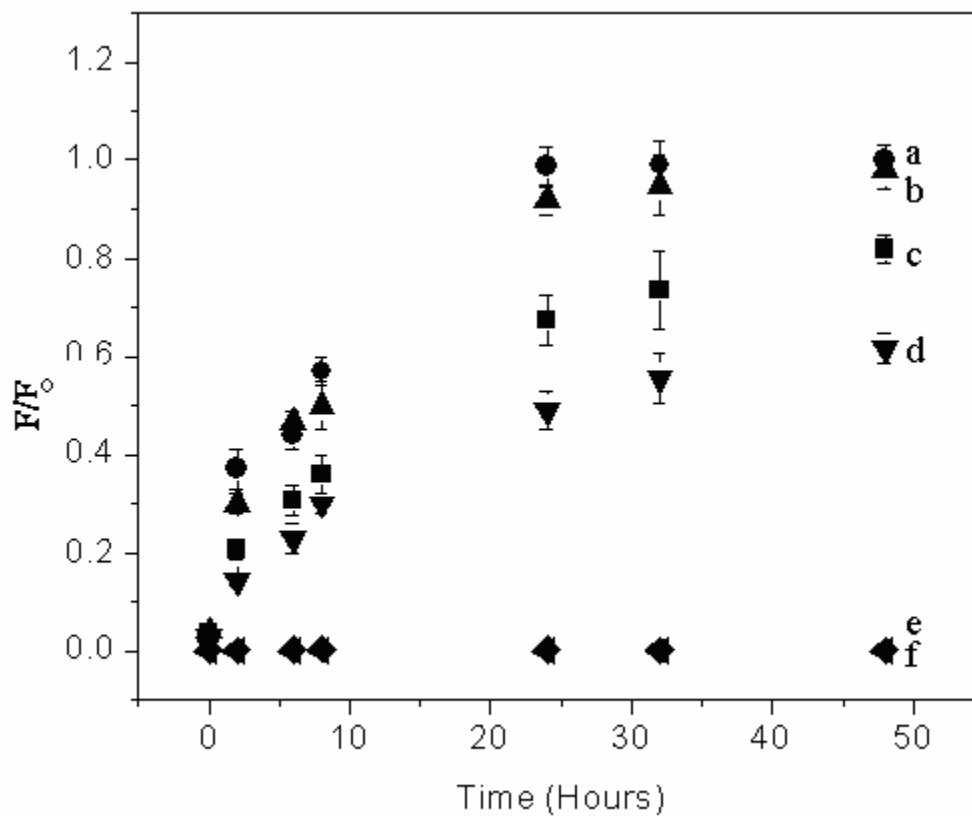


Figure 5.3. Effect of collagenase concentration on BODIPY-vinblastine release from HSA nanoparticles. a) 10  $\mu\text{g/mL}$  collagenase, b) 8  $\mu\text{g/mL}$  collagenase, c) 6  $\mu\text{g/mL}$  collagenase, d) 2  $\mu\text{g/mL}$  collagenase, e) 0  $\mu\text{g/mL}$  collagenase, and f) unlabeled HSA particles with 10  $\mu\text{g/mL}$  collagenase.

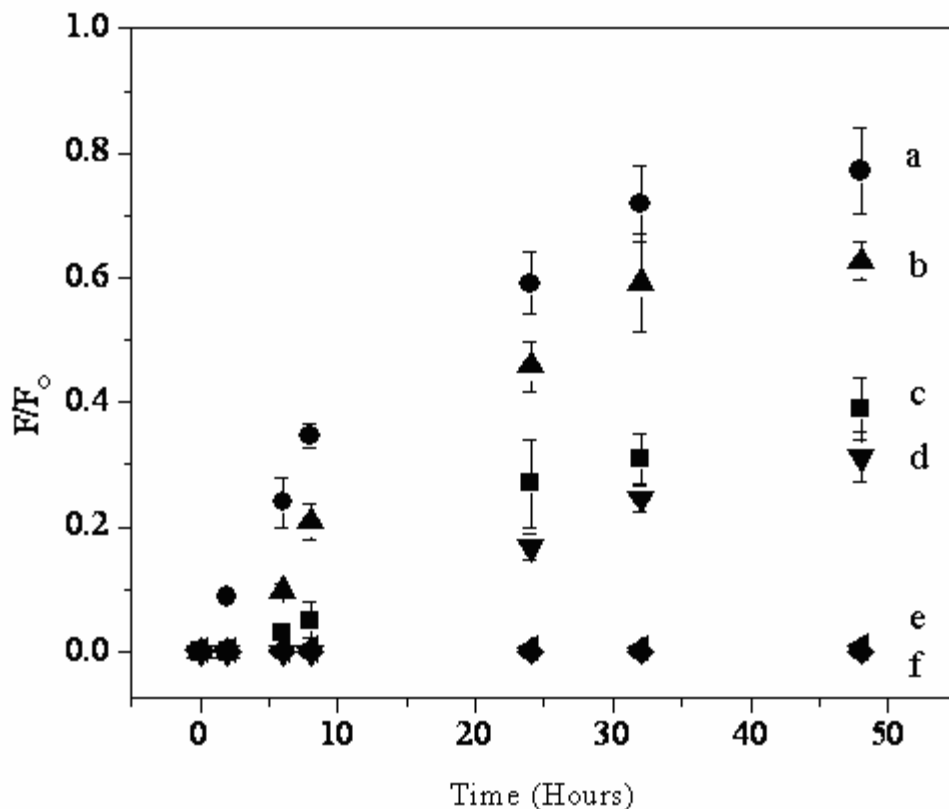


Figure 5.4. Effect of MMP-11 concentration on BODIPY-vinblastine release from HSA nanoparticles. a) 10 µg/mL MMP-11, b) 8 µg/mL MMP-11, c) 6 µg/mL MMP-11, d) 2 µg/mL MMP-11, e) 0 µg/mL MMP-11, and f) unlabeled HSA particles with 10 µg/mL MMP-11.

### 5.4.3 Control experiment for the release of BODIPY Vinblastine from HSA

To ensure that the enzyme is in fact degrading the HSA particles and releasing the material in solution, 8 µg/mL of MMP-11 was added to five solutions of magnetic, fluorescent particles without anti-PR on the surface. After various exposure times, the solution was placed near a magnet for separation, and the fluorescence intensities of the supernatants were measured. Each solution was measured at different time points. Figure 5.5 shows the fluorescence spectra and a corresponding plot of fluorescence intensity vs time for the release of BODIPY - vinblastine from HSA nanoparticles. The solution without any MMP-11 added showed no

fluorescence in the supernatant (data not shown). At 0 hours of incubation with MMP-11, there was very little fluorescence signal. The fluorescence intensity continued to increase from 6 to 32 hours. The increase in fluorescence intensity of the supernatants indicates enzyme degradation of the HSA particles. Because there is no antibody present, the possibility of antibody degradation initiating the release of non- degraded particles in solution is ruled out.

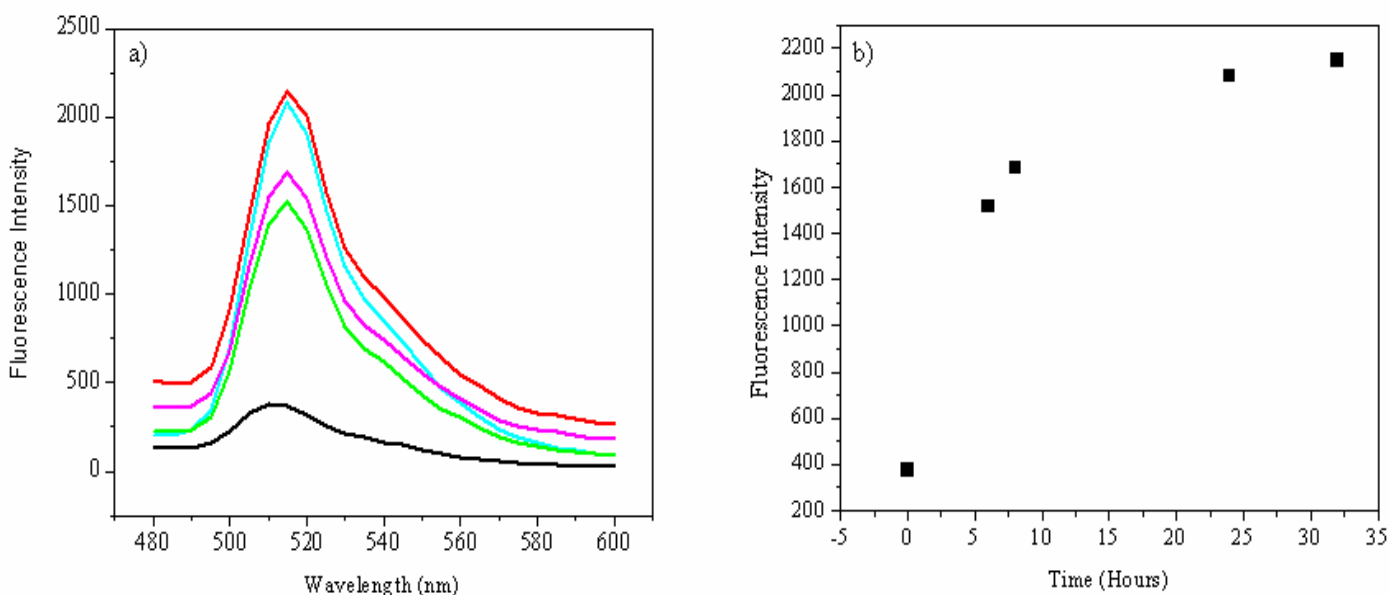


Figure 5.5. Effect of MMP-11 concentration of BODIPY-vinblastine release from HSA nanoparticles suspended in solution. a) fluorescence spectra and b) corresponding plot of the fluorescence intensity of supernatant as a function of enzyme degradation time

#### 5.4.4 Determination of BODIPY Vinblastine encapsulation in HSA nanoparticles

To determine whether BODIPY was encapsulated inside the HSA particles and not on the surface, varying concentrations of KBr were added and the quenching effects were determined by measuring the decrease in fluorescence intensity. Figure 5.6 shows the Stern-Volmer plot of free BODIPY and BODIPY encapsulated in HSA.  $F_0$  represents the fluorescence intensity of

BODIPY in the absence of KBr, and  $F$  represents the fluorescence intensity in the presence of KBr. The plot for free BODIPY shows a very linear response ( $R^2 = 0.9985$ ) as a function of KBr concentration. According to the Stern-Volmer equation  $F_0/F = K[Q] + 1$ , where  $K$  is the Stern-Volmer constant and  $Q$  is the quencher concentration,  $K$  (determined by the slope) for free BODIPY is  $3.18 \text{ M}^{-1}$ . This clearly indicates one fluorophore population that is entirely accessible to quencher. The plot for BODIPY encapsulated in HSA shows a nonlinear response that curves downward towards the x-axis. This downward curvature suggests the presence of two fluorophore populations: one with BODIPY on the surface and one buried inside the HSA. The population on the surface is easily accessible to KBr quenching; whereas, the population inside HSA is not. The downward curvature clearly indicates that BODIPY is entrapped inside the HSA. This is important because it can be released specifically upon enzyme degradation of the HSA particles in diseased tissue which eliminates any premature release.

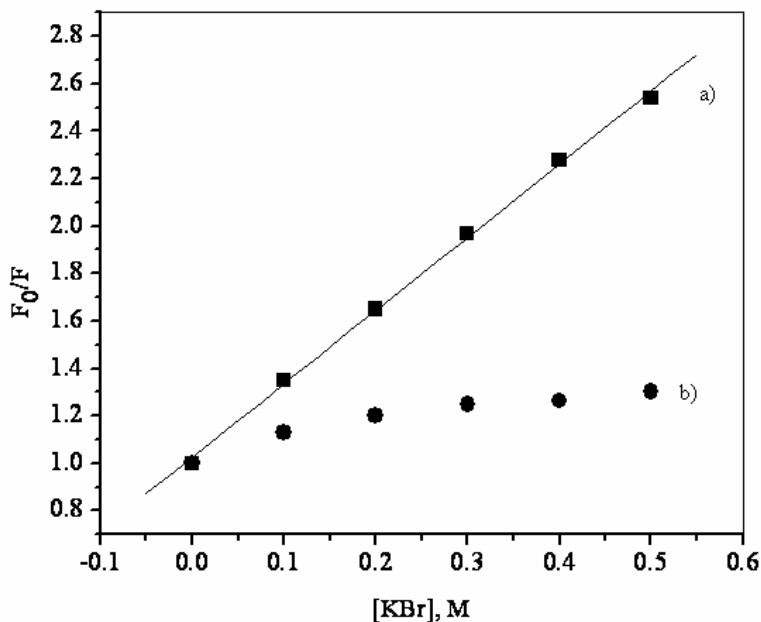


Figure 5.6. Stern-Volmer plot of fluorophore populations. a) Free BODIPY and b) BODIPY inside HSA nanoparticles

## 5.5 Summary and Conclusions

HSA nanoparticles loaded with magnetite particles and a fluorescent drug analogue, BODIPY- vinblastine were prepared. The method of preparing the HSA composite particles was simple and reproducible. HSA has several advantages including the availability of surface functional groups for covalent attachment of biomolecules, biocompatibility, and biodegradability. This study showed, *in vitro*, the release of the drug analogue as a function of enzyme concentration. Collagenase was superior at degrading the HSA particles compared to MMP-11. The release was complete within 24 hours. It was proven that the enzymes do degrade HSA and that BODIPY was successfully encapsulated inside the particles and not just on the surface. The incorporation of magnetic particles into HSA makes them candidates for theranostics. The antibody – labeled composite particles could be used to detect diseased sites, image the diseased sites with MRI, and treat the diseased sites by either releasing a drug in the presence of an oscillating magnetic field or magnetic hyperthermia. HSA nanoparticles have a very bright future in biomedicine. One example is the FDA approved Abraxane. Future work will focus on optimizing the conditions for the release of BODIPY-vinblastine by magnetic nanoparticles in the presence of an oscillating magnetic field.

## 5.6 References

1. Deo, S. K.; Moschou, E. A.; Peteu, S. F.; Bachas, L. G.; Daunert, S.; Eisenhardt, P. E.; Madou, M. J., Peer Reviewed: Responsive Drug Delivery Systems. *Analytical Chemistry* **2003**, 75, (9), 206 A-213 A.
2. Farokhzad, O. C.; Jon, S.; Khademhosseini, A.; Tran, T.-N. T.; LaVan, D. A.; Langer, R., Nanoparticle-Aptamer Bioconjugates: A New Approach for Targeting Prostate Cancer Cells. In 2004; Vol. 64, pp 7668-7672.
3. Rosenholm, J. M.; Meinander, A.; Peuhu, E.; Niemi, R.; Eriksson, J. E.; Sahlgren, C.; Linden, M., Targeting of Porous Hybrid Silica Nanoparticles to Cancer Cells. *ACS Nano* **2008**, 3, (1), 197-206.
4. Wu, X. L.; Kim, J. H.; Koo, H.; Bae, S. M.; Shin, H.; Kim, M. S.; Lee, B.-H.; Park, R.-W.; Kim, I.-S.; Choi, K.; Kwon, I. C.; Kim, K.; Lee, D. S., Tumor-Targeting Peptide Conjugated pH-Responsive Micelles as a Potential Drug Carrier for Cancer Therapy. *Bioconjugate Chemistry*.
5. Shi, X.; Wang, S. H.; Shen, M.; Antwerp, M. E.; Chen, X.; Li, C.; Petersen, E. J.; Huang, Q.; Weber, W. J.; Baker, J. R., Multifunctional Dendrimer-Modified Multiwalled Carbon Nanotubes: Synthesis, Characterization, and In Vitro Cancer Cell Targeting and Imaging. *Biomacromolecules* **2009**, 10, (7), 1744-1750.
6. Gelperina, S.; Kisich, K.; Iseman, M. D.; Heifets, L., The Potential Advantages of Nanoparticle Drug Delivery Systems in Chemotherapy of Tuberculosis. In 2005; Vol. 172, pp 1487-1490.
7. Cho, K.; Wang, X.; Nie, S.; Chen, Z.; Shin, D. M., Therapeutic Nanoparticles for Drug Delivery in Cancer. In 2008; Vol. 14, pp 1310-1316.
8. Diagaradjane, P.; Shetty, A.; Wang, J. C.; Elliott, A. M.; Schwartz, J.; Shentu, S.; Park, H. C.; Deorukhkar, A.; Stafford, R. J.; Cho, S. H.; Tunnell, J. W.; Hazle, J. D.; Krishnan, S., Modulation of in Vivo Tumor Radiation Response via Gold Nanoshell-Mediated Vascular-Focused Hyperthermia: Characterizing an Integrated Antihypoxic and Localized Vascular Disrupting Targeting Strategy. *Nano Letters* **2008**, 8, (5), 1492-1500.
9. Dhar, S.; Daniel, W. L.; Giljohann, D. A.; Mirkin, C. A.; Lippard, S. J., Polyvalent Oligonucleotide Gold Nanoparticle Conjugates as Delivery Vehicles for Platinum(IV) Warheads. *Journal of the American Chemical Society* **2009**, 131, (41), 14652-14653.
10. Rosenholm, J. M.; Peuhu, E.; Eriksson, J. E.; Sahlgren, C.; Linden, M., Targeted Intracellular Delivery of Hydrophobic Agents using Mesoporous Hybrid Silica Nanoparticles as Carrier Systems. *Nano Letters* **2009**, 9, (9), 3308-3311.

11. Anhorn, M. G.; Wagner, S.; Kreuter, J. r.; Langer, K.; von Briesen, H., Specific Targeting of HER2 Overexpressing Breast Cancer Cells with Doxorubicin-Loaded Trastuzumab-Modified Human Serum Albumin Nanoparticles. *Bioconjugate Chemistry* **2008**, 19, (12), 2321-2331.
12. McKinnon, B.; Li, H.; Richard, K.; Mortimer, R., Synthesis of Thyroid Hormone Binding Proteins Transthyretin and Albumin by Human Trophoblast. In 2005; Vol. 90, pp 6714-6720.
13. Gelos, M.; Hinderberger, D.; Welsing, E.; Belting, J.; Schnurr, K.; Mann, B., Analysis of albumin fatty acid binding capacity in patients with benign and malignant colorectal diseases using electron spin resonance (ESR) spectroscopy. *International Journal of Colorectal Disease* 25, (1), 119-127.
14. Liu, X.; Du, Y.; Sun, W.; Kou, J.; Yu, B., Study on the interaction of levocetirizine dihydrochloride with human serum albumin by molecular spectroscopy. *Spectrochimica Acta Part A: Molecular and Biomolecular Spectroscopy* **2009**, 74, (5), 1189-1196.
15. Jahanshahi, M.; Babei, Z., Protein nanoparticle: A unique system as drug delivery vehicles. *African Journal of Biotechnology* **2008**, 7, (25), 4926-4934.
16. Dreis, S.; Rothweiler, F.; Michaelis, M.; Cinatl Jr, J.; Kreuter, J.; Langer, K., Preparation, characterisation and maintenance of drug efficacy of doxorubicin-loaded human serum albumin (HSA) nanoparticles. *International Journal of Pharmaceutics* **2007**, 341, (1-2), 207-214.
17. Anhorn, M. G.; Mahler, H.-C.; Langer, K., Freeze drying of human serum albumin (HSA) nanoparticles with different excipients. *International Journal of Pharmaceutics* **2008**, 363, (1-2), 162-169.
18. Wagner, S.; Rothweiler, F.; Anhorn, M. G.; Sauer, D.; Riemann, I.; Weiss, E. C.; Katsen-Globa, A.; Michaelis, M.; Cinatl Jr, J.; Schwartz, D.; Kreuter, J.; von Briesen, H.; Langer, K., Enhanced drug targeting by attachment of an anti [alpha]v integrin antibody to doxorubicin loaded human serum albumin nanoparticles. *Biomaterials* In Press, Corrected Proof.
19. Steinhauser, I. M.; Langer, K.; Strebhardt, K. M.; Spänkuch, B., Effect of trastuzumab-modified antisense oligonucleotide-loaded human serum albumin nanoparticles prepared by heat denaturation. *Biomaterials* **2008**, 29, (29), 4022-4028.
20. Rowinsky, E. K.; Donehower, R. C., Paclitaxel (Taxol). In 1995; Vol. 332, pp 1004-1014.
21. Desai, N.; Trieu, V.; Yao, Z.; Louie, L.; Ci, S.; Yang, A.; Tao, C.; De, T.; Beals, B.; Dykes, D.; Noker, P.; Yao, R.; Labao, E.; Hawkins, M.; Soon-Shiong, P., Increased antitumor activity, intratumor paclitaxel concentrations, and endothelial cell transport of cremophor-free, albumin-bound paclitaxel, ABI-007, compared with cremophor-based paclitaxel. In 2006; Vol. 12, pp 1317-1324.

22. Gradishar, W. J.; Tjulandin, S.; Davidson, N.; Shaw, H.; Desai, N.; Bhar, P.; Hawkins, M.; O'Shaughnessy, J., Phase III Trial of Nanoparticle Albumin-Bound Paclitaxel Compared With Polyethylated Castor Oil-Based Paclitaxel in Women With Breast Cancer. In 2005; Vol. 23, pp 7794-7803.
23. [www.abraxane.com](http://www.abraxane.com).
24. Green, M. R.; Manikhas, G. M.; Orlov, S.; Afanasyev, B.; Makhson, A. M.; Bhar, P.; Hawkins, M. J., Abraxane(R), a novel Cremophor(R)-free, albumin-bound particle form of paclitaxel for the treatment of advanced non-small-cell lung cancer. In 2006; Vol. 17, pp 1263-1268.
25. De Paoli, V. M.; De Paoli Lacerda, S. H.; Spinu, L.; Ingber, B.; Rosenzweig, Z.; Rosenzweig, N., Effect of an Oscillating Magnetic Field on the Release Properties of Magnetic Collagen Gels. *Langmuir* **2006**, 22, (13), 5894-5899.
26. Wang, D.; He, J.; Rosenzweig, N.; Rosenzweig, Z., Superparamagnetic Fe<sub>2</sub>O<sub>3</sub> Beads CdSe/ZnS Quantum Dots Core Shell Nanocomposite Particles for Cell Separation. *Nano Letters* **2004**, 4, (3), 409-413.
27. [http://www.ncbi.nlm.nih.gov/bookshelf/br.fcgi?book=meds&log\\$=drug\\_bottom\\_one&part=a682848](http://www.ncbi.nlm.nih.gov/bookshelf/br.fcgi?book=meds&log$=drug_bottom_one&part=a682848).
28. Harmsen, S.; Meijerman, I.; Febus, C.; Maas-Bakker, R.; Beijnen, J.; Schellens, J., PXR-mediated induction of P-glycoprotein by anticancer drugs in a human colon adenocarcinoma-derived cell line. *Cancer Chemotherapy and Pharmacology*.
29. Zu, Y.; Zhang, Y.; Zhao, X.; Zhang, Q.; Liu, Y.; Jiang, R., Optimization of the preparation process of vinblastine sulfate (VBLS)-loaded folate-conjugated bovine serum albumin (BSA) nanoparticles for tumor-targeted drug delivery using response surface methodology (RSM). *Int J Nanomedicine* **2009**, 4, 321-333.
30. Manuel, G.; Lluís, M. M.; Stéphane, O., Competitive and Non-Competitive Inhibition of the Multidrug-Resistance-Associated P-glycoprotein ATPase. In 1997; Vol. 244, pp 664-673.
31. Pradhan, P.; Banerjee, R.; Bahadur, D.; Koch, C.; Mykhaylyk, O.; Plank, C., Targeted Magnetic Liposomes Loaded with Doxorubicin. In *Liposomes*, pp 279-293.
32. Mauro Comes, F.; Giovanni, B.; Daniele, B.; Denis, G.; Guido, G.; Alessandro, L.; Maurizio, C.; Patrick, M.; Jessica, P.; Edoardo, M.; Uliano, G.; Luigi, S.; Paolo, G.; Costanza, R.; Alfredo, R., Bovine Serum Albumin-Based Magnetic Nanocarrier for MRI Diagnosis and Hyperthermic Therapy: A Potential Theranostic Approach Against Cancer. In 2009; Vol. 9999, p NA.
33. Hergt, R.; Dutz, S.; Müller, R.; Zeisberger, M., Magnetic particle hyperthermia: nanoparticle

- magnetism and materials development for cancer therapy. *Journal of Physics: Condensed Matter* **2006**, 18, (38), S2919-S2934.
34. Langer, K.; Balthasar, S.; Vogel, V.; Dinauer, N.; von Briesen, H.; Schubert, D., Optimization of the preparation process for human serum albumin (HSA) nanoparticles. *International Journal of Pharmaceutics* **2003**, 257, (1-2), 169-180.
  35. Kunigal, S.; Lakka, S. S.; Joseph, P.; Estes, N.; Rao, J. S., MMP-9 Inhibition Downregulates Radiation-induced NF- $\kappa$ B Activity Leading to Apoptosis in Breast Tumors. *Clin Cancer Res.* **2008**, 14, 3617-3626.
  36. London, C. A.; Sekhon, H. S.; Arora, V.; Stein, D. A.; Iversen, P. L.; Devi, G. R., A novel antisense inhibitor of MMP-9 attenuates angiogenesis, human prostate cancer cell invasion and tumorigenicity. *Cancer Gene Ther* 10, (11), 823-832.
  37. Vu, T. H.; Shipley, J. M.; Bergers, G.; Berger, J. E.; Helms, J. A.; Hanahan, D.; Shapiro, S. D.; Senior, R. M.; Werb, Z., MMP-9/Gelatinase B Is a Key Regulator of Growth Plate Angiogenesis and Apoptosis of Hypertrophic Chondrocytes. **1998**, 93, (3), 411-422.
  38. Curran, S.; Murray, G. I., Matrix metalloproteinases: molecular aspects of their roles in tumour invasion and metastasis. *European Journal of Cancer* **2000**, 36, (13), 1621-1630.
  39. Stamenkovic, I., Matrix metalloproteinases in tumor invasion and metastasis. *Seminars in Cancer Biology* **2000**, 10, (6), 415-433.
  40. Maeda-Yamamoto, M.; Kawahara, H.; Tahara, N.; Tsuji, K.; Hara, Y.; Isemura, M., Effects of Tea Polyphenols on the Invasion and Matrix Metalloproteinases Activities of Human Fibrosarcoma HT1080 Cells. *Journal of Agricultural and Food Chemistry* **1999**, 47, (6), 2350-2354.
  41. Pan, W.; Arnone, M.; Kendall, M.; Grafstrom, R. H.; Seitz, S. P.; Wasserman, Z. R.; Albright, C. F., Identification of Peptide Substrates for Human MMP-11 (Stromelysin-3) Using Phage Display. *The Journal of Biological Chemistry* **2003**, 278, 27820-27827.
  42. Lijnen, H. R., Matrix Metalloproteinases and Cellular Fibrinolytic Activity. *Biochemistry (Moscow)* **2002**, 67, (1), 92-98.
  43. Kohrmann, A.; Kammerer, U.; Kapp, M.; Dietl, J.; Anacker, J., Expression of matrix metalloproteinases (MMPs) in primary human breast cancer and breast cancer cell lines: New findings and review of the literature. In 2009; Vol. 9, p 188.
  44. Peruzzi, D.; Mori, F.; Conforti, A.; Lazzaro, D.; De Rinaldis, E.; Ciliberto, G.; La Monica, N.; Aurisicchio, L., MMP11: A Novel Target Antigen for Cancer Immunotherapy. In 2009; Vol. 15, pp 4104-4113.

45. Gall, A.-L.; Ruff, M.; Kannan, R.; Cuniasse, P.; Yiotakis, A.; Dive, V.; Rio, M.-C.; Basset, P.; Moras, D., Crystal structure of the stromelysin-3 (MMP-11) catalytic domain complexed with a phosphinic inhibitor mimicking the transition-state. *Journal of Molecular Biology* **2001**, 307, (2), 577-586.

## **Chapter 6**

### **Discussion**

This dissertation has discussed the use of fluorescent quantum dots and protein nanoparticles in biological applications. Quantum dots offer several advantages over conventional fluorophores such as broad absorption spectra, narrow emission spectra, high quantum yield, high photostability, high chemical stability, and size dependent luminescence. Human serum albumin protein nanoparticles have the advantages of being inexpensive, nonimmunogenic, biocompatible, and biodegradable.

One of the most desirable characteristics of quantum dots is their ability to multiplex. Several research groups have used quantum dots in multiplexed assays to detect biomolecules such as multiple DNA targets to specific neurotoxins. Chapter 3 discussed the incorporation of CdSe/ZnS quantum dots emitting at 545 nm and 655 nm into 35 nm pores of 3  $\mu\text{m}$  mesoporous silica particles. The quantum dots were stably encapsulated in the pores via strong hydrophobic interactions between the TOPO molecules on the quantum dot surface and the C-18 hydrocarbon chain in the mesopore. It was also possible to precisely control the ratio the different emission wavelength quantum dots in the pores which makes it possible to make several optical codes. Unlike costly and laborious methods such as spray pyrolysis and microemulsions, the method of preparing the fluorescent mesoporous silica particles was both rapid and simple. The incorporation of the quantum dots into the mesoporous silica spheres was completed in 30 minutes. The quantum dot- silica composites were employed as signal transducers for the

detection of the breast cancer marker HER2/neu. TEM, SEM, and EDS showed the presence of quantum dots in the silica pores. Unlike polystyrene microparticles, the rigid silica particles were resistant to structural deformation. The quantum dot – silica composites showed high photostability compared to dye labeled mesoporous silica particles and free quantum dots. This is likely due to the silica shielding the quantum dots from photo-oxidation or photocorrosion. The composite particles were most stable when stored under argon in the dark. Mesoporous silica loaded with a 1:1 ratio of 1 $\mu$ M 545 nm and 655 nm quantum dots and labeled with anti-HER2 via biotin/avidin interactions successfully detected the HER2/neu. The HER2/neu assay had a limit of detection of 85 ng/mL with a linear range between 85 ng/mL and 10  $\mu$ g/mL of HER2/neu.

The ability to screen for multiple biomarkers is very desirable. The current gold standards for detecting breast cancer are fluorescence in situ hybridization (FISH) and immunohistochemistry (IHC), neither of which can identify multiple biomarkers simultaneously and are invasive. Chapter 4 discussed in more detail the use of quantum dot – silica composites for the multiplexed detection of multiple breast cancer markers. Unlike FISH and IHC which analyze tissue samples, this detection method was minimally invasive in that it analyzed breast cancer marker concentration in serum samples. Quantum dots emitting at 495 nm, 560, nm, and 655 nm were used to detect HER2/neu, ER $\alpha$ , and PR individually and simultaneously. The direct detection method which involved the nonspecific adsorption of protein to a glass well plate was only able to measure abnormal levels of protein. To improve the sensitivity of the assay a sandwich assay was performed by covalently binding a capture antibody to the glass plate via EDC/NHS chemistry and using the antibody labeled quantum dot – silica composites as the

detection. The sandwich assay had approximately a 20 to 30-fold improvement in detection and was able to detect both normal and abnormal levels of protein. One major disadvantage of CdSe/ZnS quantum dots is their toxicity. We wanted to demonstrate the capability of nontoxic InP quantum dots to simultaneously detect the breast cancer markers. The multiplexed detection with InP quantum dots was successful but had inferior detection limits compared to mesoporous silica loaded with CdSe/ZnS. These quantum dot encoded particles are novel in that they could potentially be used in the early detection of HER2/neu, ERα, or PR positive breast cancer. By using the minimally invasive technique of collecting serum samples, the use of SiQDs as signal transducers could potentially be used in the early diagnosis of breast cancer and can possibly be used to either replace or complement FISH and IHC.

A highly attractive alternative to conventional chemotherapy is the controlled release and targeting of drug agents specifically to diseased sites. Chapter 5 discussed the use of anti-PR labeled human serum albumin nanoparticles for the in vitro detection of the breast cancer marker progesterone receptor and the effect of matrix metalloproteinase (MMP) concentration on the release of drug analogue from the composite particles. Several research groups have used human serum albumin nanoparticles for the detection and delivery of hydrophobic drug molecules to diseased cells. In our study, human serum albumin nanoparticles were loaded with 10 nm magnetite particles and a fluorescent drug analogue, BODIPY-vinblastine. Cryo-TEM images revealed spherical, monodispersed particles. The particles were proven to be both fluorescent and magnetic by mounting the sample vial on a magnet. After 15 minutes, the particles moved toward the magnet, leaving a clear supernatant. The solution fluoresced under illumination with a UV lamp. The release was complete within 24 hours with increasing collagenase

concentration; whereas, the release was still not complete after 48 hours with increasing MMP-11 concentration. The novelty of the antibody – labeled composite particles is their potential use as a theranostic tool to detect diseased sites, image the diseased sites with MRI, and treat the diseased sites by either releasing a drug in the presence of an oscillating magnetic field or magnetic hyperthermia.

## **VITA**

The author was born in Shreveport, Louisiana. She obtained her Bachelor's degree in chemistry from Louisiana State University in 2005. To pursue a PhD in analytical chemistry, she joined the University of New Orleans chemistry graduate program and became a member of Professor Zeev Rosenzweig's and Professor Matthew Tarr's research groups in 2005 and 2007, respectively.